Structural health monitoring of concrete structures using diffuse waves

Fröjd, Patrik

2018

Document Version:
Publisher's PDF, also known as Version of record

Structural health monitoring of concrete structures using diffuse waves

PATRIK FRÖJD
ENGINEERING GEOLOGY | FACULTY OF ENGINEERING | LUND UNIVERSITY

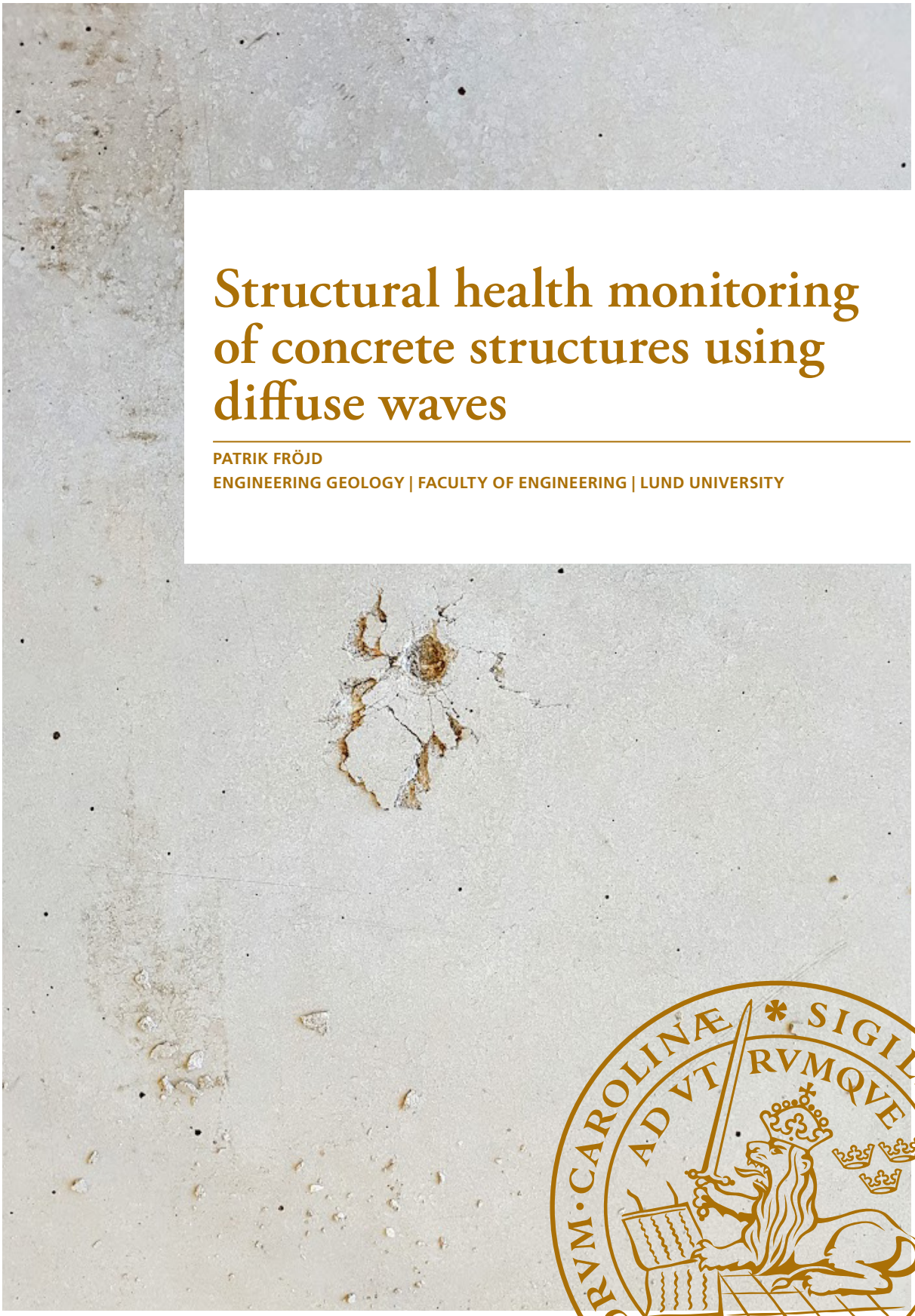

Printed by Media-Tryck, Lund 2018 NORDIC SWAN ECOLABEL 3041 0903

LUND UNIVERSITY
Faculty of Engineering
Engineering Geology
ISBN 978-91-7753-581-2
ISRN LUTVDG/(TVTG-1039)/1-142/(2018)

Department of Biomedical Engineering

Division of Engineering Geology

ISRN: LUTVDG/(TVTG-1039)/1-142/(2018)

ISBN: 978-91-7753-581-2 (print) | 978-91-7753-582-9 (pdf)

DOCTORAL THESIS

STRUCTURAL HEALTH MONITORING OF CONCRETE STRUCTURES USING DIFFUSE WAVES

Patrik Fröjd

Printed by Media-Tryck, LU, Sweden, 2018.

Abstract

The work presented in this thesis has aimed to investigate and implement techniques for ultrasonic measurements in structural health monitoring applications for civil structures. The focus of the work has been to make these systems practical in real applications, where the large size of the structures, and the changing environments they are exposed to, pose problems for many methods which otherwise fare well in laboratory settings.

There is an increasing demand on the safety and reliability of the civil structures that make up our cities and infrastructure. The field of structural health monitoring aims to provide continuous non-destructive evaluation of such structures. Large concrete structures, such as nuclear power plants or bridges, provide a challenge when implementing such systems. Especially if minor damage is to be detected and even located.
Methods based on propagating mechanical waves are known to be useful for detecting structural changes, due to the coupling between the properties of such waves and the mechanical properties of the material. The sensitivity of such measurements generally increase with higher frequencies, and ultrasonic waves can be used to detect minor cracks and early signs of damage. Unfortunately, concrete is a complex material, with aggregates and reinforcement bars on the same order of size as the wavelengths of ultrasonic waves. Ultrasonic waves are quickly scattered and attenuated, which makes traditional pitch-catch measurements difficult over long distances. However, multiply scattered waves contain much information on the material in the structure, and have been shown to be very sensitive to material changes.

In this project continuous wave excitation has been used when creating the multiply scattered wave fields. This enables narrow-band detection, which is shown to enable the detection of significantly weaker signals, and thus increase the maximum distance between transducers. Techniques for localizing damage using such continuous wave fields, as well as methods for compensating for effects of changing environmental conditions, are demonstrated. Recommendations are also given for future designers of structural health monitoring systems, as to the choice of frequency, when using multiply scattered wave fields.

Sammanfattning

Arbetet som presenteras i denna avhandling har haft som mål att evaluera och implementera tekniker för ultraljudsmätningar inom strukturövervaknings-applikationer. Arbetets fokus har varit att göra sådana system praktiska i verkliga applikationer, där strukturernas storlek, och de varierande omgivningarna de exponeras för, innebär problem för många metoder som annars fungerar bra i laboratoriemiljö.

Det finns ett ökat behov av säkerhet och pålitlighet för de byggnadskonstruktioner som våra städer och infrastrukturer består av. Forskningsfältet strukturövervakning strävar efter kontinuerlig observation av sådana strukturer med icke-förstörande provningsmetoder. Stora betongkonstruktioner, såsom kärnkraftverk eller broar, innebär en stor utmaning när sådana system ska implementeras. Särskilt om även små skador ska kunna detekteras.
Det är känt att metoder som bygger på propagerande mekaniska vågor är användbara för att upptäcka strukturella förändringar, på grund av kopplingen mellan egenskaperna hos sådana vågor och de mekaniska egenskaperna i byggnadsmaterialet. Känsligheten i sådana mätningar ökar generellt för högre frekvenser, och ultraljudsvågor kan användas för att detektera små sprickor och tidiga tecken på skada. Tyvärr är betong ett komplext material, med ballast och armeringsjärn i samma storleksordning som våglängden hos ultraljud. Ultraljudvågor sprids och dämpas snabbt, vilket gör att traditionella mätmetoder blir svåra att använda över längre avstånd. Dock innehåller spridda vågor mycket information om materialet i strukturen, och har visats kunna användas för mätningar som är mycket känsliga för förändringar i materialet.

I detta projekt har kontinuerliga vågor genererats för att skapa vågfält av spridda vågor. Detta möjliggör smalbandsdetektering, vilket visas göra det möjligt att detektera väsentligt mycket svagare signaler, och därmed öka det maximalt möjliga avståndet mellan sändare och mottagare. Tekniker för att lokalisera skada med kontinuerliga vågfält, samt metoder för att kompensera för föränderliga miljövillkor, demonstreras. Rekommendationer ges också för framtida skapare av övervakningssystem, vad gäller val av frekvens, när vågfält ska användas.

Acknowledgements

The work presented in this thesis has been carried out at the division of Engineering Geology at LTH, Lunds Tekniska Högskola, in Lund, Sweden. The work is funded by the Swedish Research Council Formas (Grant number 244-2012-1001).

First of all I want to thank my main supervisor Peter Ulriksen for all his support and guidance over the course of my PhD studies.

I also want to thank my assisting supervisor, Nils Rydén, and all of my colleagues and friends at the department. You have all provided an environment which inspired me, and every time I got stuck on a problem there was somebody to help me.

Thank you, also, to my parents, family and friends for all your support. The biggest thanks, however, goes to my wife Maria and our beloved daughter Malou for all of the support and love you have brought into my life!

List of appended papers

The following papers are included in the thesis. Patrik Fröjd wrote the necessary code and performed all the experiments in the reported studies. He is the main author and has, as such, performed most of the writing and all correspondence with the scientific journals which published the papers.
Papers I and III, and IV in manuscript form, were included in Patrik's Licentiate thesis (Fröjd 2016).

Paper I
"Efficiency of some voice coil transducers in low frequency reciprocal operations"
P. Fröjd and P. Ulriksen
Journal of Acoustical Society of America Express Letters, 137(6), Jun. 2015. Doi: 10.1121/1.4922011.

Paper II
"Frequency selection for coda wave interferometry in concrete structures"
P. Fröjd and P. Ulriksen
Ultrasonics, 80:1-8, Sep. 2017. Doi: 10.1016/j.ultras.2017.04.012.

Paper III
"Amplitude and phase measurement of continuous diffuse fields for structural health monitoring of concrete structures"
P. Fröjd and P. Ulriksen
NDT & E International, 77:35-41, Jan. 2015. Doi: 10.1016/j.ndteint.2015.10.003.

Paper IV
"Continuous wave measurements in a network of transducers for structural health monitoring of a large concrete floor slab"
P. Fröjd and P. Ulriksen
Structural Health Monitoring, 15(4), 2016. Doi: 10.1177/1475921716642139.

Paper V
"Detecting damage events in concrete using diffuse ultrasound structural health monitoring during strong environmental variations"
P. Fröjd and P. Ulriksen
Structural Health Monitoring. First published March 26 2017. Doi: 10.1177/1475921717699878.

Related publications

"Voice-coils as reciprocal transducers in structural health monitoring applications"
P. Fröjd and P. Ulriksen
7th European Workshop on Structural Health Monitoring (EWSHM 2014). Nantes, 8-11 Jul, pp. 457–464.

"A comparison between pulse and continuous guided wave pitch-catch testing of concrete beams"
P. Fröjd and P. Ulriksen
International Symposium Non-Destructive Testing in Civil Engineering (NDTCE 2015). Berlin, 15-17 Sep.

"Amplitude and Phase Measurements of Continuous Diffuse Fields for Structural Health Monitoring of Concrete Structures"
P. Fröjd and P. Ulriksen
Abstracts of ATEM: International Conference on Advanced Technology in Experimental Mechanics: Asian Conference on Experimental Mechanics. Toyohashi, 2015(14), pp. 81.

"Structural health monitoring of large concrete structures"
P. Fröjd
Licentiate thesis, Lund University, Division of Engineering Geology. ISBN: 9789176236611.

"Narrow-band diffuse ultrasonic wave field measurements in a network of reciprocal transducers for monitoring of a large concrete floor slab"
P. Fröjd and P. Ulriksen
8th European Workshop on Structural Health Monitoring (EWSHM 2016). Bilbao, 5-8 Jul.

"The sensitivity of coda wave interferometry in different scattering regimes"
P. Fröjd and P. Ulriksen
8th European Workshop on Structural Health Monitoring (EWSHM 2016). Bilbao, 5-8 Jul.

"Feedback resonance frequency as an SHM indicator (The Larsen effect)"
P. Ulriksen and P. Fröjd
8th European Workshop on Structural Health Monitoring (EWSHM 2016). Bilbao, 5-8 Jul.

Abbreviations

AD	Analogue to digital
AE	Acoustic emission
AMA	Actively modulated amplitude
CC	Correlation coefficient
CWI	Coda wave interferometry
DC	Decorrelation coefficient
DI	Damage index
NDT	Non-destructive testing
NWMS	Nonlinear wave modulation spectroscopy
PZT	Lead zirconate titanate (piezoelectric ceramic)
SHM	Structural health monitoring
SNR	Signal-to-noise ratio

Contents

Part I - Overview of work

1 Introduction

1.1 Nondestructive testing and structural health monitoring

Concrete is the most commonly used building material in the world; twice as much concrete is used as steel, wood, plastics and aluminum combined, in terms of mass. Modern society relies on concrete structures more than ever and the number of new structures, as well as the age of existing ones, are increasing rapidly. This means that there is an increasing demand on the safety, maintenance planning and environmental impact of such structures.
Innumerable people depend on the strength of e.g. bridges and apartment buildings every day, and failure in these can have catastrophic consequences for human lives. Therefore it is vital that owners of such structures continuously investigate their condition and are made aware of sudden changes in the behavior of the structure.
Often, when a significant damage to a structure is discovered, the deterioration has already progressed far and the required reparations are substantial and expensive. Not rarely will the structure be demolished and a new one constructed in its place. This is both costly and has a negative effect on the environment.
Even minor cracks in the concrete can expose the steel reinforcement bars inside to the environment. This will lead to corrosion, which will expand the steel bars and cause further cracking to the concrete. Thus, it is increasingly important to be able to detect very early defects and degradation, before these evolve into more substantial damage. Figure 1 shows a photograph of significant damage to a concrete structure, where a reinforcement bar has corroded.
The most common methods of testing are visual inspections and core sampling. Visual inspections only yield information of the status of the surface of a structure and often only rather far progressed signs of damage can be detected. In core sampling, a piece of concrete is cut from the structure and brought to a laboratory. There, the sample is subjected to tests which yield information on the strength of the concrete. Core sampling yield very detailed information of the material of the sample. However, in such analysis only the material at the sample point is investigated; the applicability of these results to the rest of the structure remain uncertain. Furthermore, such sampling affects the structure, since a piece of the material is removed. Core sampling is thus a *destructive testing* method.

The field of *non-destructive testing*, or NDT, aims to provide information on the condition of the structure in such a way that the testing itself does not affect its health status. Many different methods exist, which make use of different physical phenomena. Examples of techniques include ultrasound, radar, acoustic, electrical and optical measurements. Methods vary in complexity from the very basic, such as an operator knocking on a wall and listening to the sound which is produced, to the

Figure 1. Severely damaged concrete, caused by corrosion of steel reinforcement bars. Original figure by MADe (licensed under CC-BY-SA-3.0)

very advanced, such as when different characteristics of propagating waves in the material are measured, analyzed and compared with computer models. Some methods aim to provide an estimation of material parameters, such as stiffness, while others attempt to create images of the interior of the material.

The benefit of NDT over destructive test methods is evident. However, most NDT methods require an operator on site to perform measurements, and each measurement usually yields information in a limited region in the vicinity of the measurement location. If a large structure is to be tested, many measurements might be required. This usually takes a lot of time and effort, and is thus expensive. Furthermore, each measurement yields information on the status of the structure only at one particular moment in time. This makes it difficult to monitor trends or detect sudden events.
These issues are addressed in *structural health monitoring*, SHM.
In SHM, transducers are permanently installed on, or inside, a structure. These automatically perform non-destructive measurements, without the need for operators on site.
The automated measuring procedure means that much data can be gathered regularly, without increase in personnel cost or effort. The amount and regularity of the measurements enables the monitoring of trends, both short- and long-term, and the detection of sudden events. Another benefit with permanently installed sensors is excellent repeatability; in traditional NDT measurements there is a possibility of human error and there is often significant variability between measurement instances.
In SHM applications, each measurement is always compared, in some regard, to either data from an undamaged structure or from some assumed values/model (Worden et al. 2007). This data is known as the *baseline*. Measurements deviating from this baseline indicates a change in the structure i.e. a possible damage or defect.

NDT and SHM are used not only in concrete structures; almost all industries are interested in the behavior of the materials used, be they metal, wood or plastic. A

notable example is the aerospace industry, where safety is paramount and the most common materials are different metals or composites. From the point-of-view of NDT, civil structures are different from most other applications for two reasons: Firstly, the structures are often very large, with bridges and buildings spanning hundreds of square meters. This makes it difficult to cover the entire structure with testing.
Secondly, concrete is a complex material which consists of cement and aggregates of different sizes randomly distributed in the material. Furthermore most concrete civil structures are reinforced with steel reinforcement bars cast into the concrete in order to increase tensile strength. This heterogeneity makes the material much harder to handle than homogeneous materials, such as steel.

The main goals of structural health monitoring systems are to detect and localize damage. Damage can be defined as changes to a structure's material or geometric properties and/or changes to the boundary conditions of the structure system. In reality all structures and materials have some defects even from the beginning of its life-cycle. Worden and Dulieu-Barton (2004) proposed the following terminology:

- A *defect* is a slight deviation from an ideally pristine material or structure, but not enough to affect its operation.
- A *damage* in a structure means it is still operational but with decreased efficiency or safety.
- A *fault* is when a structure is so damaged it can no longer operate safely or satisfactory.

SHM systems can be classified based on what information they provide about the structure and damage (Rytter 1993):

- Level 1: The method gives a qualitative indication that damage might be present in the structure. (Detection).
- Level 2: The method gives information about the probable location of the damage. (Localization).
- Level 3: The method gives information about the size of the damage. (Assessment).
- Level 4: The method gives information about the actual safety of the structure given a certain damage state. (Consequence).

It should be noted that most SHM applications are limited to level 2 or possibly level 3, according to the above definitions. Methods available for large structures today will not yield very detailed information on the damage. However, for a very large structure it would be of great use to be able to detect a significant deviation from normal conditions in a general region. In such a case operators can move on site and perform measurements with other NDT methods, restricted to the region indicated

by the SHM system. The most realistic procedure is such a combination of SHM and NDT. Furthermore multiple SHM and NDT methods, based on different physical properties of the material, can be combined using data fusion to give a more robust measure of the health status of the structure as described by e.g. Garnier et al. (2014) and Ploix et al. (2009).

1.2 Common SHM techniques

SHM systems make use of different NDT methods that are suitable for automation and permanently installed transducers. Following are some examples of common SHM methods, applicable for concrete structures.

1.2.1 Acoustic emission SHM

When the material in a structure undergoes stress which creates deformations or microscopic cracks, mechanical waves are generated. This is called acoustic emission (AE). If appropriate transducers are placed in contact with the structure these waves can be detected. Since the wave propagation velocity of the material generally is known, the location of the crack can be deduced from the difference in arrival times of different wave types or based on the time of arrival at different sensors.
Analysis of the amplitudes, phases and frequency content of the emitted acoustic signals can give information about different properties of the cracks, such as orientation, size and development of the whole damage process.
These factors make AE a useful method for NDT and SHM. The history, and initial development, of AE is described by Drouillard (1996).
Most methods require several measurements before characterization is possible, but this is generally not a problem as clusters of up to hundreds of acoustic emissions often are recorded in certain regions and locations.
The emitted acoustic signals have high frequencies, between 10 kHz-1 MHz, and are heavily damped in concrete. Because of this, the range of each AE sensor is limited. Acoustic emission is therefore best suited for monitoring crucial locations, such as joints. If very large structures are to be monitored it would require an unpractically large amount of sensors.

1.2.2 Impedance SHM

Impedance based SHM utilize the fact that the electrical impedance of a piezoelectric transducer, placed on a structure, is affected by the mechanical impedance of the surrounding material in the structure. If the structural integrity of the material is compromised, the mechanical impedance will be affected, which will be detectible by measuring the change in electrical impedance of the piezoelectric

transducer. This is the *electromechanical coupling* property of the piezoelectric material.
The sensitivity of this method is frequency dependent; the wavelength of the vibration must be smaller than the characteristic length of the cracks to be detected (Park et al. 2006). However, vibrations with too high frequencies will be heavily damped and thus reducing the effective range. Thus, there is a trade-off in sensitivity and range when deciding the frequency of an impedance based SHM system. Typical frequency ranges are 30-400 kHz. The sensing radius of each transducer can vary significantly depending on the material of the structure; around 0.4 m for composite structures to 2 m for metal beams (Park et al. 2006).
Similar to AE, impedance based SHM systems require a dense network of transducers, which means very many transducers are needed to cover a large concrete structure.

1.2.3 Modal analysis

Modal analysis is a common method for SHM applications. Modal analysis is in itself a wide field with different approaches. They all have in common the fact that it is inherent dynamic properties, modal parameters, of the structure that are measured. The basic modal parameters are natural frequencies, mode shapes and damping, which all depend on the geometry, material and boundary conditions of the structure. The fundamental idea of modal analysis SHM is that the modal parameters are affected by damage to the structure. Comparison between a current measurement and measurements from an undamaged structure can therefore give indications of the current health status of the structure.
Excitation of the structure can be accomplished with different methods, e.g. impact hits or vibrators. It is also possible to utilize the vibrations the structure is naturally subjected to in operational environments, e.g. wind, machinery or traffic.
The most common method for measuring the vibrations is by accelerometers placed in contact with the structure. Contact-less methods exist, e.g. laser vibrometer and radar measurements.
The most basic modal analysis is simply measuring the natural frequencies of the structure, which can shift as the structure is damaged. As these are global properties of the structure, it is generally not possible to localize any damage with only this data. For more detailed information concerning the damage, mode shape analysis and other, more advanced techniques, are required. Modal analysis was already a well-established field before it was utilized in SHM and is thus probably the most developed branch within the field of SHM. Extensive literature reviews exist on the subject, e.g. by Doebling et al. (1996), Carden and Fanning (2004) and Fan and Qiao (2011).

1.2.4 Strain and movement monitoring

Due to external influences, such as humidity and temperature, even a healthy structure will exhibit some movement. This can be monitored using sensors for measuring strain, deflection, inclination, etc.
It is normal to see seasonal patterns in the material strain and movement, as the ambient temperature shifts. However, if the overall trend continue to increase or decrease over long periods of time it can be an indicator of slow degradation of the structure. Deviations in relationships between different measurements, e.g. strain in the concrete and the strain in pre-stressed steel tendons, can be of particular interest. Creep and shrinkage, which is caused by drying of the concrete and chemical processes, can also be monitored with these types of measurements.
These types of monitoring systems benefit from combined measurements of a wide array of parameters, including environmental conditions, such as temperature. Examples of such systems can be found in the works presented by Hu et al. (2017) and Sousa et al. (2011), both of which describe monitoring of a large variety of parameters in different long-spanned pre-stressed concrete bridges.
These measurements provide information on the general behavior of the structure at large, and are useful for monitoring trends. Additional information can be deduced by updating and tuning finite element models of the structure using these sort of measurements, as reported by e.g. Sousa et al. (2013).

1.2.5 Bridge weigh-in-motion

The main purpose of bridge weigh-in-motion (BWIM) systems is to measure the loading on a bridge caused by traffic. A few transducers, normally strain gauges, measure the response of the bridge material as vehicles drive across, and the BWIM system can estimate the characteristics of the loads. Knowing what loads a bridge is subjected to is crucial when planning maintenance and predicting remaining life of bridges. The information provided by a BWIM system can also be used to detect changes in bridge behavior, possibly caused by damage, as reported by e.g. Gonzalez and Karoumi (2015). An overview of recent developments in BWIM is presented by Lydon et al. (2016).

1.2.6 Propagating wave SHM

Methods based on acoustic and ultrasonic waves have been successfully implemented in NDT and SHM systems and applied on concrete structures. A large variety of techniques can be used for measuring different properties of the material. I refer to e.g. the review by McCann and Forde (2001) and the work presented by Garnier et al. (2013) and Wiggenhauser and Niederleithinger (2013) for overlooks of the field.

The behavior of propagating waves vary greatly with the ratio between the wavelength and the geometry of the propagation medium. If the wavelength is significantly smaller than the geometry, the waves will propagate in any direction in the 3D volume. This is typical for ultrasonic waves in large structures. If the wavelength is larger than, or of the same order as, some dimension of the geometry, the waves will be guided by the boundaries of the structure. These are then called *guided waves*.

Propagating wave SHM make use of acoustic or ultrasonic waves transmitted between two, or more, transducers. The basic principle is that defects in the material will affect the propagating wave, which can be seen in the acquired signal. Guided wave and ultrasonic systems have been implemented in NDT and SHM and have been shown to provide both high sensitivity to damage and large range. There are many different methods for generating and analyzing waves, but it is not trivial to implement for SHM in very large concrete structures, such as nuclear power plants. The attenuation of mechanical waves in concrete is significant and varies greatly depending on the composition of the material and of the frequency of the signal. Examples of reported attenuations are ~7-20 dB/m for 19.7 kHz signals (Abdullah & Sichani 2008), 25-75 dB/m for 100-200 kHz signals (Deroo 2009) and 134 dB/m for 150 kHz signals (Garnier et al. 2013). The high attenuation means that the amplitude of transmitted high frequency signals in a concrete structure quickly decreases with distance.

1.3 Aim

The field of SHM is still relatively new, and owners of civil structures have yet to accept and embrace the possibilities. This is largely due to the fact that systems which have been demonstrated to function very well in laboratory environments encounter a range of issues when deployed in a real scenario. These issues include:

- The large size of most civil structures means that systems which are capable of detecting early signs of damage require dense networks of transducers if the entire structure is to be monitored. This is both expensive and impractical.
- Civil structures are subjected to a wide range of environmental variations, such as variations in temperature, humidity, traffic, etc. All types of measurements are affected by some of these variations, and this can mask the effects of damage or give rise to false alarms.
- There is a general lack of standards and regulations for the design of propagating wave SHM systems. A set of recommendations would serve well as guidance for both investors and designers. Of importance here are also clarifications as to what the systems can and cannot detect, so that expectations are kept at a realistic level.

The aim of the research presented in this thesis is to address these issues, and help push the state of the field in a direction where it is practical and applicable in real civil structures.

1.4 Significance of research

The purpose with this research is to make propagating wave SHM more attractive to investors and owners of structures, by presenting tools and guidelines for addressing the issues listed above. New techniques have been developed and evaluated, which show potential for practical health monitoring of civil structures.

1.5 Limitations

The results presented herein are based on work done on various concrete samples in laboratory settings. Although attempts have been made to scale up the experimental setups compared to those often presented in similar work, it should be noted that these studies should be repeated on even larger samples and real structures under ambient conditions. The time-frames for the induced damages to the concrete specimens have been short. Many realistic damage scenarios include material deterioration over several years. Such slowly developing damage has not been included in this work.

1.6 Summary of appended papers

1.6.1 Paper I

The aim of the first paper was to investigate the use of voice coil transducers as reciprocal transmitters and receivers of acoustic signals. The motivation for this was the fact that such transducers often are constructed for use in low frequency ranges, which have potential to be useful in concrete SHM applications where attenuation of high frequency signals is a major issue. It was speculated that voice coil transducers could be a more efficient alternative to piezo electric transducers in very low frequency regions.
The experiments showed that voice coil transducers could indeed function as reciprocal transmitters and receivers of acoustic waves. In particular geophones, which are common voice coil transducers used in seismic measurements, were found to be efficient. The geophone was more efficient in reciprocal transmission than the PZT disc included in the study for frequencies up to ~3.5 kHz, while also being more resilient to electromagnetic coupling.

1.6.5 Paper II

There is a general lack of guidelines for designing SHM system based on diffuse ultrasound, such as coda waves. Often the choice of frequency is left uncommented in published articles discussing coda wave interferometry. The aim of this paper is to provide some guidance as to the choice of frequency of the signals, and how this influences the types of damage which can be expected to be found. In general, higher frequency signals are more sensitive to smaller cracks than lower frequency signals, but are also significantly more attenuated.
Different types of damage, with different sizes, was inflicted on concrete samples in a controlled manner. The sensitivity of coda wave interferometry measurements to these damages, using signals with widely different central frequencies, were compared. It was found that relatively low frequency signals, in the range 50-150 kHz, could be used to detect the appearance of holes which were smaller than the aggregates in the concrete, corresponding to less than 1/10 of the wavelength of the ultrasound. These signals could also be used to detect developing microcracks, due to bending, with a sensitivity not far from higher frequency signals (~500 kHz). It was concluded that, for many SHM applications, the superior possible transmission length of these relatively low frequency transmissions should outweigh the increased sensitivity of higher frequency signals

1.6.2 Paper III

For very large concrete structures the strong attenuation of high frequency waves is an issue; the signals will be obscured by noise after a certain propagation distance. By transmitting a continuous sinusoidal signal, high energy is put into the structure, focused in one specific frequency. Such a continuous wave signal can be detected with a lock-in amplifier, which is known to accurately measure amplitude and phase even if the signal is well below the noise floor. This gives the potential to transmit mechanical waves relatively far, even in concrete.
Both transient coda wave measurements and continuous wave measurements, with similar frequency, were applied on a concrete specimen which was subjected to cyclically increased loading. It was shown that the continuous wave field measurements tracked the progressing damage with very similar sensitivity as the transient measurements.
Furthermore, it was also shown that the transient measurements lost correlation to damage level when the signal level was decreased to the same order as the noise, even after filtering and averaging. The continuous wave field measurements maintained the sensitivity to damage even when the noise level was 100 times (40 dB) greater than the signal level. Continuous wave transmissions thus show great potential to be used with large transducer spacing, with sensitivity to damage comparable with transient coda wave interferometry.

1.6.3 Paper IV

The results from the study presented in Paper III indicated that transmitting a continuous wave and measuring the amplitude and phase of the resulting diffuse wave field can be used to detect damage over relatively long distances. The aims of Paper IV were to implement the measurement technique on a larger structure, in order to verify that a large transmission range can be yielded, and to investigate whether damage could be localized using a network of reciprocal transducers.
An 8 x 2 m concrete floor slab was instrumented with a network of 30 transducers, and local damage was induced with impact hits. It was shown that 50 kHz continuous wave transmissions could successfully be sampled and the damage could be detected in the signal, as deviations from the baseline. Furthermore, by implementing a tomographic procedure, the probable location of the damage could be roughly established.

1.6.4 Paper V

Variations in the environmental conditions, such as temperature, is known to greatly influence all SHM measurements. This is particularly problematic for diffuse ultrasound measurements; though these types of measurements are well documented to be very sensitive to damage in the monitored material, they are also extremely sensitive to environmental variations. This manifests as noise, which can mask the influence of damage or falsely indicate damage when none is existent.
In this paper, a similar continuous, diffuse wave field SHM system as used in paper IV was used to monitor a large concrete floor slab over a couple of weeks, while subjected to significant environmental variations.
Mahalanobis distance was used as a tool for teaching the SHM system to differentiate between fluctuations in the data caused by normal environmental variations and the effects of damage in the structure.
It was shown that the machine learning process could be used to enable damage detection and localization in the structure, whereas otherwise the effects of the damage was completely masked by the noise caused by the environmental variations.

2 Guided wave and ultrasonic SHM

This chapter discusses different aspects of SHM based on propagating mechanical waves, since the work in this thesis is based on these phenomena. Some fundamental properties are discussed, and how these relate to NDT and SHM. The chapter serves as background and motivations for the choices made in this research. The final section of the chapter summarizes the identified issues which are addressed in appended papers I, II, III and IV.

2.1 Mechanical wave propagation

There are two fundamental types of waves that propagate in an infinite medium; P-waves, or compression waves, are body waves which cause particle displacement parallel to the direction of propagation. S-waves, or shear waves, cause particle displacement perpendicular to the wave propagation. Figure 2 illustrates the displacement of particles in P-waves and S-waves respectively.
P-waves have the highest wave propagation velocities (hence the name P-wave which is short for primary wave). S-wave, or secondary wave, propagation velocity is approximately half that of P-waves.

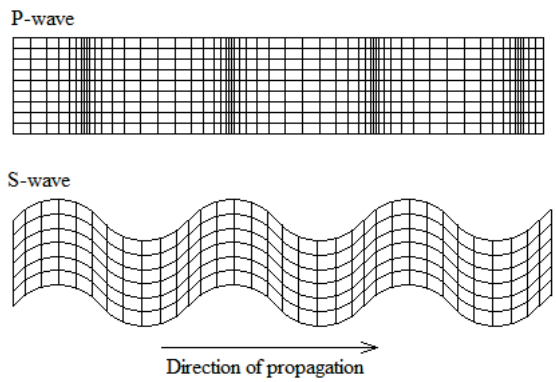

Figure 2. Illustration of the particle displacement in P-waves and S-waves.

In infinite bodies only these two types of waves exist, but in real bodies there are boundaries, either between layers of different materials or at the edge of the body itself. At these boundaries, given the boundary conditions, P- and S-waves interact to form new types of waves that are guided along the boundary. These are called guided waves. Guided waves which propagate along the surface of the structure are called surface waves. The theory behind these interactions was first presented by Rayleigh (1885) and Lamb (1917).

Rayleigh waves are surface waves that propagate along a single surface of a solid. They have components of motion both parallel to the direction of propagation and normal to the surface, and propagate at a velocity slightly less than S-waves. The depth of the influence of the Rayleigh wave is approximately one wavelength (Graff 1975). One notable characteristic of a Rayleigh wave is that it is attenuated with $\frac{1}{\sqrt{r}}$, where r is radial distance from the source, which is more slowly than body waves, which are attenuated with $\frac{1}{r}$ (Richart et al. 1970). This makes them suitable for applications where long distances are desired between source and receiver.

If the geometry of a structure is such that it has two surfaces close and parallel to each other, as in a plate, the two boundaries form special types of waves, called Lamb waves. Two families of Lamb waves can propagate in a plate; one family which displaces particles symmetrically about the midplane of the plate (S-mode) and one family which displaces them anti-symmetrically about the midplane (A-mode). For low frequencies (when the wavelength is large compared to the plate thickness) only one wave of each family exist. These are the zero-order modes, S_0 and A_0. As the frequency increases, higher-order modes come into existence which can be thought of to be oscillating around modal planes in the plate.
Lamb waves are often visualized in dispersion plots, where phase- or group velocity is plotted against the product of frequency and plate thickness. Numerically calculated, or experimentally measured, such plots show that at low frequency-thickness products indeed only the zero-order modes exist. As the frequency increases, both the phase- and group velocities of S_0 and A_0 converge towards the Rayleigh velocity and those of the higher order modes converge towards the shear wave velocity.
Guided waves consist of a mixture of these types of modes and are complex and difficult to analyze separately. However, knowledge of the material properties in regard to the different modes can lead to increasingly sensitive measurement methods in NDT and SHM.
One approach is to construct the hardware and software of the measurement instruments in such a way that one or two simple modes are enhanced while others are suppressed. This can make the signals much less difficult to analyze, while preserving the sensitivity to damage. This is called *tuning*.
Surface waves, and Lamb waves in particular, are widely used in NDT applications.

2.2 Measurement parameters

Within wave propagation-based SHM applications there exist many different measurement parameters that can be used as indicators of damage. The most basic parameters are accounted for here.

2.2.1 Velocity

Pulse velocity is defined as the speed at which a pulse signal propagates through a material. The common way to measure this is by measuring the time-of-arrival of a pulse at a transducer. Since the location of the transmitter and the time of transmission is known it is a simple task to calculate the velocity. Cracking of the concrete can lead to changed material properties which can decrease the speed of a pulse. However, it has been shown that wave propagation speed is rather insensitive to early damage processes in concrete, being unchanged up to about 80% of the compressive capacity of the concrete (Kamada et al. 1997). The wave propagation velocity in concrete depends on the type of mortar and aggregates, but a rough estimate is a P-wave velocity of 4000-5000 m/s and an S-wave velocity of 2000-2500 m/s.
As further detailed in section 2.3, the coda wave interferometry stretching method measures the velocity difference for many scattered wave paths rather than just the direct one. This heightens the sensitivity since more of the damaged material is passed by the waves.

2.2.2 Attenuation

Signal attenuation measurements are based on the fact that mechanical waves are more strongly attenuated in a damaged material than in a pristine one. By comparing the strength, or energy content, of a signal between a current measurement and one from an undamaged structure one can acquire an indication of possible damage. Attenuation measurements are regarded to be more sensitive to damage than pulse velocity but is strongly dependent on coupling factors for reliability (Daponte et al. 1995; Van Hauwaert et al. 1998). This is less of an issue for SHM than for NDT due to transducers being permanently fixed on the structure in SHM, which gives good repeatability. Several articles describe methods where attenuation is successfully used as damage indicator in concrete, and I refer to work by e.g. Song et al. (2007), Liao et al. (2011) and Moradi-Marani et al. (2014).

2.2.3 Nonlinearity

Velocity and attenuation measurements are both based on linear properties of the material in the structure. Cracking in materials like concrete give rise to nonlinear effects on a propagating wave. The simplest way to envision this effect is to consider a single, smooth microcrack. The compressive and tensile components of a wave passing through the crack will alternatively compress and decompress the interfaces. During the compression phase the two sides will be in contact while in the tensile phase the interfaces will be pulled apart (Richardson 1979). This is commonly referred to as *breathing* cracks. In reality cracks will not be smooth and

will appear in clusters which forms complex properties. The resulting nonlinearity is thus dependent on the amount of microcracks in the material.
Nonlinearity will affect a propagating wave in that it will shift its spectral energy away from the fundamental frequency of the original wave. This can be seen by the appearance of sub- and superharmonics, as presented by Thompson (1977). Measuring the amplitude ratio between the fundamental frequency and e.g. the second harmonic gives an indication of the nonlinearity, and therefore the damage state, of the material, see work by e.g. Zhou et al. (2013).
It should be noted that concrete is inherently nonlinear even in a relatively undamaged state, being a highly heterogeneous material with varying bonding stiffness between the surfaces of the materials. Operators should also beware of nonlinearities in transducers, measurement instruments and in the coupling between transducer and structure (Worden et al. 2007; Brotherhood et al. 2003).
Another way of detecting nonlinearity in a material is to measure the dependence on resonant frequencies to strain amplitudes. An increase in signal amplitude increase the opening and closing of cracks and thus increase the nonlinear properties of the material. By sweeping the amplitude it is possible to detect a drift in the natural frequencies of the structure. This drift is then a measure of the nonlinearity of the material.

In the method known as nonlinear wave modulation spectroscopy (NWMS) a secondary stress wave, with lower frequency than the measurement signal, is introduced to the structure. This lower frequency oscillation will cause the existing cracks in the structure to open and close periodically and thus modulate the measurement signal. The result is a shift in spectral energy towards frequencies corresponding to the original frequency plus/minus the secondary oscillation frequency. An analytical model of this phenomenon is presented by Warnemuende and Wu (2004; 2005).
Warnemuende and Wu (2000; 2004) concluded that nonlinear-based damage indicators are more sensitive than the linear-based ones presented above. It was also shown that NWMS, there also referred to as AMA (actively modulated acoustic) approach, was much more sensitive to damage than “passive” nonlinearity measurements, i.e. merely measuring harmonics.
AMA can successfully be combined with other nonlinearity measurement techniques in order to increase sensitivity, e.g. coda wave interferometry (Y. Zhang et al. 2013; Hilloulin et al. 2014).

2.2.4 Damage index and measurement features

As stated earlier, SHM systems always compare each measurement to baseline measurements, acquired when the structure was in a known condition. Since the measured data can take on different forms, depending on the nature of the measurement parameters, it is often converted to a generic Damage Index, or

Damage Indicator (sometimes abbreviated as “DI”). This damage index then describes the deviation of the current measurements from the normal conditions. It is often weighted to range between 0 and 1, or is expressed in some statistical manner depending on the variation of the baseline data set.

2.3 Diffuse wave propagation

2.3.1 Wave scattering

Mechanical waves do not simply propagate in a straight line between a source and a receiver; they scatter on boundaries and on heterogeneities in the material. The first signal to arrive to a point is the wave travelling in a direct path from the source. These direct waves are sometimes called *ballistic waves*. The rest of the signal is a mixture of all the scattered energy that has travelled in indirect paths. These latter parts, of an emitted signal, that are measured at a specific location, are called coda waves (Aki 1956), or diffuse waves.
Scattering is more prominent in heterogeneous materials, such as concrete, than in homogeneous materials, such as metals. Concrete is therefore more problematic for traditional ultrasonic measurements, as transmitted short pulses quickly become convoluted, and attenuated, from the scattering.
The nature of the scattering in a material depends on the ratio between the typical size of the heterogeneities and the wavelength. Planés and Larose proposed the following naming conventions for four different scattering regimes and how they apply to concrete (Planès & Larose 2013). The transitions between regimes are smooth and depends greatly on the typical size of the aggregates used in the concrete mix.

- *The Stationary wave regime*, for frequencies below 10-20 kHz, is mostly associated with modal analysis. In this regime the wavelength is on the same order of length as the structure as a whole, and thus much larger than the aggregates in the concrete. The interaction between the waves and the aggregates is mostly negligible. The signals can, however, reverberate in the structure, due to reflections in boundaries. This will lead to diffuse wave fields and create codas in a measured signal.
- *The simple scattering regime*, for frequencies between the stationary wave regime and up to approximately 100-150 kHz, is the range commonly used for traditional ultrasonic investigation of concrete. The regime is defined by the wavelengths being shorter than the size of the structure, but longer than the size of the aggregates and reinforcement bars in the concrete. The waves interact weakly with the heterogeneities, and the codas in this regime thus often consist of a mix of scatterings and reflections in boundaries.

- *The multiple scattering regime*, for frequencies between the simple scattering regime and up to approximately 1 MHz, is the range where the wavelengths of the ultrasound is shorter than the general size of the aggregates. In this regime the waves are strongly affected by the heterogeneity and the direct/coherent wave is strongly attenuated. Measured signals then mostly consists of a coda, created by multiple scatterings. Most publicized work on CWI in concrete operate in this regime.
- *The attenuation regime*, for frequencies above 1 MHz, is the range where the ultrasound is so strongly attenuated, from both scattering and intrinsic absorption, that applications involving anything other than very small test objects in laboratories are infeasible. Applications with signals in this frequency regime thus have little use in practice, and is mostly neglected in SHM applications.

Two properties which are useful for describing the scattering behavior for a given material, at a given signal frequency, are the *scattering mean free path*, ℓ, which is defined as the average distance between two scattering events, and the *transport mean free path*, ℓ^*, which is the average travel distance after which the direction of propagation for each wave packet is completely randomized. For isotropic scattering, i.e. if the angle of reflection for each scattering event is completely random, then $\ell = \ell^*$. If the scatterings are anisotropic, then $\ell < \ell^*$, since more than one scattering event is required to completely randomize the direction. Alternatively, one can instead use the *scattering mean free time* and *transport mean free time* which correspond to the time between two scattering events and time after the wave direction is randomized, respectively.
At each scattering event there is a chance of mode conversion, i.e. the conversion of a P-wave into an S-wave or vice versa. For diffuse wave fields, i.e. after many scatterings, a steady-state in the ratio between P-wave energy and S-wave energy is obtained. This ratio depends on the velocities of the respective wave modes as (Weaver 1982; Snieder 2002):

$$\left(\frac{E_P}{E_S}\right) = \frac{1}{2}\left(\frac{v_s}{v_p}\right)^3 \qquad \textit{Eq. 1}$$

Where E_P and E_S are P-wave and S-wave energies respectively, and v_s and v_p are P-wave and S-wave velocities respectively.
For concrete, assuming a P-wave velocity of 4500 m/s and an S-wave velocity of 2600 m/s, the ratio is ~0.096. This means that the wave energy in diffuse wave fields in concrete is dominated by S-waves.

2.3.2 Intensity models

Individual scattered waves are generally not possible to accurately predict or model with any detail. Instead different models can be employed to describe the overall propagation of intensity of the mechanical energy in the material. This can be thought of as modeling the envelopes of the waveforms, in time and space.

The most basic, commonly used, intensity model is the *diffusion* model. If several scattering events have occurred, then the time evolution of the intensity is expected to behave as a diffusion process, and thus described by the diffusion equation:

$$\frac{\partial P(\mathbf{r},t)}{\partial t} - D\Delta P(\mathbf{r},t) + \sigma P(\mathbf{r},t) = S(\mathbf{r},t)\ \forall \mathbf{r} \in \Omega \qquad \textit{Eq. 2}$$

$P(\mathbf{r},t)$ is the intensity of the mechanical energy at point **r** and time t, D is the diffusivity, which describes the rate at which the diffusion covers an area, σ is the dissipation rate. Both D and σ depend on frequency. $S(\mathbf{r},t)$ is the intensity of the source. Ω denotes the body of material in which the energy propagates and Δ is the Laplacian operator.

If the material can be assumed to be an infinite body the solution to the diffusion equation is given by:

$$P(\mathbf{r},t) = \frac{P_0}{(4D\pi t)^{\frac{d}{2}}} \cdot e^{\frac{-r^2}{4Dt}} \cdot e^{-\sigma t} \qquad \textit{Eq. 3}$$

Where P_0 is the amplitude of the source pulse, r is the distance between the source and point **r**, and d is the dimensionality (e.g. 2 for 2D models). Here can clearly be seen that σ describes an exponential decay of the diffuse wave field.
It is possible to estimate solutions to the diffusion equation for finite structures, which is necessary in applications where the size and geometry of the structure is such that boundary reflections can be expected to contribute to the measured result. A solution for the diffusion equation in a 3D cuboid, with sides a, b and c can be found using Fourier series (Hill & Dewynne 1987; Deroo et al. 2010; Ramamoorthy et al. 2004):

$$\begin{aligned} P(x,y,z,t) = P_0 e^{-\sigma t}\{1 &+ [g(x,x_0,a)g(y,y_0,b)g(z,z_0,c)] \\ &+ [g(x,x_0,a) + g(y,y_0,b) + g(z,z_0,c)] \\ &+ [g(x,x_0,a)g(y,y_0,b) \\ &+ g(x,x_0,a)g(z,z_0,c) \\ &+ g(y,y_0,b)g(z,z_0,c)]\} \end{aligned} \qquad \textit{Eq. 4}$$

where

$$g(x, x_0, a) = 2\sum_{m=1}^{\infty} \cos\left(\frac{m\pi x}{a}\right) \cos\left(\frac{m\pi x_0}{a}\right) e^{-D\left(\frac{m\pi}{a}\right)^2 t} \qquad \textit{Eq. 5}$$

Here, a pulse excitation is assumed in the point (x_0, y_0, z_0) and no flux outward from the boundaries.

If a diffuse, time-domain waveform is measured at a specific location, and the location and amplitude of the source is known, it is thus possible to fit the solution to the diffusion equation to the envelope of the waveform. This yields values of the diffusivity and dissipation for the material. Figure 3 shows an example of a measured 50 kHz waveform, together with a solution of the diffusion equation, which have been fitted to the envelope of the coda.

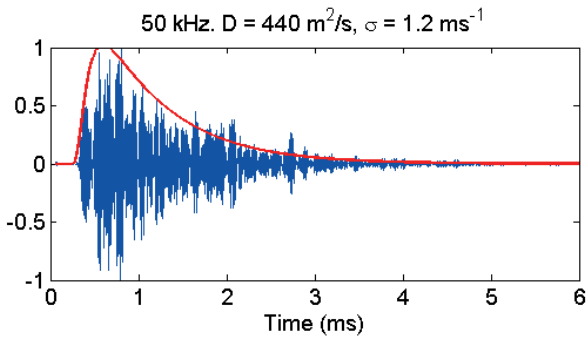

Figure 3. Example of a 50 kHz waveform with coda, and a fitted solution of the diffusion equation. In this example, the diffusivity was estimated to 440 m^2/s and the dissipation to 1200 s^{-1}. Image from Fröjd and Ulriksen (2017).

The diffusivity is known to be decreased by developing microcracks in concrete, while the dissipation is only minimally influenced, as shown e.g. by Deroo et al. (2010). Diffusion models have also been used to determine the depth of cracks in concrete, e.g. by Ramamoorthy et al. (2004).

From the estimated value of the diffusivity it is possible to also estimate the transport mean free path, as shown by Sheng (1995), by:

$$\ell^* = \frac{dD}{v_e} \qquad \textit{Eq. 6}$$

Where the average velocity of the transport of energy, v_e, could be thought of as the velocity of the envelope, and d is the dimensionality.

The diffusion model assumes completely random propagation, which is not accurate for wave packets which have traveled less than a transport mean free path (or reciprocally, have travelled for less than a transport mean free time). An alternative is to use the *radiative transfer* intensity model. This model also takes into account the coherent wave between transmitter and defect (and between defect and receiver), and is therefore more accurate for waves which are not yet completely randomized. The model is based on the Boltzmann equation (Chandrasekhar 1960; Ishimaru 1978):

$$\frac{1}{v_e}\cdot\frac{\partial}{\partial t}P(\mathbf{r},t,\hat{s})+\hat{s}\cdot\nabla P(\mathbf{r},t,\hat{s})+\left(\ell^{-1}+\ell_a^{-1}\right)P(\mathbf{r},t,\hat{s}) = \frac{1}{\ell}\int\frac{1}{\Omega_d}\cdot P(\mathbf{r},t,\hat{s}')d\hat{s}'+\frac{1}{v_e}S(\mathbf{r},t,\hat{s}) \qquad \textit{Eq. 7}$$

Where $P(\mathbf{r},t,\hat{s})$ is the intensity of the mechanical waves at the point **r**, time t, and in the direction $\hat{s}$. ℓ is the scattering mean free path, ℓ_a is the absorption length and S is the source term. Ω_d is the surface area of the unit sphere in d-dimensional space.

For rigorous solution of the equation, the reader is referred to Paasschens (1997). The 2D average intensity model, assuming isotropic scattering and disregarding absorption, is given by:

$$P(\mathbf{r},t)=\frac{1}{2\pi r}e^{\frac{-v_e t}{\ell}}\delta(v_e t-r)+\frac{e^{\frac{1}{\ell}\left(\sqrt{v_e{}^2t^2-r^2}-v_e t\right)}}{2\pi\ell v_e t\cdot\sqrt{1-r^2/v_e{}^2t^2}}\Theta(v_e t-r) \qquad \textit{Eq. 8}$$

Where δ is Dirac's delta function, Θ is the Heaviside function and r is the distance between the source and point **r**. The first term on the right-hand side is the contribution of the coherent wave, which can be seen to decay exponentially with time. At very long propagation times the radiative transfer solution approach the diffusion model solution.

2.3.2 Coda wave interferometry

The coda in a measured signal, while easily mistaken for random noise, is actually highly repeatable, and the full waveform contains much information which can be used to detect minute changes in the propagating material. In c*oda wave interferometry* (CWI) the coda of a measured waveform is compared to that of a baseline measurement from the exact same location. CWI has been shown to be a sensitive method for detecting damage in different materials. The sensitivity of coda waves can be explained by the fact that the measured signal is composed of waves that have propagated in the damaged material for longer periods of time, and has thus been more affected than ballistic waves.

Different techniques are described in the literature for using coda waves to detect change in a material before and after a possible damage event.

2.3.2.1 Decorrelation

One basic method for evaluating codas is to calculate the decorrelation between the baseline waveform and the current measurement, in a certain time-window:

$$DC = 1 - \frac{\int_{t_1}^{t_2} \varphi^0(t) \cdot \varphi(t) dt}{\sqrt{\int_{t_1}^{t_2} \varphi^0(t)^2 dt \cdot \int_{t_1}^{t_2} \varphi(t)^2 dt}} \quad \textit{Eq. 9}$$

Here, φ^0 is the baseline waveform and φ is the current waveform. The time window is given by the interval $[t_1, t_2]$. Generally, the decorrelation increases for later time windows, as the waves have spent more time in the material. This method does not differentiate between time-dilation and convolution of the waveform, and is therefore not suitable for distinguish between global velocity changes and changes in local scattering behavior.

2.3.2.2 Stretching method

An alternate technique is called the *stretching method* (Lobkis & Weaver 2003; Hadziioannou et al. 2009). Here the reference coda signal is interpolated at times $t(1+\alpha)$ with various values of α. This corresponds to a stretching or compressing of the reference signal which is then compared to the measurement signal from the possibly damaged structure by computing the correlation coefficient:

$$CC(\alpha_i) = \frac{\int_{t_1}^{t_2} \varphi^0\big(t(1+\alpha_i)\big)\varphi(t) dt}{\sqrt{\int_{t_1}^{t_2} \varphi^0\big(t(1+\alpha_i)\big)^2 dt \int_{t_1}^{t_2} \varphi(t)^2 dt}} \quad \textit{Eq. 10}$$

Where φ^0 and φ are the reference signal and the signal from the damaged structure respectively. α_i are different stretching factors. The α that maximizes the correlation coefficient is equal to the relative modification of the propagation velocity.

Alternatively, decorrelation coefficient (DC) can be used instead of correlation coefficient (CC), where

$$DC = 1 - CC \quad \textit{Eq. 11}$$

CWI, using the stretching method, have been shown to be able to track different changes to concrete specimens, including cracks (Deroo et al. 2010; Planès & Larose 2013; Schurr et al. 2011), thermal damage (Schurr et al. 2011) and stress (Zhang et al. 2011; Zhang et al. 2016; Shokouhi et al. 2010; Niederleithinger 2014). In these

works it is shown that CWI is sensitive to variations in temperature and some compensation techniques are proposed.
It is also shown that the choice of time window parameters, t_1 and t_2, are vital for the analysis; using late parts of the Coda will result in a higher sensitivity, since this part of the signal corresponds to the waves which have been reflected and scattered the most times.

2.3.2.3 Nonlinear CWI

When CWI is used to track stress in concrete the acoustoelastic effect is used. The acoustoelastic effect is a nonlinear phenomenon which describes how the velocities of propagating mechanical waves are affected by the stress fields of the material (Zhang et al. 2012; Lillamand et al. 2010; Planès and Larose 2013; Abraham et al. 2014). Measuring nonlinear effects has been shown to yield higher sensitivity than linear effects. Analogous to the nonlinear wave modulation spectroscopy described in section 2.2.3, CWI has been used in conjunction with low frequency modulation, in order to increase nonlinear effects (Y. Zhang et al. 2013; Hilloulin, Zhang, Abraham, Loukili, et al. 2014). Low frequency, high energy acoustic "pump" signals are input to the structure while coda wave analysis is performed with a high frequency "probe" signal. The pump signal will open and close microscopic cracks in the concrete resulting in a larger relative velocity change of the high frequency probe signal.
Using different amplitudes of the pump signal and investigating the effect on the high frequency signal gives a measure of the nonlinear behavior of the material.

2.3.2.4 Localization with CWI

One advantage of diffuse wave measurements is that not only the material located in a direct line between transmitting and receiving transducers is probed; the multiple scattered waves traverse a wider region of the material, and volumes of the structure which are hard to reach using ballistic waves can be probed. Figure 4 provides an illustration of this. It means that CWI could fill the gap between the global, but insensitive, modal analysis methods and local, detailed NDT point measurements. This is a very promising prospect for SHM applications.

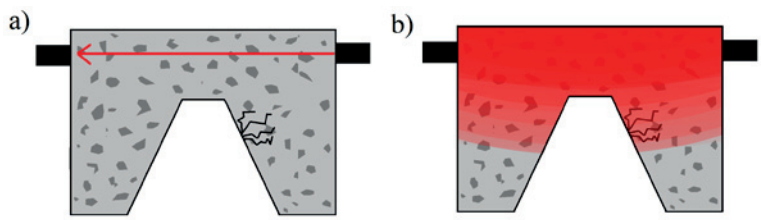

Figure 4. Illustration of probed region. a) Ballistic waves probe the material directly between transducers. b) Diffuse wave fields probe a wider region between transducers.

This advantage also makes localizing a damaged region more problematic; the probed region for ballistic waves, i.e. a straight line between the transducers, is known, and simple tomographic procedures can be employed.

For diffuse wave fields, models of the propagation of energy can be used to construct sensitivity kernels (Pacheco and Snieder 2005; Obermann et al. 2013). These are maps that show the density of waves around each point in space and time, following the transmission from a transmitting to a receiving transducer. Figure 5 shows an example of a sensitivity kernel, constructed using the diffusion model. It can be seen that the sensitivity of CWI is highest close to either transmitting or receiving transducer, and in a region in between them.

By acquiring waveforms from several different transducer-receiver pairs and evaluating the shift in the codas at a set of different times, it is possible to fit this data to the sensitivity kernels, and find the likely location of damage through an inversion procedure. A notable such algorithm is the Locadiff algorithm, developed by Planès, Larose and Rossetto (Planès et al. 2013; Rossetto et al. 2011).

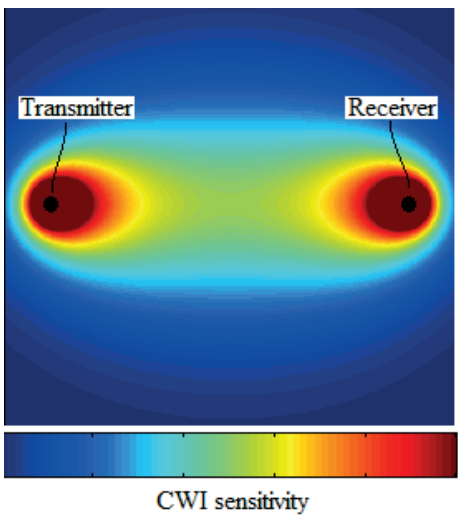

Figure 5. Sensitivity kernel based on the diffusion energy transfer model. The width of the high sensitivity region is on the same scale as the transport mean free path

This procedure is significantly improved if the sensitivity kernels are constructed from solutions of the radiative transfer model, instead of the diffusion model, since these also take into account the coherent wave between transmitter and defect (and between defect and receiver). This is necessary in order to accurately localize damage close to either transducer, i.e. within one or a few mean free paths (Planès et al. 2014).

Mayor et. al. (2014) and Margerin et. al. (2016) have shown that the sensitivity kernels appear different depending on whether the defects influence the absorption or scattering properties of the material. In the case of scattering, the kernels are more complex, with alternating signs of the sensitivity. Overall, however, they showed that absorption affects codas more than scattering.

An alternative to the kernels based on analytical models of the propagation of intensity is to use numerically generated kernels. These can be used to construct kernels with very complex evolution in space and time, which is realistic in a structure which cannot be accurately approximated with isotropic scattering (Kanu and Snieder 2015; Kanu and Snieder 2012).

2.4 Transducers and signals

2.4.1 Transducers

2.4.1.1 Piezoelectric transducers

In an application where a mechanical wave is to be generated by one transducer and received by another, it is convenient, from both a practical and economical point-of-view, if the same type of transducer can be used as both actuator and receiver. This is one of the reasons why piezoelectric transducers have become popular. Piezoelectric materials generate an electric potential over its poles if subjected to a strain. Conversely, if an electric potential is applied over the poles the piezoelectric material will generate a strain. This makes the material ideal for constructing transducers which are reciprocal actuators and receivers.
The most common piezoelectric material used as transducers in SHM application is lead zirconate titanate (PZT), which is a ceramic material.

Piezo electric transducers can be embedded into the concrete as the structure is created, yielding excellent connection to the material and protection from physical damage. PZT discs are be brittle, and can be damaged during the construction, but it has been shown that first encasing the PZT in mortar provides good protection for the transducers (Song et al. 2007; Gu et al. 2006; Song et al. 2008). Some transducers are particularly developed for embedment in concrete and are suitable for SHM applications, e.g. those reported on by Niederleithinger et. al. (2015).

2.4.1.2 Voice coil transducers

An alternate type of transducers, to PZTs, for measuring vibrations are voice coil transducers, which are electromagnetic transducers. One notable example is the geophone which is a type of transducer very commonly used as receivers in seismic geological measurements. These are based on the principle of a spring-mounted coil that moves within a magnetic field. Due to its own inertia, the coil remains stationary while the case moves with ambient vibrations or vice versa. The coils' relative motion through the magnetic field generates a voltage proportional to the velocity. Thus the transducer measures velocity of the vibration, as opposed to accelerometers which measure acceleration.
Voice coils can also be used as actuators, by applying an electric signal over the poles. This will cause the coil to move within the magnetic field with a velocity proportional to the applied voltage. There exist several types of such commercial

actuators with different designations, such as inertial force actuators and electrodynamic exciters. These are used as vibrators or for vibration control. Figure 6 shows a sketch of a typical voice coil transducer.

Though there are many commercial transducers for either reception or transmission, there are few mentions of transducers meant for reciprocal use. Conservation of energy implies that the responsivity of the coil-magnet system as a force transducer, in N/A, and its sensitivity as a velocity transducer, in V/(m/s), are identical properties (Gabrielson 1997; Wielandt 2012). Thus, voice coil transducers can be used reciprocally as both receivers and transmitters of mechanical waves.

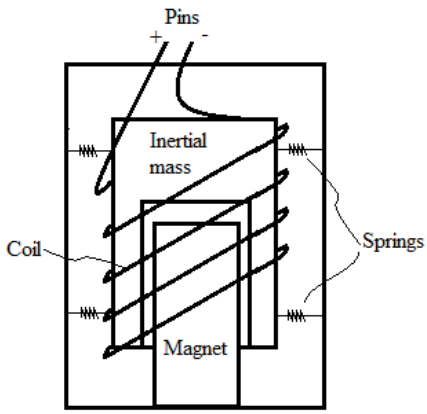

Figure 6. Illustration of the main components in a typical voice coil transducer.

2.4.2 Continuous wave measurements

2.4.2.1 Continuous wave vs. pulse measurements

In ultrasonic SHM the transmitting transducer is commonly excited with either a transient pulse (spike), resulting in a transmitted signal with frequency content determined by the impulse response of the transducer, or with a burst signal specifically designed for the purpose. Such bursts are usually a number of periods of a sinusoidal signal, either with a single frequency or with swept frequency, in the case of chirps. Bursts are usually windowed, in order to avoid an impulse response by the transducer. However, all transient signals include frequencies in a certain interval, and are thus broad-band, by definition. Figure 7 illustrates different types of excitation signals in both time-domain and frequency domain.

The maximum strength of the transmitted signal is generally determined by the amplifier driving the transducer, which is limited to a certain voltage, or power. In a broad-band transmission the energy is distributed in the frequency domain, depending on the excitation signal and characteristics of the transducer.

On the receiving end, a transducer registers the mechanical vibrations and an AD-converter is used to sample the data. This sampling must be made to include signal components in a range of frequencies, since the signal itself is broad-band. Analog or digital filters can be used to remove measured noise components lower and higher than the frequency range of interest. However, noise components in the same frequency range as the signal of interest cannot be filtered out.

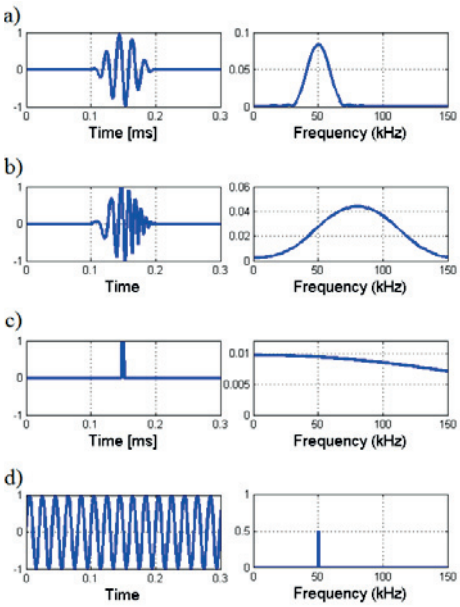

Figure 7. Different types of common excitation signals, in time domain (left) and frequency domain (right).
a) Windowed sinusoidal burst.
b) Windowed chirp signal.
c) Impulse (spike).
d) Continuous sinusoidal wave

If the distance between the transmitting and receiving transducers is large enough the received signal will be obscured by the noise. The *signal-to-noise ratio*, SNR, can be increased by averaging several measurements. If the noise is white, i.e. completely random and uniformly distributed in the frequency domain, the SNR is increased with the square root of the number of averages. This requires that the measurement signal and measurement system are stable over the time data is collected. Coherent noise with a certain frequency characteristic, i.e. from some machinery, will not be removed by averaging.

As previously stated, the amplitude of a transmitted signal is limited by the amplifier driving the transmitting transducer. However, by transmitting continuously, with a sinusoidal signal of a certain frequency, more energy is input into the structure, and all energy is concentrated in one frequency.
Furthermore, since the transmitted signal is a single frequency, narrow-band reception is possible. By only collecting data with a specific frequency component, most noise will be rejected. A lock-in amplifier can be used to detect signals with a

known frequency at extremely low SNR. A lock-in amplifier yields the amplitude of the continuous wave field and its phase, relative to a reference signal. The operation of lock-in amplifiers is further detailed in the next section.

If a single frequency is transmitted continuously into a structure, a steady-state diffuse field will stabilize after a short period of time, consisting of direct propagation, reflections in boundaries and scattered waves. The signal measured at any receiver location will then be a superposition of all possible propagation paths between actuator and receiver. This removes any temporal information in the measured signal, which impedes spatial resolution. However, an advantage is the increase in energy of the scattered and reflected waves, which otherwise rapidly attenuate below the noise floor. Figure 8 (a) shows an example of the development of a steady-state, measured at a particular position of a concrete floor slab, after a continuous wave transmission is started. The ballistic waves, traveling in a direct line between transmitter and receiver, are first measured, similarly as for transient pulses. However, since more energy is continuously put into the structure, new ballistic waves are measured simultaneously as the scattered and reflected waves start to reach the receivers. Due to superposition of the waves, the different paths will interfere in complex patterns, which is why the overall amplitude is not strictly increasing with time. After a time, the waves from all possible propagation paths have been superimposed, and a steady state is formed. This steady state is given by an amplitude and a phase, at each receiver position. The variations in the steady-state in the figure are mostly artifacts from the plotting. Figure 8 (b) shows a zoomed in view of the steady state, corresponding to the red rectangle in Figure 8 (a).
Since transmitting continuously results in a diffuse wave field, it is quite similar to coda waves, as these too, by definition, are diffuse signals. The same reasoning explaining the high sensitivity of CWI should hold for continuous diffuse wave fields. A change in the wave velocity in the propagation material will result in a change in phase of the continuous wave field.

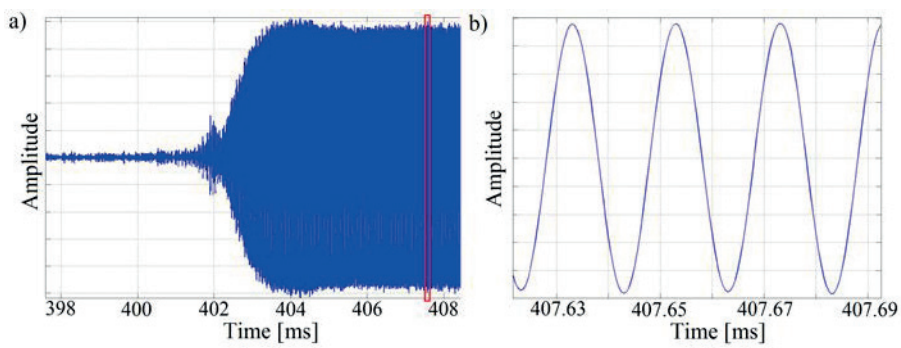

Figure 8. a) Development of a steady state diffuse wave field from a single frequency continuous wave transmission. b) Zoomed in view of steady state.

2.4.2.1 Lock-in amplifier

A lock-in amplifier is an instrument used for measuring the amplitude and phase of a continuous signal, relative to a single-frequency reference signal. The reference signal can be either externally provided, or generated internally by an oscillator. The basic principle of a lock-in amplifier is to multiply the measured signal with the reference signal and integrate the result over a specified period of time, much longer than the period of the reference. Due to the orthogonality of sinusoidal functions, signal components with a different frequency will approach zero in this operation. The components of the signal with the same frequency will yield a DC value, which depends on the amplitude of the component. The DC value will also depend on the phase difference between the reference and measurement signal. The lock-in amplifier is thus a phase-sensitive detector.

Modern lock-in amplifiers have two such detectors, where one has a 90 degree phase shift relative the reference signal. The result from this detector is called the quadrature component, while that of the detector with no phase-shift is called the in-phase component. Together these can yield both amplitude and phase of the component of the measured signal which has the same frequency as the reference signal.

The resulting value output by a lock-in amplifier with a sinusoidal reference signal can be expressed as

$$U_{out}(t) = \frac{1}{T}\int_{t-T}^{t} \sin(2\pi f_{ref}\tau + \gamma)U_{in}(\tau)d\tau \qquad \textit{Eq. 12}$$

where U_{in} is the input signal, Υ is a phase setting on the lock-in amplifier, f_{ref} is the frequency of the reference signal and T is the averaging time.

Provided that the averaging time is much longer than the signal period, the in-phase component, X, and quadrature component, Y, are given by

$$X = V_{in}\cos(\varphi) \qquad \textit{Eq. 13}$$

$$Y = V_{in}\sin(\varphi) \qquad \textit{Eq. 14}$$

where V_{in} is the amplitude of the component with frequency f_{ref} of the input signal, and φ is the phase difference of the reference and input signal.

The magnitude, V_{in}, of the measured signal is then given by

$$V_{in} = \sqrt{X^2 + Y^2} \qquad \textit{Eq. 15}$$

The phase, φ, relative to the reference signal is given by

$$\varphi = \tan^{-1}\left(\frac{Y}{X}\right) \qquad \textit{Eq. 16}$$

The result is an instrument which measures amplitude and phase of a single frequency component at a time and rejects other frequency components extremely well. Random noise manifests as an AC component on the relevant DC output, but this can easily be removed with a low-pass filter. Lock-in amplifiers can thus be used to detect continuous signals even if these are indistinguishable from noise in time domain.

2.5 Strategy for thesis work

The substantial attenuation of high frequency waves in concrete needs to be addressed in order for mechanical wave-based SHM systems to be practical in large civil structures. Many presented CWI applications are used to transmit signals over less than 1 m. This would necessitate an unreasonable amount of transducers to cover very large civil structures in an SHM system. This issue was approached in two ways in the scope of this thesis work:

1) Investigate the possibility to use low frequency signals to detect minor damage. Attenuation of mechanical waves is frequency dependent, with high frequency waves being more strongly attenuated. In literature can be found examples of CWI applications ranging from single kHz measurements to almost 1 MHz measurements. No comprehensive study has been presented where identical measurements, but in different frequency ranges, are used to follow the same damage evolution. This is the scope of paper II in this thesis.
   Signals in the lower end of this wide frequency range is most often generated by impact hits. This is not suitable for SHM applications. In paper I, the efficiency of voice coil transducers as reciprocal transmitters and receivers of mechanical waves in concrete is investigated. These could serve as viable alternatives to PZT transducers in very low frequency applications, where PZT:s are not very efficient.
2) Investigate the use of continuous wave measurements, as opposed to using transient pulses. Continuous wave measurements can be sampled with a lock-in amplifier, which enables the successful detection of signals, even if they are significantly weaker than the ambient noise. The ability to detect weaker signals should equal the ability to transmit signals over longer distances, and the noise rejection should make the system less

affected by external disturbances. Continuous wave measurements and transient CWI measurements are compared in paper III.

Transmitting continuously, at only one, or a few, frequencies means that full waveforms are not acquired. Any temporal information in the signal is lost, and the localization methods developed for CWI, e.g. Locadiff, are not possible. In paper IV the possibility to use these measurements to provide rough localization of the damaged region using a simple tomography is investigated.

3 Environmental variations

This chapter addresses the issue of changing environmental conditions, and how this is a problem for the field of SHM in general. Some common methods for countering this issue are briefly discussed, with emphasis on the tools used within the scope of the thesis. The final section discusses this choice of tools and the methodology with which the issue of environmental variations is handled in the appended paper V.

3.1 Issues in SHM

One of the greatest challenges of SHM is the fact that most structures are situated in environments where conditions vary greatly during measurements. Examples are exposure to changes in weather, traffic, temperature, hydrostatic pressure etc. Variations in conditions like these can change stiffness, damping and even geometry of structures, without posing any problems for the safety.
The problem is that the baseline, that is the data for an undamaged structure, is highly dependent on these environmental conditions. These variations can often affect the measured data more than actual damage. This can easily lead to the SHM system either missing real damage or giving a false alarm when no actual damage is present.

3.2 Choice of feature

Ideally an SHM system would measure a parameter which gives good indications of damage but which is not affected by environmental conditions. In general, no such physical quantity exists. But some aspects of measured data are less sensitive to environmental variations than others. The choice of *measurement feature* is therefore often crucial in SHM. Some basic examples of features are given in section 2.2, and in section 2.3 for CWI. Features based on measurements of nonlinear parameters are generally less dependent on environmental variations, as demonstrated by e.g. Zhang et al. (2017).
In practice, no damage-sensitive feature is completely independent of environmental variations. Instead SHM applications will have to compensate for the effects of environmental conditions to the measured parameters. Some such methods of compensation are described in the next section.

3.3 Common compensation methods

In this section, some common methods for compensating for environmental variations in SHM are briefly outlined.

3.3.1 Optimal baseline selection

With the *optimal baseline selection* method, multiple baselines are acquired, at different values for the environmental factors (e.g. temperature). The baseline corresponding to the least difference from the current measurement point is used for each damage index (DI) calculation**.**
The baseline which gives the smallest residue is chosen, not the one at the closest environmental parameter. This is shown to yield a better result than if the baseline at e.g. the exact same measured temperature was chosen (Konstantinidis et al. 2007).
For the method to work well, very many baselines are needed, spanning a large number of combinations of environmental conditions. This is not trivial, or even possible, in many practical implementations on real structures.
The method can be extended by interpolation of the acquired set of baselines, which can produce a baseline closer to the current measurement (Scheerer & Lager 2014; Clarke et al. 2010). This can lead to fewer baseline measurements required.

3.3.3 Baseline signal stretch

When wave propagation velocity in a structure is homogeneously changed relative to a single baseline, the time domain signal of a wave is stretched. *Baseline signal stretch* is a method where the signal is stretched in such a way that the fit to the baseline is optimized. This way, good results can be achieved in comparisons with a single baseline, even if the baseline is acquired at e.g. a different temperature (Lu & Michaels 2005). However, the difference in temperature between the baseline and the current measurement cannot be too high, or the method will not work. This gap depends on signal complexity and mode purity – if Lamb waves are used (Clarke et al. 2010).
This method can be used to compensate for environmental effects that result in a homogenous, isotropic change in guided wave velocity, such as temperature and hydrostatic pressure. However, effects such as application of a load in a particular direction that cause anisotropic changes in wave velocity cannot be compensated for using this method (Croxford et al. 2010).

3.3.4 Reference object control

It is possible to differentiate between the effects of damage and environmental effects by the use of a reference object. A protocol has been proposed by Zhang et al. (2013) where one such reference object is placed to be subjected to the same environmental conditions as the real test object of interest. The reference object is not subjected to the loads and damage as the test object. By subtracting the measured variations in the reference object, attributed to the environment, from the measurements in the test object, only the effects of the damage remains. The

proposed method was shown to be successful for CWI on concrete specimens in laboratory. Further tests with a combination of CWI and NWMS has also been presented (Abraham et al. 2014). It should be noted that it is not trivial to transfer this technique to a large structure in uncontrollable environmental conditions.

3.4 Machine learning

In real applications, an SHM system will likely be affected by variations in many environmental conditions simultaneously, in complex combinations. In practice, it will not be possible to measure all of these environmental parameters, nor will it be possible to gather baselines from all combinations of conditions. By simply letting an SHM system run over a certain period of time, on a structure subjected to normal variations, large amounts of data are gathered. The variations in the data, due to environmental variations, are most often too complex for a human mind to analyze. However, this is a perfect application for various types of *machine learning*. In machine learning, different algorithms can analyze large amounts of data and can determine whether a new data point is within normal conditions or if it deviates in some manner. The collection of data over several years means that a system can learn e.g. seasonal and diurnal patterns, which will further improve the accuracy.
Machine learning is a large field in itself, with rapidly growing number of applications. In this thesis, no attempt to develop new machine learning tools is made, but over the course of the work commonly used tools have been applied to new types of measurements. For an extensive review and overlook of machine learning in SHM applications the reader is referred to the book by Farrar and Worden (2013).
A brief overlook is given here, as well as a slightly more detailed description of the tool specifically used in the thesis work.

3.4.1 Supervised and unsupervised

If algorithms have access to data sets from both undamaged and damaged structures it can be taught all the characteristics of both (all) these cases. This is *supervised learning*. Such a system can theoretically classify each new measurement to a specific group and thus differentiate between e.g. different types of damage.
Supervised learning requires training data from the undamaged structure, as well as every type of damage which should be classifiable. This is generally not possible for applications on civil structures.

Instead, algorithms have to be trained on data from only the undamaged structure. These are *unsupervised learning* algorithms. These can only detect changes, not identify different types of changes. Being able to detect changes from normal behavior is called *novelty detection*. Like already mentioned, this is not trivial for systems exposed to environmental variations, as these variations can be orders of

magnitude larger than the variations caused by damage. So unsupervised machine learning algorithms need to be employed for normalization of the data, before novelty detection is possible. Many techniques exist which are suitable for such tasks, e.g. principal component analysis, cointegration, Mahalanobis distance and artificial neural networks. A description of Mahalanobis distance is given here, as this was identified as the tool best suited for the developed SHM system within this thesis work.

3.4.2 Mahalanobis distance

One method for analyzing the difference between a multivariable data point and a set of such points is to calculate the Mahalanobis distance (Mahalanobis 1936).
The Mahalanobis distance between a multivariable point **x** and a set of points **Y** is given by

$$\mathrm{D} = \sqrt{(\mathbf{x} - \overline{\mathbf{Y}})^{\mathrm{T}} \mathbf{S}^{-1} (\mathbf{x} - \overline{\mathbf{Y}})} \qquad \textit{Eq. 17}$$

Where $\overline{\mathbf{Y}}$ is the mean of the set of baseline data points, **S** is the covariance matrix of **Y** and superscript T means transpose.
The Mahalanobis distance equals the distance between the current measurement and the mean of the baseline data set, expressed in the number of standard deviations of the baseline data in the specific direction in the multidimensional space.
Thus, if the baseline measurements have large variations in a certain direction in the multidimensional space, a larger absolute deviation from the mean of the baseline, in this direction, is needed to pronounce a measurement value as an outlier.

Figure 9 shows an illustration of Mahabalonis distance for synthetic 2-dimensional data. The features here could be any measurement parameter, such as pulse velocity and attenuation. Even though the two points, A and B, are equally far from the mean of the baseline data set in Euclidian space, the Mahalanobis distance for point A is ~1.3 while the Mahalanobis distance of point B is ~5.6. Point B is therefore different from the baseline data set, while point A is not.
It is worth noting that point B is not separated from the baseline data set in either the feature 1 or the feature 2 directions. If this data point were to be evaluated by feature 1 or feature 2 separately, it would most likely be classified as an inlier. However, using the Mahalanobis distance it can easily be classified as an outlier.
This is a simple 2-dimensional example, where it is trivial for a human to see that one of the points is an outlier and the other is not. However, for data sets with higher dimensionality, it can be impossible to visualize this without some sort of computer algorithm.

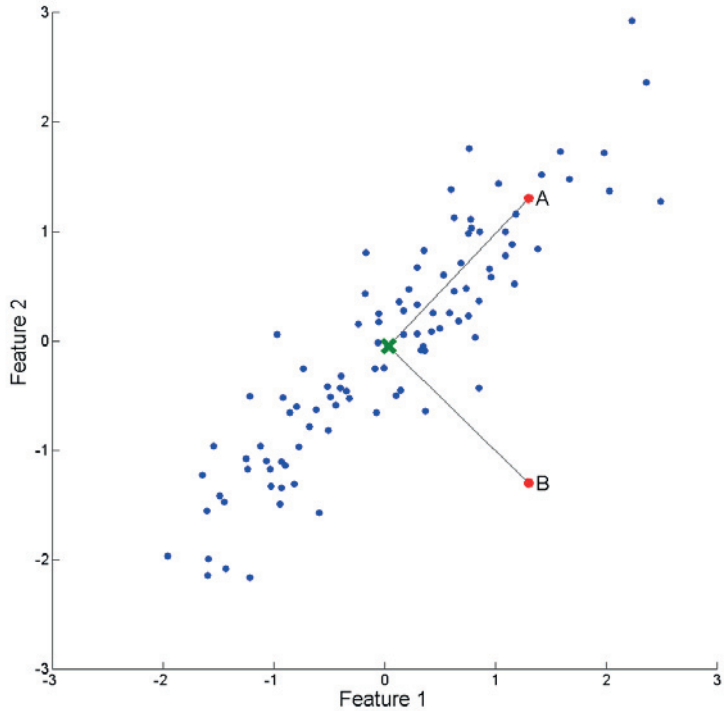

Figure 9. Illustration of Mahalanobis distance. Blue points are a set of 2-dimensional data points which make up the baseline. The green cross is the mean of the baseline data set. Point A and point B are equally far from the mean of the baseline data in both feature 1 and feature 2 dimensions. However, the Mahalanobis distance between the baseline data set and point A is ~1.3 while that of point B is ~5.6. This is because the variance of the baseline data is much larger in the direction given by the mean point and point A, than the variance in corresponding direction for point B.

3.5 Strategy for thesis work

The SHM system mainly developed within the scope of this thesis make use of narrow-band amplitude and phase measurements of continuous diffuse wave fields, as stated in section 2.5. The similarity of these measurements to CWI measurements have already been established in this thesis, and unfortunately they also display similarly strong sensitivity to environmental variations as their transient counterpart.
The continuous wave measurements are by nature low-dimensional; only two scalar values, amplitude and phase, are yielded for each single-frequency measurement. These measurements thus inherently contain less information with which to construct features which are less affected by environmental variations, than compared to full time-domain waveforms. The obvious first approach is to make use of more frequencies, to add more information; in theory, if measurements were performed at all possible frequencies, this information could be used to construct full waveforms, through inverse Fourier transformation. In practice, a number of frequencies are chosen, making use of resonant frequencies of the transducers.

This can be viewed as each measurement yielding a multi-dimensional data point (with two dimensions per included frequency), with a complex dependency on both environmental variations and damage. These high dimensional points are very hard to interpret by humans, but are well suited for machine learning, as described in the previous section. The second approach was therefore to employ the Mahalanobis distance, as a damage index. The SHM system can be set to gather baseline data over a period of time, with strong variations in the multi-dimensional space due to environmental variations. The sudden appearance of damage will then affect the features of each new data point in a way which is somewhat orthogonal to the variations caused by environmental variations, resulting in a relatively large Mahalanobis distance.
This is the scope of appended paper V.

4 Methodology and results

This chapter is intended to give an overview of the experiments carried out within the scope of the thesis, which were designed according to the strategies formulated in sections 2.5 and 3.5. All experiments are described in more detail in the papers appended in the second part of this thesis. Conclusions from the combined results from the different studies are given in chapter 5.

4.1 Voice coils as reciprocal transducers

The usefulness of voice coil transducers as reciprocal transmitters and receivers of low frequency mechanical waves in concrete was to be investigated. For this end, a set of five such transducer types were evaluated; two geophones (ION SM6 3500Ω and SM6 375Ω), an inertial force actuator (Motran IFX30-100) and two electro dynamical exciters (Visaton EX60S and EX45S). None of the transducers are designed for reciprocal use, i.e. they are meant to be used as either actuators or receivers of mechanical vibrations. A piezoelectric disc (Ferroperm Pz27) was put through the same experiments, in order to provide some reference. The transducers efficiency were investigated in three different experiments. These are more detailed in Paper I, appended to this thesis (Patrik Fröjd & Ulriksen 2015).

The first experiment evaluated the force output per unit of current from the transducers, when used as actuators. The transducers were mounted on top of a force transducer, and was excited by a driving signal whose frequency was stepped through the interval 10 – 5000 Hz. The results are shown in Figure 10 (a).
The second experiment evaluated the sensitivity of the transducers as receivers by mounting them on top of a shaker. The frequency of the vibrations of the shaker was stepped through the same interval as for the actuation experiment, and the velocity was measured. With this information, the voltage generated by the transducers per unit of velocity of the ambient vibrations could be established. The results are shown in Figure 10 (b).
The main conclusions from these tests are that the force responsivity measurements are very similar to the reception sensitivity measurements, which speaks to the reciprocity of the voice coils. In fact, the force responsivity, in N/A, and sensitivity, in V/(m/s), are identical units. This can easily be seen if one express these in SI-units only ($\mathrm{kg} \cdot \mathrm{m} \cdot \mathrm{A}^{-1} \cdot \mathrm{s}^{-2}$). The geophones, SM6 3500Ω in particular, display very similar behavior in both modes of operation, and are more efficient than the PZT disc for frequencies up to ~3.5 kHz.

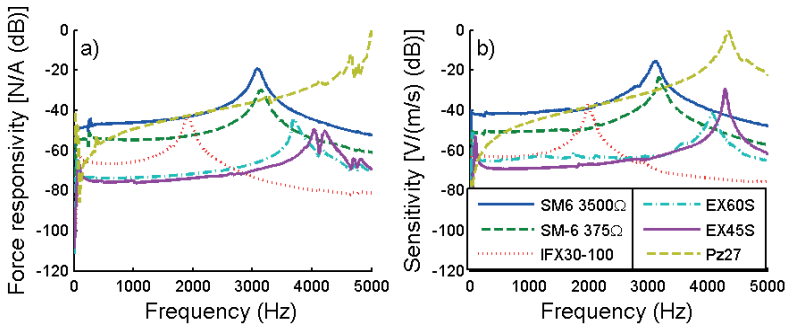

Figure 10. (a) The responsivity, in N/A, as a function of frequency for the investigated transducers. (b) The receiving sensitivity, in V/(m/s), as a function of frequency, for the evaluated transducers. In both sets of graphs the amplitudes are in decibel scale, normalized relative to the highest value in each diagram. Image from Fröjd and Ulriksen (2015).

In the third experiment, a pair of each transducer was used, for reciprocal transmission. These were attached to either side of a 0.4 m cubic concrete block, and one of the transducers was used as transmitter and the other as receiver. The actuating transducer was excited with stepped frequency, in the same range as above. The experiment was repeated for each pair, with the roles of the transducers reversed. This was done to additionally illustrate the reciprocity of the transducers. Figure 11 (a) and (b) show the measured output divided by the input current, as a function of frequency, for the initial and reversed transducer configuration respectively. In these graphs, the transmission between the PZT discs at first seem to be most efficient over most of the range. However, the measured signal up to ~3.5 kHz is purely due to capacitive coupling between the transducers, and is unrelated to the generation of mechanical waves. This was confirmed by the fact that the response of the PZT:s, between 10 Hz and 3.5 kHz, was identical if the experiment was repeated with the transducers suspended in the air, without mechanical coupling to the concrete between them. Additionally, the noise in the PZT signal between ~10-1000 Hz are most likely components picked up from ambient disturbances in the room. The voice coil transducers seemed less sensitive to these disturbances. As expected, the SM6 3500Ω geophone proved to be the most efficient for frequencies below ~3.5 kHz. This, combined with the fact that they behave relatively linearly and appear resilient to electrical disturbances, make them a viable alternative to PZT transducers in reciprocal generation and reception of low frequency mechanical vibrations.

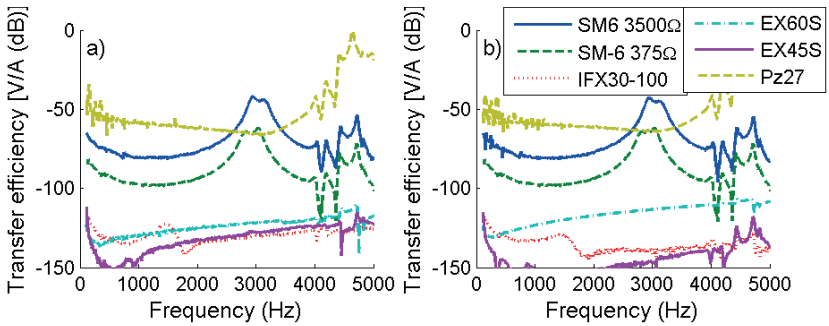

Figure 11. Transmission efficiency, in V/A, between a pair of identical transducers, for all transducers investigated in the study. All plots are in decibel scale, normalized relative to the highest values in the diagrams. The measured signals in the PZT transducers for frequencies below ~3.5 kHz correspond to capacitive coupling between transmitter and receiver. In (a) one of the transducers, for each pair, acts as transmitter and the other as receiver. In (b) the transmission is reversed. Image from Fröjd and Ulriksen (2015).

4.2 CWI at different frequencies

In order to provide some guidance to designers of SHM systems based on diffuse mechanical waves, as to the choice of signal frequency, two sets of experiments were designed. The overall aim was to investigate the different abilities of CWI in widely different frequency ranges to detect and track the same damage, and illustrate the difference in possible transmission distance. The work, and results, summarized here, are given in more detail in appended paper II (P. Fröjd & Ulriksen 2017). The evaluated signal central frequencies were 3.1, 50, 150, 250 and 500 kHz, which span the first three, useful, scattering regimes in concrete (see section 2.3.1). Two different types of damage were to be detected; extra scatterers, in the shape of boreholes, and cracking due to bending loads. The boreholes were assumed to not result in global velocity changes, and thus the simple decorrelation method was used, according to Eq. 9. For the bending cracks in the beam, a velocity change is a more valid model. Thus, the stretching method, according to Eq. 10, was used. This yields both the estimated relative velocity change and remaining decorrelation, after optimal stretching.

In the first experiment, the goal was to detect boreholes in an 8x2 m concrete floor slab. A separate pair of transducers were used for each of the signal frequencies. The 3.1 kHz signals were transmitted between two geophones, and all other signals were generated by PZT discs. All signals were 5-cycle, Hanning windowed sinusoids. Since the higher frequency signals are significantly more attenuated in the concrete than the lower frequency signals, the transducer pairs were separated by a distance

corresponding to 20 wavelengths. This correspond to 10, 20, 33 and 100 cm for the 500, 250, 150 and 50 kHz signals respectively. The 3.1 kHz signals gives rise to Lamb waves, with wavelengths on the order of the size of the structure. 20 such wavelengths are longer than the lengths of the slab and the geophone transducers were instead placed 4 m apart. For a structure this size, regardless of the placement of the low-frequency transducers, the measured signals will consist of waves that have been reflected from the boundaries many times. The distance between the geophones is therefore not crucial.

At the specified transducer distances for the different frequency transmissions, all signals had similar signal-to-noise ratios, ~50 dB, at the largest peak. This highlights the difference in order of magnitude of the attenuation and thus the useful maximum range between actuator and receiver.

The five pairs of transducers were placed with these individual distances, all centered at roughly the center of the concrete slab. Figure 12 shows a sketch of the transducer placement.

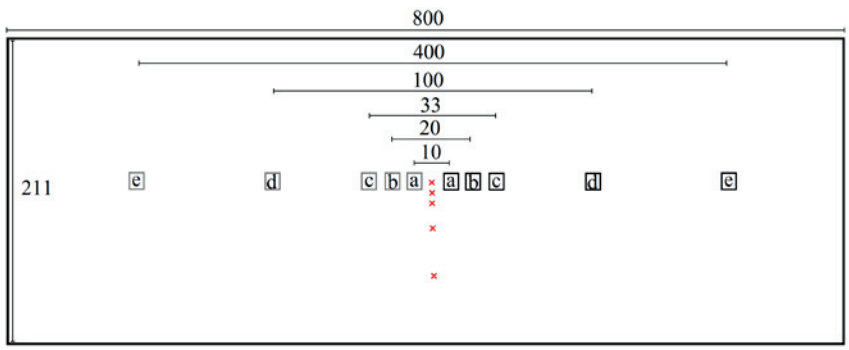

Figure 12. Layout of the concrete floor slab, transducers, and boreholes. Dimensions are given in cm. The transducer pairs denoted by a-e in the figure were used for signals with frequencies 500, 250, 150, 50, and 3.1 kHz, respectively. The transducers to the right of the center were used as transmitters and those to the left as receivers. The red crosses indicate the location of the boreholes. The boreholes are located 0, 5, 10, 20 and 40 cm from the centerline, between the transducers. The sketch is not to scale and the transducers were placed slightly off-center on the slab due to other instrumentation on the concrete. Image from Fröjd and Ulriksen (2017).

Holes were drilled in the floor slab, in the middle between the transducers. The holes were first drilled with a diameter of 4 mm, and a depth of 1 cm. Then the diameters were expanded to 8, 10 and 12 mm. This was repeated for a number of holes, situated at different distances from the center of the floor slab, according to the red crosses in Figure 12. This was done in order to investigate the width of the probed region between the transducers, and if this corresponds well with the

models which predict this region to be on the order of a mean free path (see section 2.3.2.4). Between each drilled hole, eight CWI measurements were performed for each of the chosen signal central frequencies.
Before evaluating the decorrelation of the codas, the scattering parameters of the concrete, at the given frequencies, were evaluated by fitting solutions of the diffusion equation to the waveforms, using Eq. 4. The estimated parameters are given in Table 1. For the stationary wave regime signal (3.1 kHz), diffusion is not a good description of the propagation of energy, as the whole structure reverberates with the vibrations. However, it is included as a rough estimate, though it is specific for the given geometry.

Frequency (kHz)	Diffusivity (m^2/s)	Dissipation (s^{-1})	Transport mean free path (cm)
500	8	13000	1.0
250	18	10000	2.1
150	39	7000	4.7
50	440	1200	35
3.1	~700	220	56

Table 1. Estimated scattering parameters for the concrete floor slab at different central frequencies.

Figure 13 shows the results from the coda decorrelation measurements for the different central frequencies and for the different boreholes. Each subplot shows measurements with one central frequency, and each curve shows a specific distance between the borehole and the centerline, according to Figure 12. The y-axis shows the coda decorrelation and the x-axis shows the measurement number. Eight measurements were performed at each borehole diameter, starting with eight measurements with no hole. The first of these measurements, with no hole, was used as the reference signal in Eq. 9.
From Figure 13, it can be seen that the absolute level of decorrelation increases with frequency. This is intuitive, as a hole of a certain diameter will affect a signal with a short wavelength more than one with a longer wavelength. However, the times when the borehole diameter was increased can clearly be seen, even in the plots corresponding to the simple-scattering regime (50 kHz) measurements. Even the smallest-diameter hole (4 mm) can be detected at this frequency. These correspond to less than a tenth of a shear wavelength and is smaller than the concrete aggregates and reinforcement bars.
The ability to resolve an event depends on the stability of the baseline measurements (measurements 2–8, in this case), which, in turn, depends on the signal-to-noise ratio and whether the variations are compensated for changes in environmental conditions. The stationary-wave-regime signals (3.1 kHz) did not register the larger-diameter drill holes, certainly not in any useful capacity.

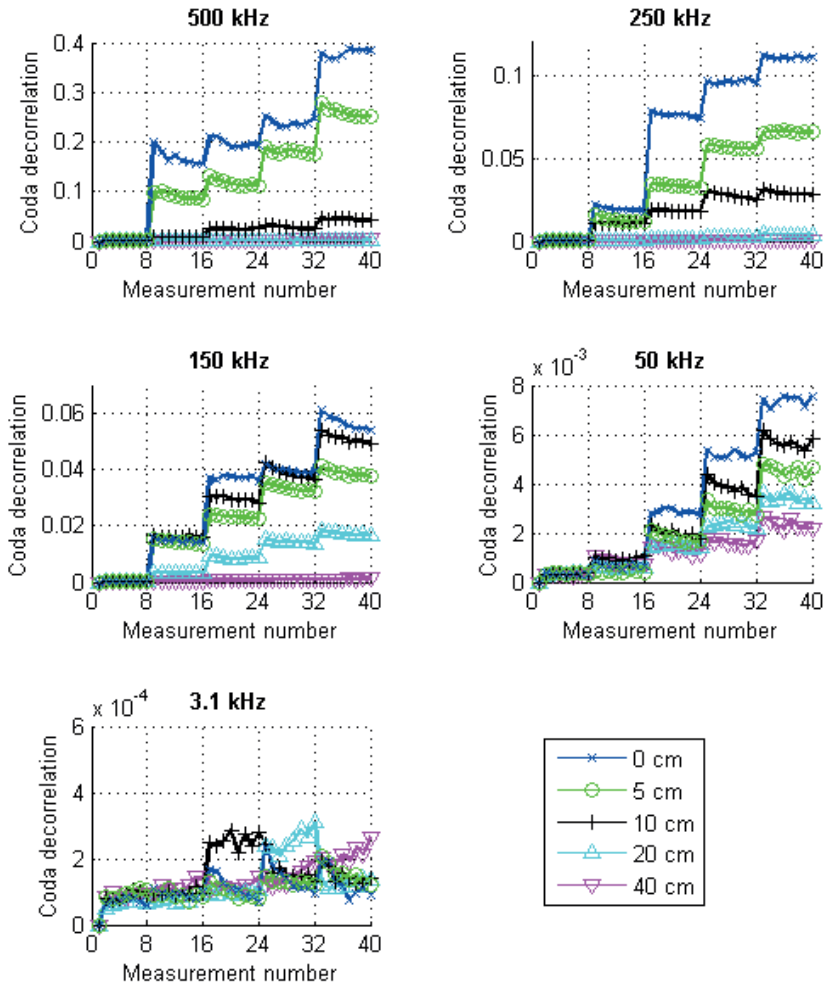

Figure 13. Decorrelation of the coda at different central frequencies. The diameter of the boreholes were expanded every eighth measurement, with diameters 4, 8, 10, and 12 mm. Each curve shows measurements with different distances between the holes and the centerline between the transducer pair (according to the red crosses in Figure 12.

The influence of the distance of the hole to the direct line between the transducers and the decorrelation of the signals can clearly be seen in the figures. The sensitivity of the coda wave analysis decreases as the distance between the hole and the direct line increases. This is caused by two factors:

1) The intrinsic absorption prevents far-traveling waves from influencing the measured signal. Evaluating the later parts of the codas results in a wider probed area, since more of the waves have time to travel further. However, the later parts of the signals will be more attenuated, resulting in lower signal-to-noise ratios. The higher-frequency signals are much more attenuated than the lower-frequency signals.
2) The probability that a measured wave packet has passed a certain point decreases with distance to the transducers and the direct connecting line between them. The second phenomenon can be visualized as a sensitivity kernel, as described in section 2.3.2.4, and the width of the zone of high sensitivity between two transducers is approximately one transport mean free path. See Figure 5 for an illustration of such a kernel. Clearly, the higher-frequency signals (with shorter ℓ^*) display a more rapid decline in sensitivity as a function of distance. There does not seem to be a significant difference in the effect of the holes within this high-sensitivity zone, which is in agreement with the resolution of sensitivity kernel–based imaging methods being on the order of ℓ^*. The 150 kHz signal measurements seem to include the holes 10 cm from the center in this high-sensitivity zone, which is more than the estimated ℓ^*, but it should be noted that the estimate is a rough approximation. In general, our measurements are in agreement with this theory.

The second experiment was used to demonstrate the different sensitivities of CWI at different frequencies when detecting bending cracks in a small concrete beam. One pair of geophones were used for the 3.1 kHz signals, and a pair of PZT transducers were used for the rest. An illustration of the experimental setup is shown in Figure 14. The measurements were evaluated using the stretching method (Eq. 10 and 11), and thus yielded relative velocity change and decorrelation after optimal stretching.

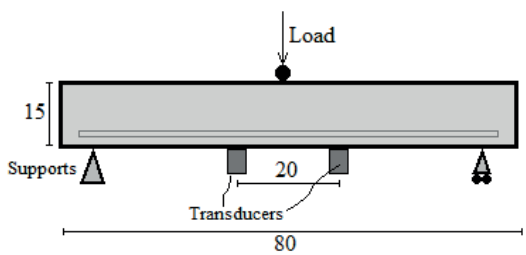

Figure 14. Illustration of the experimental setup for the beam bending experiment. Dimensions are given in cm. Image from Fröjd and Ulriksen (2017)*.*

A downward load was applied at the center of the beam. The load was applied in steps with increasing force. Between each load step, the load was released before the CWI measurements were performed. The measurements were thus made on

the unloaded slab, and any effect on the coda should therefore be attributed to damage to the concrete rather than stress.
In contrast to the case with drilled holes in the floor slab, it was not possible to know the exact damage state of the concrete at the various load steps. It was simply assumed that the level of damage in the concrete increased with the maximum bending load experienced by the beam. For low loads, it was assumed that only microscopic cracks formed. As the load increased, larger internal cracks were created, and at a load of ~12 kN, the first visible crack appeared while the load was applied.

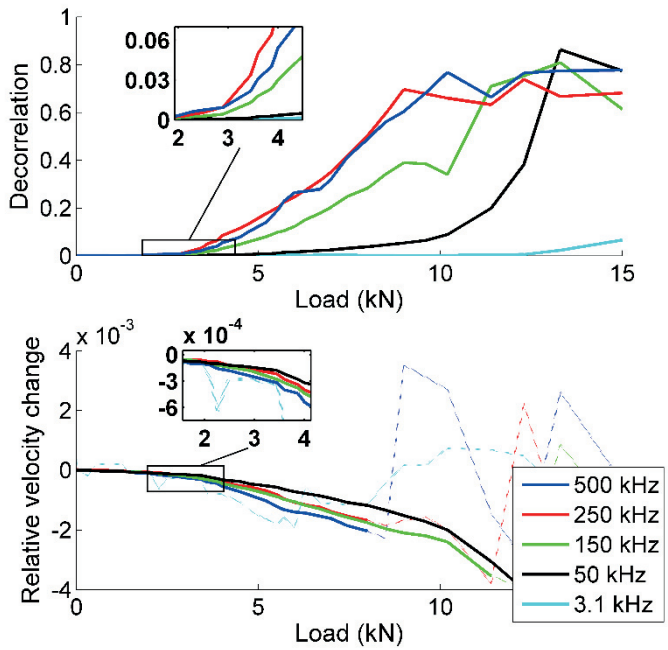

Figure 15. Decorrelation (upper) and relative velocity change (lower) of the different frequency coda signals as a function of maximum bending load experienced by the beam. The relative velocity change measure is not relevant after the signal has been very distorted, since the degree of optimal stretching then is somewhat random. These data are shown with dotted lines, in order to increase visibility in the graphs. The relative velocity change for the 3.1 kHz signals are also shown with a dotted line since the stretching method did not seem useful for this frequency. Image from Fröjd and Ulriksen (2017).

Figure 15 shows the relative velocity change (lower subplot) and remaining decorrelation after optimal stretching (upper subplot). The horizontal axis shows the bending load of the load step before each measurement.

From the results, it is evident that the ultrasonic (50-500 kHz) CWI measurements registered an effect in the material at loads less than one-fourth of the load that produced visible cracks. This can be seen both from the relative velocity change and remaining decorrelation.
As the damage progresses, the relative velocity change decreases and the remaining decorrelation increase. After the beam has been loaded up to 8.5 kN, both the 500 and 250 kHz signals are so perturbed, and the decorrelation so high, that the estimated velocity change is not accurate. This data is shown with dotted lines in the relative velocity change plot, for improved visibility of the other curves.
The 3.1 kHz signals display large fluctuations in the relative velocity change, with no clear relation to the progressing damage. At some points an increase in velocity is registered, which is counterintuitive. It is speculated that this is due to the fact that the coda, for these stationary wave regime signals, is created from the beam reverberating. In fact, there are several structural modes within the frequency spectra of the signal, which are excited. The time stretching procedure cannot be said to necessarily estimate the relative velocity change at these circumstances. Therefore, the line which corresponds to the 3.1 kHz signal in the lower subfigure in Figure 5 is shown dotted, in order to increase visibility of the other lines. The decorrelation is a more straight-forward parameter, which should be applicable even if the measured coda is caused by modal reverberations. From the these measurements it is clear that the stationary wave regime signals do not display significant decorrelation until after such loadings that visible cracks appear in the concrete.
The results from both decorrelation and relative velocity change measurements indicate that the 500 kHz measurements does not give much higher sensitivity than the 250 and 150 kHz measurements; all three configurations show some indication of change after ~2 kN load. The 50 kHz measurements yield measurements with only slightly lower sensitivity in the decorrelation, and register a change after ~3 kN load, though the absolute measurement values are lower than the high frequency counterparts. In the relative velocity change measurements, the 50 kHz signals display very similar sensitivity as the higher frequency signals.

The combined results, from both experiments, indicate that CWI with signals in the simple-scattering regime (~50–150 kHz in concrete) are quite suitable for SHM applications. These signals can be used to detect minor damage to concrete, by which we mean either a local hole or crack that is smaller than the aggregates in the concrete, or early signs of stress-induced cracking, such as a region of microcracks. The increase in sensitivity when using higher-frequency signals might not outweigh the downside of significantly higher attenuation, which necessitates a much denser transducer network in an SHM system. The simple-scattering regime signals also exhibit a larger probed area between two transducers, which is also an attractive prospect in SHM applications.

In both the presented experiments, the time windows for the codas were placed at the times when the measured signals had an SNR of ~25 dB. Selecting later coda windows yields measurements with greater sensitivity, but at the cost of lower SNR, which introduces more uncertainty and fluctuations. In SHM applications, in particular, care should be taken to choose a time window where a high-enough SNR is obtained, as noise and disturbances are likely to be more prevalent than in laboratory environments.
It should be noted that it is common to use chirp signals over a wide range of frequencies. Such a signal was not included in this study, as we focused on distinguishing the influences of different frequency signals. The benefits of including a wide range of frequencies in the signals are clear, but it should be noted that, for larger distances, the high-frequency components are significantly more attenuated than the lower-frequency components.

4.3 Continuous and transient diffuse wave measurements

As stated in section 2.4.2, exciting a transducer with a continuous wave, will give rise to a diffuse wave field in the structure. This is similar to the wave fields created by scattered and reflected pulses, but instead of being transient, after a short time, a steady state will be created. An experiment was created to demonstrate the similarity of measuring shifts in such a continuous wave field to transient CWI measurements. The experiment and results are detailed further in appended paper III (P. Fröjd & Ulriksen 2015).
A reinforced concrete slab, with dimensions 120 x 80 x 15 cm, was instrumented with two PZT transducers on the lower side. The transducers were placed 70 cm apart. The concrete slab, and transducers are shown in Figure 16.

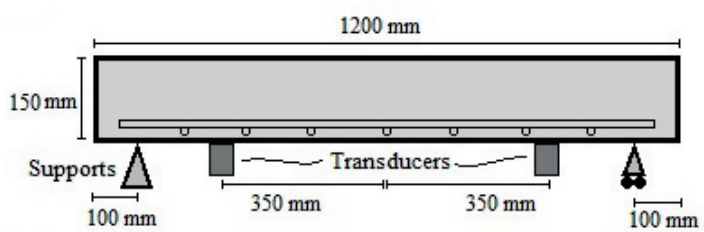

Figure 16. Concrete dimensions, reinforcement layout and transducer locations. Image from Fröjd and Ulriksen (2015).

A system was set up which enabled the transmission and measurement of both pulses and continuous waves, centered around 47 kHz. The continuous waves were sampled with a lock-in amplifier, which yielded the amplitude and phase of the continuous wave field, as detailed in section 2.4.2.1. The transient pulses were evaluated by the relative velocity change, as estimated with the stretching method

(see section 2.3.2.2), and the attenuation. The energy content of each measured pulse was calculated as

$$E = \sum_{k=1}^{N} \left[\frac{1}{2}(A_k + A_{k+1})\right]^2 \cdot \Delta t \qquad \textit{Eq. 18}$$

where A_k is the amplitude of the signal at sample k, Δt is the sample time and N is the number of samples. The energy measured for pulses transmitted through the undamaged sample was used as baseline. The dissipated energy for each state of damage was defined as the ratio between the current pulse energy and the baseline energy.

A downward load was applied at the center of the beam. The load was applied in steps with increasing force. Between each load step, the load was released before both continuous and pulsed measurements were performed. The measurements were thus made on the unloaded slab, and any effect on the coda should therefore be attributed to damage to the concrete rather than stress. Each measurement was repeated with a range of different driving signal amplitudes. This was done in order to create different signal-to-noise ratios. The signals with lower SNR are intended to simulate a greater distance between the transducers.

The amplitude of the continuous signals and the energy content of the pulses are shown in Figure 17 as a function of the concrete deflection during the preceding load step. The values are normalized with regard to the first measured energy/amplitude. Each sub-figure shows the amplitude and energy ratio for decreasing transmission signal levels. The uppermost left sub-figure shows data from measurements with a high signal-to-noise ratio. It can clearly be seen that the transmitted signal is increasingly attenuated as the concrete is damaged. The continuous and pulse transmissions show very similar sensitivity to the damage.
However, as the transmission signal level is decreased the pulse measurements become less coherent, and show little or no relation to the level of damage in the concrete. It is clear that the pulse is simply not measurable below the noise, even after averaging and filtering. The continuous signal data, however, measured by the lock-in amplifier, maintains its sensitivity to changes in the concrete even for extremely low signal levels; only for the lowest SNR is there some variance in the data at each load level. The results indicate that the continuous transmission display the same sensitivity as pulsed transmission, but is functional at lower signal levels.

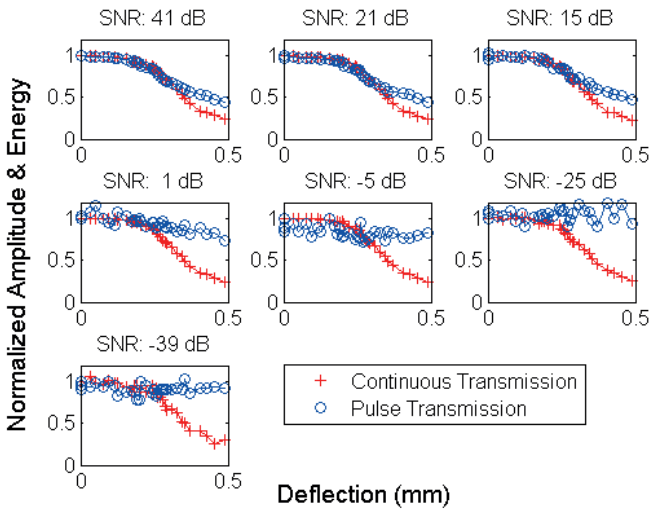

Figure 17. Amplitude measurements from continuous measurements and energy measurements from pulse measurements as a function of deflection of the concrete slab. The amplitude and energy are normalized relative the baseline measurement. The horizontal axis of each subplot corresponds to the deflection of the concrete slab during the preceding load step. Each consecutive subplot shows measurements for decreasing signal-to-noise (SNR) ratio.

In order to compare the sensitivity of the velocity change measurements for pulse transmission and the phase measurements for the continuous transmission, both data sets were normalized to the minimum value in the set of measurements before yielding of the reinforcement bars. These normalized relative values are shown in Figure 18, as a function of previous deflection of the slab. Each sub-figure displays similar measurements with decreasing signal-to-noise ratio.
As can be seen in Figure 18, for the transmissions with high signal-to-noise ratio, the velocity and phase measurements display very similar sensitivity to damage, with a clear relation to the previously experienced deflection of the concrete slab.
Similarly as for the attenuation measurements, in Figure 17, it is clear that for very low SNR the pulse measurements cannot distinguish between the pristine and damaged concrete due to the signal being buried under the noise. The phase measurement maintains it sensitivity even at extremely low signal levels.

The results show that both amplitude and phase measurement of continuous waves give indications of damage equal to similar measurements with pulse transmission, with the added benefit of being able to detect much weaker signals. The pulse transmissions lose their sensitivity to damage when the measured signal is of the same order of magnitude as the noise, while the continuous measurements maintain their sensitivity even at a SNR of ~-40 dB, and possibly lower.

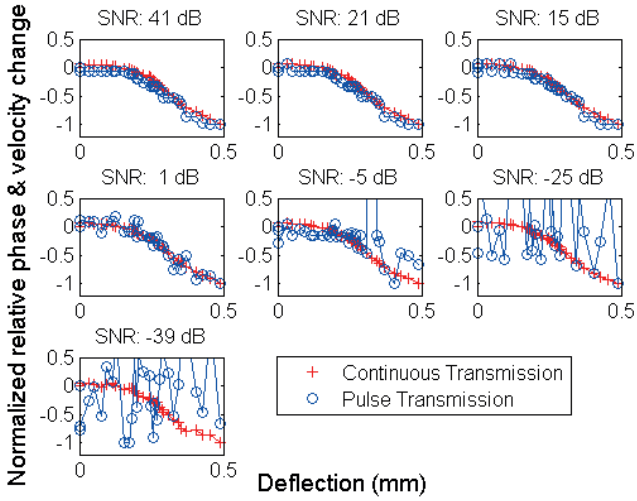

Figure 18. Phase measurements from continuous measurements and relative velocity change measurements from pulse measurements as a function of deflection of the concrete slab. The phase and velocity change are normalized relative the minimum value of the set of measurements before the yielding of the reinforcement bars. The horizontal axis of each subplot corresponds to the deflection of the concrete slab during the preceding load step. Each consecutive subplot shows measurements for decreasing signal-to-noise (SNR) ratio.

The presented pulse measurements are averaged with 20 samples of the waveform. Theoretically, SNR increases with the square-root of the number of samples, provided that the noise is truly white and the channel is stable. Under such conditions, this means that the pulse measurements would need to be averaged 10000 times in order to maintain sensitivity at -40 dB SNR.

The phase measurements give slightly earlier warning than the amplitude measurements, but both values are obtained simultaneously from the lock-in amplifier which means it is very little effort to design an SHM application which makes use of both parameters. The time-stretching method, used for the transient measurements, is computationally intensive as each measurement is correlated to many stretched baseline signals. In contrast, the phase measurements are read from the lock-in amplifier in almost real-time.

4.4 Locating damage using continuous diffuse wave fields

When using continuous diffuse wave fields, it is not possible to use localization schemes such as Locadiff, where the time evolution of the decorrelation of codas are used. However, it is reasonable to assume that damage which is located somewhat in between transmitting and receiving transducer will affect the wave

field more, compared to a distant region of damage. This is in agreement with the shape of sensitivity kernels for transient pulses, as described in section 2.3.2.4. Therefore it is possible to provide some rough localization of a damaged region, using a network of transducers. Such a network, consisting of 30 PZT transducers in a 3x10 grid, was installed on an 8x2 meter concrete floor slab. The system, and results are given in more detail in appended paper IV (Fröjd & Ulriksen 2016).

In each measurement cycle, each transducer once acted as transmitter, while all others acted as receivers. The transmitting transducer was excited with a 50 kHz continuous sinusoidal signal, and a multi-channel lock-in amplifier was used to measure the amplitude and phase at all receiver locations simultaneously. Then the system switched to the next transducer in line to act as transmitter, etc. Thus each measurement cycle yielded 30x29 amplitude and phase measurements. In order to acquire a single damage indicator, the amplitude and phase were used as input features in a Mahalanobis algorithm, according to section 3.4.2. It was found that this yielded more robust measurements than considering amplitude and phase separately.

In order to investigate the possibility of locating any damaged region, the floor slab was divided into a grid with the same layout as the grid formed by the transducers. Each box in the grid was thus slightly less than a square meter, and was assigned a value corresponding to the mean of the Mahalanobis distance for all transducer pairs whose direct propagation path intersects the box. Figure 19 shows, as an example, lines between the transducers in the pairs which are included in the evaluation of the grid coordinate between transducers 3, 4, 13 and 14. The grid coordinate is highlighted in red. Since all transducers are used reciprocally as transmitters and receivers, each one transducer pair provides two measurements, with reversed transmission. For example, the grid coordinate corresponding to the location of damage include both measurements from transmissions between transducer 3 and 4 and between transducer 4 and 3.

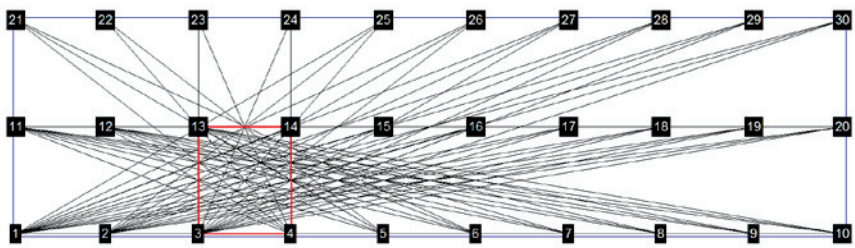

Figure 19. Illustration of the 8x2 meter concrete floor slab, and the layout of the transducers (numbered black squares). The black lines illustrate the transmitter-receiver pairs which were used to create the graphic value in the grid box between transducers 3, 4, 13 and 14 (red square). Image from Fröjd and Ulriksen (2016).

Damage was introduced to the concrete by use of a bolt gun. The bolt gun was not loaded with any bolts, but the piston was used to inflict impact damage in a repeatable manner. The shots were fired in the middle of the square defined by the transducers 3, 4, 13 and 14, as given in red in Figure 19. The visible damage to the concrete was superficial, with the deepest hole about 5 mm. The width of the holes varied from less than 1 cm to 4.5 cm. Figure 20 shows a close-up of the damage, as well as the order of the shots. Some superficial cracking can be seen around the holes, e.g., around hole number 1.

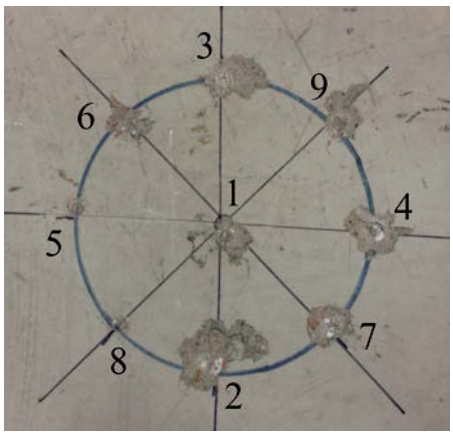

Figure 20. Close up of the damaged region after bolt gun shots to the surface of the concrete floor. For reference, the diameter of the blue circle is 15 cm

Between the shot events, continuous wave measurements were performed. Figure 21 displays the resulting images from the tomographic procedure. The grayscale shows the deviation from the baseline measurements, i.e. before any shots. The subfigures show the results after increasing the number of shots, as indicated by the red dots. The imaging method successfully identifies the grid coordinate of the damage as the box with the highest mean Mahalanobis distance from the baseline data.

Additionally, it is evident that the deviation from the baseline increases as the damage level increases. This increase is seen over the entire floor slab, and there is a misleading particularly high indication in the grid box 8-9-18-19, but at all damage levels the correct grid box is assigned the highest value.

It should be noted that even the first damage level yields a mean Mahalanobis distance of 72 in the grid box corresponding to the damaged area. This is a substantial deviation, corresponding to 72 standard deviations from the mean of the baseline data set, and the possibility of detecting even slighter damage seems likely.

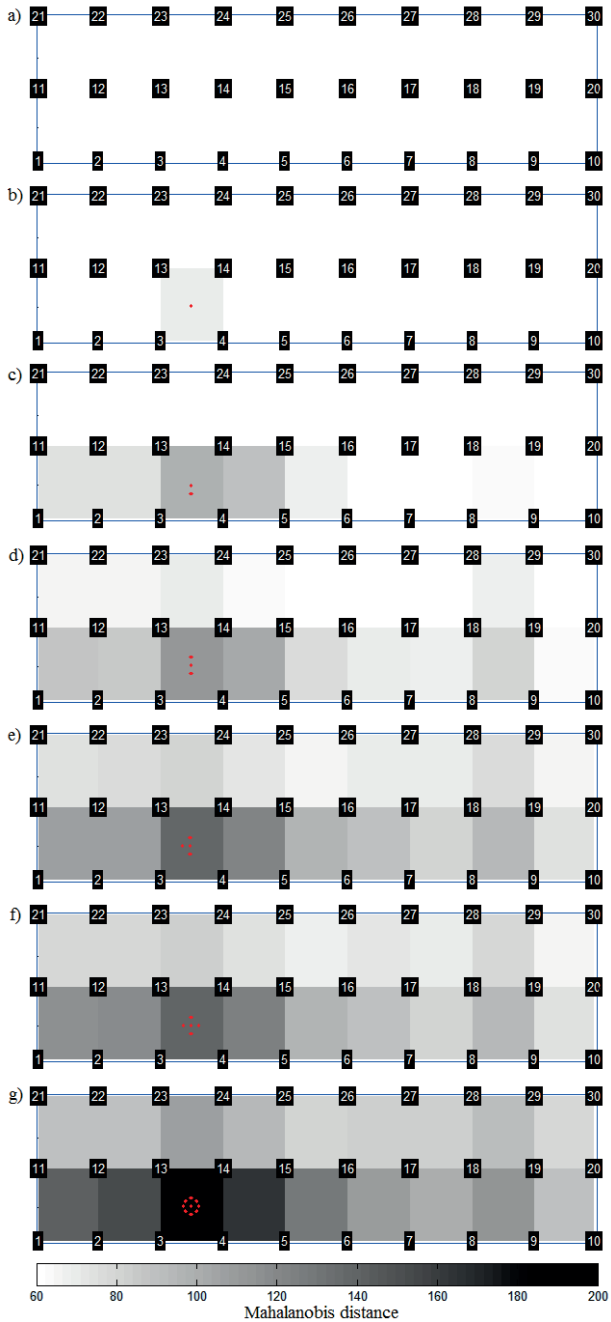

Figure 21. Mahalanobis distance from the baseline data for measurements at different damage levels. a)-g) results after 0, 1, 2, 3, 4, 5 and 9 shots. The red dots indicate locations of bolt gun shots. Image from Fröjd and Ulriksen (2016).

It is of interest to see if similar localization is possible with a sparser network of transducers. An example is shown in Figure 22 (a), where only transducers 4, 8, 11, 20, 22, 26 and 30 are used. It is evident from the figure that it is possible to localize the damage with sparser networks. Further removal of transducers resulted in a gradual loss of ability to locate the damage.
Figure 22 (b) shows a lower resolution localization using only the data from the four transducers in the corners of the slab. This is encouraging for the scalability of the system; a system similar to that in the presented study but with several meters between the closest transducers would have great utility. Scaling the experiment is not straightforward, however, as the distance to the reflective boundaries affects the emerging diffuse wave field.

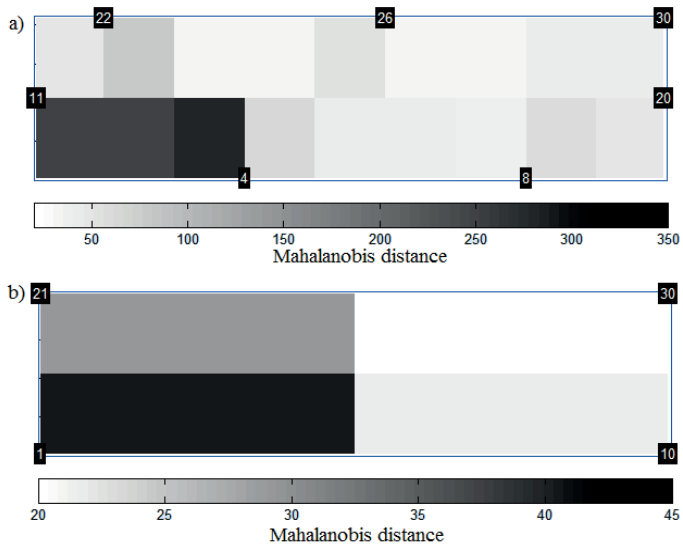

Figure 22. Mahalanobis distance from the baseline data for sparse networks of transducers at damage level 6. a) Transducers 4, 8, 11, 20, 22, 26 and 30 were used. b) Transducers 1, 10, 21, and 30 were used. Image from Fröjd and Ulriksen (2016).

4.5 Compensation of environmentally induced variations

As previously stated, diffuse wave field measurements are sensitive to variations in environmental conditions. Even when left undisturbed, the previously mentioned SHM system on the 8x2 meter concrete floor slab yielded data with large variations over time. These variations can be attributed mainly to temperature variations in the laboratory and exposure of the concrete and transducers to sunlight. Figure 23 shows a photograph of the concrete floor slab in the laboratory environment, with the large windows admitting the sun in different angles over the course of each day.

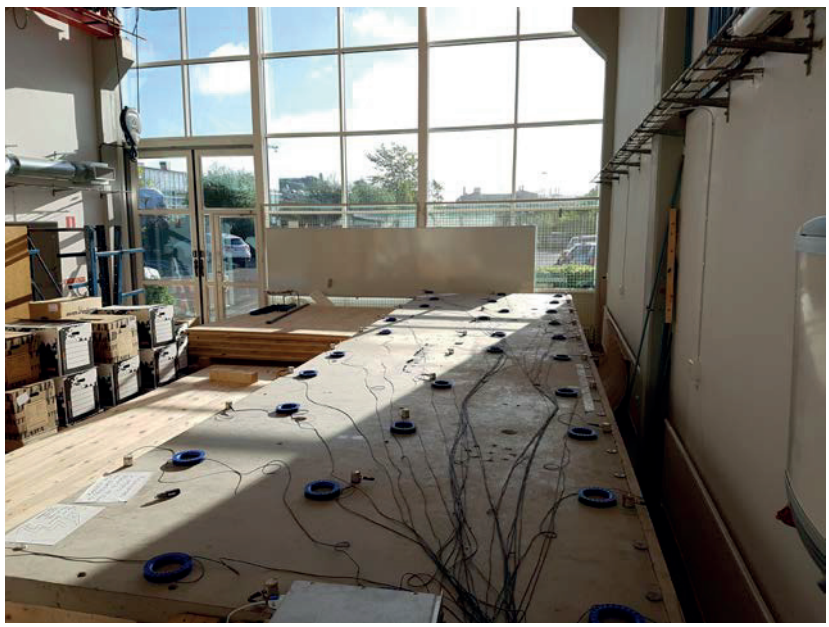

Figure 23. The concrete floor slab, used throughout the course of the thesis work. During the summer the sunlight raise the temperature in the room significantly and rapidly.

As discussed in section 3.5, a machine learning method is necessary to compensate for the environmental variations, so that actual damage can be detected. An experiment was set up to demonstrate the usefulness of the Mahalanobis distance, to enable the detection of sudden damage events using continuous diffuse wave fields, even in the presence of severe environmental variations. This work is presented in more detail in appended paper V (Patrik Fröjd & Ulriksen 2017).
The same SHM system as described in the previous section was used to monitor the floor slab over the course of 25 days. In order to retrieve more information, measurements were performed at six different frequencies, as opposed to only one;

13, 40, 42, 46, 48, and 50 kHz. These frequencies were chosen to correspond to the resonant frequencies of the transducers. The lower frequency signals, at 13 kHz, were assumed to be rather insensitive to damage but sensitive to temperature variations. Thus, they can be useful in the algorithm to differentiate between changes caused by damage and those caused by temperature. Higher frequencies could not be included as the available multichannel lock-in amplifier can only measure signals with frequencies below ~50 kHz.
Only eight of the PZT transducers on the floor were included, as this more resembles a realistic network spacing. The transducers used were numbers 1, 4, 7, 10, 21, 24, 27 and 30, according to Figure 19.
Measurements were performed every 35 minutes. The general temperature in the laboratory was also monitored, and is displayed in Figure 24.

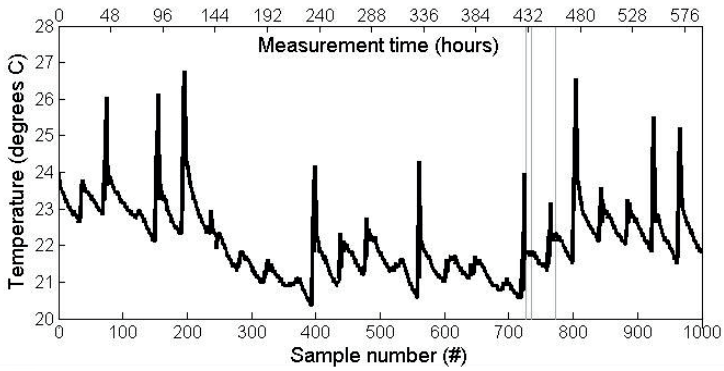

Figure 24. The temperature in the laboratory during the 25 day experiment. The upper x-axis shows time, in hours, while the lower shows sample number of the SHM system. Image from Fröjd and Ulriksen (2017).

Damage was introduced to the concrete by impact hits from a bolt gun, similarly as in the previous section. All shots were performed between transducers 27 and 18, according to the numbering in Figure 19. Two shots were performed on the 20:th day, at 430 and 435 hours, and one on the 21:st day, at 457 hours. This corresponds to just before the SHM samples 727, 735 and 773. The times for the three shots are indicated by the gray vertical lines in Figure 24. The damage was similar to the previously described study; superficial holes in the concrete, on the scale of 1 cm.

If only one measured feature is viewed, it is obvious that the variations caused by the environmental conditions are of the same order as, and even larger than, the effects of the impact hits. As an example, Figure 25 shows the amplitude and phase of the 50 kHz measurements between transducers 7 and 27. The samples which correspond to the measurements directly after each shot are again highlighted by vertical gray lines. From neither of these plots can the times of the impact hits be deduced.

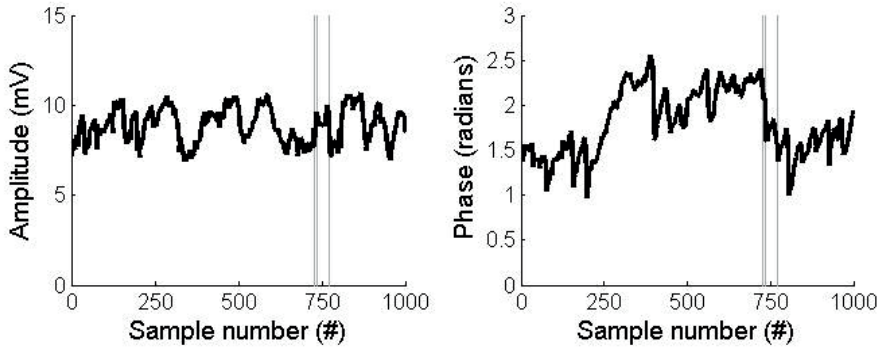

Figure 25. Amplitude (left) and phase (right) as a function of sample number for the frequency 50 kHz. Data are taken from the transmissions between transducers 27 and 7. The gray vertical lines indicate the times of the damage events. Image from Fröjd and Ulriksen (2017)*.*

In order to normalize the data, the Mahalanobis distance was used. The amplitude and phase for each of the six frequencies were used as features in the algorithm. Each new measurement made use of the previous 300 data points as baseline. This means that the baseline is continuously updated, in a moving window fashion. This works well when sudden appearance of damage is to be detected, as was the aim in this study. This means that the second measurement after an introduced damage will have a sample from the damaged structure included in its baseline. It will therefore be assigned a lower Mahalanobis distance. Each damage event will therefore appear as a spike, in a time-flow curve of the Mahalanobis distance.

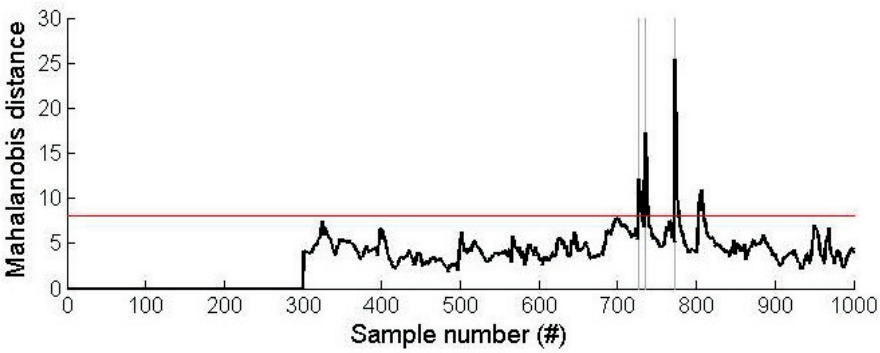

Figure 26. Mahalanobis distance for the measurements between transducers 27 and 7. A threshold line is set at a Mahalanobis distance of 8 (red horizontal line). The gray vertical lines indicate the times of the damage events. Image from Fröjd and Ulriksen (2017)*.*

Figure 26 shows the Mahalanobis distance for the course of the 25 days of the experiment. The first 300 measurements are used as the first baseline and are set to zero. For every new measurement, the baseline window is moved one sample ahead. Some inherent deviation from the baseline is present at all times, with some variation. This is expected, since the environmental variation compensation is not perfect and there are some uncertainties in each measurement. However, some measurements clearly stand out in the figure, and these can be distinguished from the normal condition by the choice of a threshold value, which results in a novelty detection method. These cases occur at sample numbers 727, 735, 773 and 805. The first three correspond to three clearly resolved damage events.
The peak around 805 is not caused directly by a damage event, but is a false positive that is not successfully suppressed by the algorithm. This has two possible explanations:

- First, as can be seen from Figure 24, this was a particularly warm day with strong sunlight. The weather had changed suddenly from the previous seven days, and the baseline did not contain enough data.
- Second, the temperature peak occurs on the first day after the last damage event. It is reasonable to assume that the influence of the environmental variations on the measurements can be altered by the damage, e.g. by tension reliefs, exposure of inner materials, etc., and that the Mahalanobis model has not yet "learned" this new behavior. If this is the case, then the variation is partly and indirectly caused by the damage, and it should rightfully be detected by the SHM system.

Figure 27 shows the results from the tomographic procedure, as detailed in the previous section. The left subfigures (a-g) are constructed using only phase data from the 50 kHz measurements. The gray scale corresponds to the deviations from the mean of the baseline data set, expressed in the number of standard deviations of the baseline set (averaged over the grid boxes in the tomography). This corresponds to a one-dimensional version of the Mahalanobis distance.
The right subfigures (h-n) are constructed from the Mahalanobis distance, where both amplitude and phase data, from all frequencies, have been used.
The sample numbers 400, 600, 700, 727, 735, 773, and 805 are shown. In the images using only one set of phase data, false positive indications are given at random times, as seen in Figure 27 (a–c), and there is no noticeable difference before and after the damage. It is not possible to distinguish between the effects of the environmental variations on the structure and the effects on the measurement system.
The images constructed with the Mahalanobis distance are better in this regard. Here, thresholds can easily be set to show no indications when there is no damage (Figure 27 (h–j)). The time stamps corresponding to the damage events (Figure 27

(k-m)) clearly indicate a deviation from normal behavior, and they also provide a rough indication as to between which transducers the damage occurred.
Some indications are seen all over the slab, which is expected since the continuous diffuse wave fields consist of multiple scattered waves and boundary reflections.

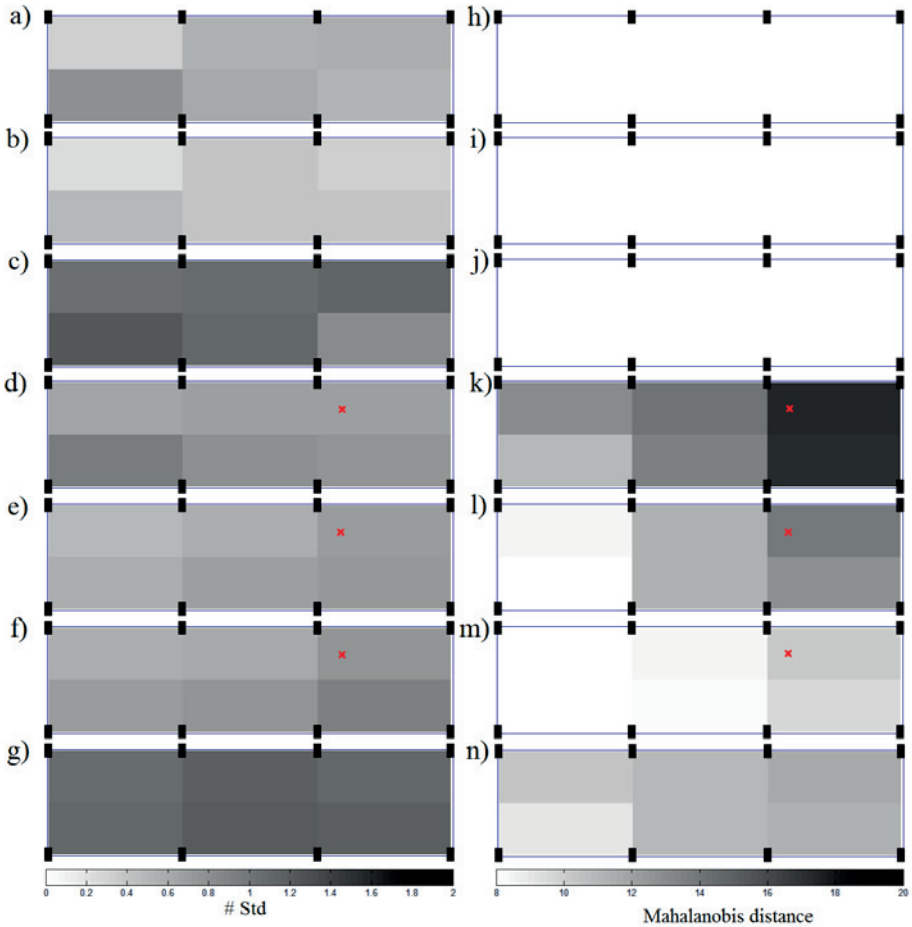

Figure 27. Results from the tomographic procedure at different samples. The left subfigures (a-g) are constructed using only phase data from the 50 kHz measurements. The right subfigures (h-n) are constructed from the Mahalanobis distance, making use of all frequencies. Subfigures (a)-(g) and (h)-(n) correspond to measurement samples 400, 600, 700, 727, 735, 773, and 805. The red crosses denote the location of the damage.

This phenomenon is expected to be somewhat less pronounced in larger structures where the transducers generally will be placed further from reflective boundaries. The images corresponding to the false positive at 805 (Figure 27 (n)) show a slightly more homogeneous deviation over the slab, which is expected for a deviation

caused by global environmental variations. However, the grid coordinate containing the damaged area shows a slightly higher deviation than the rest of the slab. This possibly supports the reasoning described above—that this peak, at least in part, is caused indirectly by real damage.

5 Conclusions and future work

5.1 Main scientific contributions

The aim of this work has been to further the knowledge of SHM systems for large concrete structures, making use of diffuse propagating mechanical waves. Rather than presenting new theory, the focus has been on experimental demonstrations and comparisons of existing techniques, as well as presenting new applications for existing types of measurements and transducers.

When scaling up monitoring systems, from laboratory scale to the scale of real civil structures, it is necessary to enable useful transmission of signals over distances of several meters. The obvious approach is to make use of signals with lower frequency than those often used in published coda wave interferometry work, as these are less attenuated as they propagate through the material. Although much work has previously been reported where diffuse waves have been used in the lower frequency domains, there was a lack of knowledge as to the trade-off between range and what sizes of damage which can be expected to be detected. By using the same techniques in different frequency ranges to detect the same damage, the work presented here gives some practical demonstrations as to this trade-off. Though additional efforts need to be put into this area, the preliminary recommendation is that signals in the simple scattering regime (~50-150 kHz) are suitable for large structures; signals in this range can easily be transmitted over relatively large distances and still be used to detect cracks and holes which are even smaller than the aggregates in the concrete. It has been demonstrated that waves in the single-kHz range are not suitable for detecting local damage, such as cracks and holes. However, earlier studies has demonstrated the use of such signals to track stress changes, and temperature variations. For such applications voice coil transducers, in particular geophones, are shown to be viable alternatives for piezoelectric transducers in both transmitting and receiving mode.

It has also been shown that transmitting continuous waves yields measurements with very similar sensitivity as traditional, transient CWI measurements. The benefit is that narrow-band methods for sampling the measured signal (e.g. by using lock-in amplifiers) can be employed, which enables the detection of significantly weaker signals and excellent noise rejection. By being able to detect weaker signals, larger distances are possible between transmitting and receiving transducers. This is particularly useful if the application necessitates higher frequency signals.

Localizing damage with diffuse waves is not trivial, and is made even more difficult when using continuous wave transmission, since all time-resolution is lost in the signals. However, by assuming a higher degree of sensitivity in a region between the

transmitting and receiving transducers than in surrounding regions, simple tomographic procedures have been shown to provide some localization of damage. This should be considered a rough localization only, with the region of interest being on the order of one, or a few, square meters, depending on the density of the used transducer network. However, it is my opinion that a rough localization is sufficient in SHM of large civil structures; it will be a long time before SHM completely replace other inspection methods, non-destructive or otherwise. SHM should initially be considered a complementary tool, where a realistic scenario would be that an SHM system detects some anomaly in a general region, whereby more traditional inspection methods are employed to provide more detailed information. A localization to within a couple of square meters is an attractive prospect in a structure which is a few hundreds of square meters large.

Diffuse waves, whether generated by continuous waves or transient pulses, are very susceptible to changes in environmental conditions. Measurements with high dimensionality, such as full waveforms, provide opportunities to extract features which are less sensitive to environmental variations. Narrow-band measurements are intrinsically low dimensional, with only scalar values of amplitude and phase of each frequency being available. It has been shown in this work that using several single-frequency measurements, and employing some machine learning algorithm, in this case the Mahalanobis distance, it is possible to create a feature which can be used to mostly distinguish between variations caused by changing environmental conditions and those caused by damage.
It is an absolute necessity to have some method with which to counter the variations caused by the environment, as these otherwise will either cause false alarms or mask cases of real damage.

5.2 Suggestions for future work

The work presented in this thesis has been aimed at developing and evaluating methods which are useful in realistic scenarios, on large civil structures. That being said, all experiments have been performed in laboratory environments on test specimens. The obvious next step is to evaluate the methods on real structures, in realistic environments, with also slow deterioration of structure materials.
This is a significant undertaking from a practical point of view, and has not been feasible during the course of this thesis work.

More advanced localization methods can most likely be created for continuous wave field measurements, than the one presented herein. For larger structures than the specimens used in these studies, some weighting by transducer distance could be useful. It is possible that inversion procedures, similar to those in e.g. Locadiff, that make use of steady-state sensitivity kernels can be employed.

The system could also make use of the transducers for passive monitoring between active measurements, and thus combine the diffuse-wave measurements with AE measurements.

Some experiments have been performed where the localization of multiple damages have been attempted. Though initial results are promising, further studies must be performed in order to draw conclusions.

The measurements presented in this thesis all make use of linear phenomena; attenuation and velocity change. Much of the latest published work in CWI make use of nonlinear modulation. These techniques are very much applicable when using continuous waves, and could be very well suited for practical SHM applications. Lock-in amplifiers could easily be used for detecting energy at emerging frequencies, like harmonics or modulation frequencies. Apart from yielding measurements which are even more sensitive to material changes than linear diffuse wave measurements, nonlinear measurements have been shown to be less sensitive to environmental variations.

Other machine learning algorithms could likely be used to improve compensation for environmental variations further. Farrar and Worden (Farrar & Worden 2013) proposed the use of principal component analysis to reduce the number of features, followed by the Mahalanobis distance procedure. The results presented in this thesis were not improved by this procedure. But, by including more transmission frequencies in the continuous wave measurements the number of features would increase, and the described procedure could be useful. If enough frequencies are included, time-domain waveforms can theoretically be constructed, using the inverse Fourier transform.
Artificial neural networks are also increasingly employed in SHM research, and could likely be of interest for diffuse wave measurements as well. In general, a combination of different compensation methods is more likely to be successful than relying on a single one.

References

Abdullah, A. & Sichani, E.F., 2008. Experimental study of attenuation coefficient of ultrasonic waves in concrete and plaster. *The International Journal of Advanced Manufacturing Technology*, 44(5–6), pp.421–427.

Abraham, O. et al., 2014. Monitoring of a large cracked concrete sample with non-linear mixing of ultrasonic coda waves. In *7th European Workshop on Structural Health Monitoring*. Nantes, pp. 1412–1418.

Aki, K., 1956. Correlogram analyses of seismograms by means of a simple automatic computer. *Journal of Physics of the Earth*, 4, pp.71–79.

Brotherhood, C.J., Drinkwater, B.W. & Dixon, S., 2003. The detectability of kissing bonds in adhesive joints using ultrasonic techniques. *Ultrasonics*, 41(7), pp.521–529.

Carden, E.P. & Fanning, P., 2004. Vibration Based Condition Monitoring: A Review. *Structural Health Monitoring*, 3(4), pp.355–377.

Chandrasekhar, S., 1960. *Radiative transfer*, Dover Publications.

Clarke, T., Simonetti, F. & Cawley, P., 2010. Guided wave health monitoring of complex structures by sparse array systems: Influence of temperature changes on performance. *Journal of Sound and Vibration*, 329(12), pp.2306–2322.

Croxford, A.J. et al., 2010. Efficient temperature compensation strategies for guided wave structural health monitoring. *Ultrasonics*, 50(4–5), pp.517–28.

Daponte, P., Maceri, F. & Olivito, R.S., 1995. Ultrasonic signal-processing techniques for the measurement of damage growth in structural materials. *IEEE Transactions on Instrumentation and Measurement*, 44(6), pp.1003–1008.

Deroo, F., 2009. *Damage detection in concrete using diffuse ultrasound measurements and an effective medium theory for wave propagation in multi-phase materials*. Georgia Institute of Technology.

Deroo, F. et al., 2010. Detection of damage in concrete using diffuse ultrasound. *The Journal of the Acoustical Society of America*, 127(L), pp.3315–3318.

Doebling, S.W. et al., 1996. *Damage identification and health monitoring of structural and mechanical systems from changes in their vibration characteristics: A literature review*, Los Alamos, NM.

Drouillard, T.F., 1996. A history of acoustic emission. *Journal of acoustic emission*, 14(1), pp.1–34.

Fan, W. & Qiao, P., 2011. Vibration-based damage identification methods: A review and comparative study. *Structural Health Monitoring*, 10(1), pp.83–111.

Farrar, C.R. & Worden, K., 2013. *Structural health monitoring - a machine learning perspective*, Chichester, West Sussex, UK: John Wiley & Sons, Ltd.

Fröjd, P., 2016. *Structural health monitoring of large concrete structures*. Lund

University. Available at: http://scitation.aip.org/content/asa/journal/jasa/137/6/10.1121/1.4922011.
Fröjd, P. & Ulriksen, P., 2015. Amplitude and phase measurements of continuous diffuse fields for structural health monitoring of concrete structures. *NDT & E International*, 77, pp.35–41.
Fröjd, P. & Ulriksen, P., 2016. Continuous wave measurements in a network of transducers for structural health monitoring of a large concrete floor slab. *Structural Health Monitoring*, 15(4), pp.403–412.
Fröjd, P. & Ulriksen, P., 2017. Detecting damage events in concrete using diffuse ultrasound structural health monitoring during strong environmental variations. *Structural Health Monitoring*.
Fröjd, P. & Ulriksen, P., 2015. Efficiency of some voice coil transducers in low frequency reciprocal operations. *The Journal of the Acoustical Society of America*, 137(6), p.EL490-5.
Fröjd, P. & Ulriksen, P., 2017. Frequency selection for coda wave interferometry in concrete structures. *Ultrasonics*.
Gabrielson, T.B., 1997. Free-mass reciprocity calibration. *Journal of the Acoustical Society of America*, 102(5), pp.2800–2808.
Garnier, V. et al., 2013. Acoustic techniques for concrete evaluation: Improvements, comparisons and consistency. *Construction and Building Materials*, 43, pp.598–613.
Garnier, V. et al., 2014. Non Destructive Testing of Concrete : Transfer from Laboratory to On-site Measurement. In *EWSHM - 7th European Workshop on Structural Health Monitoring*. pp. 1489–1496.
Gonzalez, I. & Karoumi, R., 2015. BWIM aided damage detection in bridges using machine learning. *Journal of Civil Structural Health Monitoring*, 5(5), pp.715–725.
Graff, K.., 1975. *Wave Motion in ElasticSolids*, Oxford University Press, London.
Gu, H. et al., 2006. Concrete early-age strength monitoring using embedded piezoelectric transducers. *Smart Materials and Structures*, 15(6), pp.1837–1845.
Hadziioannou, C. et al., 2009. Stability of monitoring weak changes in multiply scattering media with ambient noise correlation: laboratory experiments. *The Journal of the Acoustical Society of America*, 125, pp.3688–3695.
Van Hauwaert, A., Thimus, J.-F. & Delannay, F., 1998. Use of ultrasonics to follow crack growth. *Ultrasonics*, 36(1–5), pp.209–217.
Hill, J.M. & Dewynne, J.N., 1987. *Heat conduction*, Blackwell Scientific Publications.
Hilloulin, B., Zhang, Y., Abraham, O., Durand, O., et al., 2014. Closed crack detection in concrete with coda wave non-linear modulation. In *7th European Workshop on Structural Health Monitoring*. Nantes, pp. 1434–1440.
Hilloulin, B., Zhang, Y., Abraham, O., Loukili, A., et al., 2014. Small crack detection in cementitious materials using nonlinear coda wave modulation. *NDT & E*

International, 68, pp.98–104.
Hu, W.-H. et al., 2017. Continuous dynamic monitoring of a prestressed concrete bridge based on strain, inclination and crack measurements over a 14-year span. *Structural Health Monitoring: An International Journal*.
Ishimaru, A., 1978. *Wave propagation and scattering in random media*, Academic Press.
Kamada, T., Nagataki, S. & Iwanami, M., 1997. Evaluation of material deterioration in concrete by nondestructive testing methods. In *International Conference on Engineering Materials, Ottawa, Canada, JSCE, 95*. pp. 453–466.
Kanu, C. & Snieder, R., 2012. Numerical computation of the sensitivity kernel for time-lapse monitoring with multiply scattered waves. *Geophysical Journal International*, 203(3), pp.1923–1936.
Kanu, C. & Snieder, R., 2015. Time-lapse imaging of a localized weak change with multiply scattered waves using numerical-based sensitivity kernel. *Journal of Geophysical Research B: Solid Earth*, 120(8), pp.5595–5605.
Konstantinidis, G., Wilcox, P.D. & Drinkwater, B.W., 2007. An Investigation Into the Temperature Stability of a Using Permanently Attached Sensors. *IEEE Sensors Journal*, 7(5), pp.905–912.
Lamb, H., 1917. On Waves in an Elastic Plate. *Proceedings of the Royal Society*, 93(648), pp.114–130.
Liao, W.-I. et al., 2011. Structural health monitoring of concrete columns subjected to seismic excitations using piezoceramic-based sensors. *Smart Materials and Structures*, 20(12), p.125015.
Lillamand, I. et al., 2010. Acoustoelastic effect in concrete material under uni-axial compressive loading. *NDT & E International*, 43(8), pp.655–660.
Lobkis, O. & Weaver, R., 2003. Coda-Wave Interferometry in Finite Solids: Recovery of P-to-S Conversion Rates in an Elastodynamic Billiard. *Physical Review Letters*, 90(25), p.254302.
Lu, Y. & Michaels, J.E., 2005. A methodology for structural health monitoring with diffuse ultrasonic waves in the presence of temperature variations. *Ultrasonics*, 43(9), pp.717–31.
Lydon, M. et al., 2016. Recent developments in bridge weigh in motion (B-WIM). *Journal of Civil Structural Health Monitoring*, 6(1), pp.69–81.
Mahalanobis, P.C., 1936. On the generalised distance in statistics. *Proceedings of the National Institute of Sciences of India*, 2(1), pp.49–55.
Margerin, L. et al., 2016. Sensitivity kernels for coda-wave interferometry and scattering tomography: theory and numerical evaluation in two-dimensional anisotropically scattering media. *Geophysical Journal International*, 204(1), pp.650–666.
Mayor, J., Margerin, L. & Calvet, M., 2014. Sensitivity of coda waves to spatial variations of absorption and scattering: Radiative transfer theory and 2-D examples. *Geophysical Journal International*, 197(2), pp.1117–1137.
McCann, D.. & Forde, M.., 2001. Review of NDT methods in the assessment of

concrete and masonry structures. *NDT & E International*, 34(2), pp.71–84.
Moradi-Marani, F. et al., 2014. Evaluating the damage in reinforced concrete slabs under bending test with the energy of ultrasonic waves. *Construction and Building Materials*, 73, pp.663–673.
Niederleithinger, E., 2014. Coda wave interferometry used to localize compressional load effects in a concrete specimen. In *EWSHM-7th European workshop on structural health monitoring*. pp. 1427–1433.
Niederleithinger, E. et al., 2015. Embedded Ultrasonic Transducers for Active and Passive Concrete Monitoring. *Sensors*, 15, pp.9756–9772.
Obermann, A. et al., 2013. Depth sensitivity of seismic coda waves to velocity perturbations in an elastic heterogeneous medium. *Geophysical Journal International*, 194(1), pp.372–382.
Paasschens, J.C.J., 1997. Solution of the time-dependent Boltzmann equation. *Physical Review E*, 56(1), pp.1135–1141.
Pacheco, C. & Snieder, R., 2005. Time-lapse travel time change of multiply scattered acoustic waves. *Journal of acoustical society of america*, 118, pp.1300–1310.
Park, S. et al., 2006. Multiple Crack Detection of Concrete Structures Using Impedance-based Structural Health Monitoring Techniques. *Experimental Mechanics*, 46(5), pp.609–618.
Planès, T. et al., 2014. Decorrelation and phase-shift of coda waves induced by local changes : multiple scattering approach and numerical validation. *Waves in Random and Complex Media*, 24(2), pp.99–125.
Planès, T. et al., 2013. LOCADIFF: Locating a weak change with diffuse ultrasound. In *AIP Conference Proceedings*. AIP Publishing, pp. 405–411.
Planès, T. & Larose, E., 2013. A review of ultrasonic Coda Wave Interferometry in concrete. *Cement and Concrete Research*, 53, pp.248–255.
Ploix, M. et al., 2009. Possibilistic NDT data fusion for evaluating concrete structures. In *NDTCE'09, Non-Destructive Testing in Civil Engineering Nantes*. Nantes, pp. 1–6.
Ramamoorthy, S.K., Kane, Y. & Turner, J.A., 2004. Ultrasound diffusion for crack depth determination in concrete. *Journal of acoustical society of america*, 115(2), pp.523–9.
Rayleigh, Lord, 1885. On waves propagated along the plane surface of an elastic solid. *London Mathematical Society Proceedings*, 17(1), pp.4–11.
Richardson, J.M., 1979. Harmonic generation at an unbonded interface—I. Planar interface between semi-infinite elastic media. *International Journal of Engineering Science*, 17(1), pp.73–85.
Richart, F.E., Woods, R.D. & Hall, J.R., 1970. *Vibrations of soils and foundations*, Prentice-Hall International Inc.
Rossetto, V. et al., 2011. Locating a weak change using diffuse waves: Theoretical approach and inversion procedure. *Journal of Applied Physics*, 109(3), p.34903.

Rytter, A., 1993. *Vibrational Based Inspection of Civil Engineering Structures*. University of Aalborg.

Scheerer, R.M. & Lager, D., 2014. Validation of temperature compensation techniques for impact damage detection and localization using ultrasonic sparse arrays. In *EWSHM-7th European workshop on structural health monitoring*. pp. 387–394.

Schurr, D.P. et al., 2011. Damage detection in concrete using coda wave interferometry. *NDT & E International*, 44(8), pp.728–735.

Sheng, P., 1995. *Introduction to Wave Scattering, Localization and Mesoscopic Phenomena*, San Diego: Academic Press Inc.

Shokouhi, P. et al., 2010. Using ultrasonic coda wave interferometry for monitoring stress-induced changes in concrete. In *Proceedings of the EEGS Annual Meeting 23rd SAGEEP, Symposium of the Application of Geophysics to Engineering and Environmental Problems, 11*. Keystone, CO, USA, pp. 650–654.

Snieder, R., 2002. Coda wave interferometry and the equilibration of energy in elastic media. *Physical Review E - Statistical, Nonlinear, and Soft Matter Physics*, 66(4), pp.1–8.

Song, G. et al., 2007. Concrete structural health monitoring using embedded piezoceramic transducers. *Smart Materials and Structures*, 16(4), pp.959–968.

Song, G., Gu, H. & Mo, Y.-L., 2008. Smart aggregates: multi-functional sensors for concrete structures—a tutorial and a review. *Smart Materials and Structures*, 17(3), p.33001.

Sousa, H. et al., 2011. Design and implementation of a monitoring system applied to a long-span prestressed concrete bridge. *Structural Concrete*, 12(2), pp.82–93.

Sousa, H., Bento, J. & Figueiras, J., 2013. Construction assessment and long-term prediction of prestressed concrete bridges based on monitoring data. *Engineering Structures*, 52, pp.26–37.

Thompson, R.B., 1977. Harmonic generation of longitudinal elastic waves. *The Journal of the Acoustical Society of America*, 62(1), p.33.

Warnemuende, K. & Wu, H.-C., 2004. Actively modulated acoustic nondestructive evaluation of concrete. *Cement and Concrete Research*, 34(4), pp.563–570.

Warnemuende, K. & Wu, H.-C., 2005. Effect of geometric non-linearity on acoustic modulation. In T. Kundu, ed. *Health Monitoring and Smart Nondestructive Evaluation of Structural and Biological Systems IV*. SPIE Press, pp. 399–405.

Warnemuende, K.L. & Wu, H.-C., 2004. High sensitivity NDE in concrete: enhancement of energy dispersion using acoustic perturbation. In T. Kundu, ed. *Health Monitoring and Smart Nondestructive Evaluation of Structural and Biological Systems III*. SPIE Press, pp. 127–138.

Weaver, R.L., 1982. On diffuse waves in solid media. *Proceedings of the U.S. National Congress of Applied Mechanics*, 1608, p.471.

Wielandt, E., 2012. Seismic sensors and their calibration. In P. Bormann, ed. *New manual of seismological observatory practice 2*. IASPEI, GFZ German Research Centre for Geosciences, pp. 1–49.

Wiggenhauser, H. & Niederleithinger, E., 2013. Innovative Ultrasonic Techniques for Inspection and Monitoring of Large Concrete Structures V. L'Hostis & R. Gens, eds. *EPJ Web of Conferences*, 56, p.4004.

Worden, K. et al., 2007. The fundamental axioms of structural health monitoring. *Proceedings of the Royal Society A: Mathematical, Physical and Engineering Sciences*, 463(2082), pp.1639–1664.

Worden, K. & Dulieu-Barton, J.M., 2004. An Overview of Intelligent Fault Detection in Systems and Structures. *Structural Health Monitoring*, 3(1), pp.85–98.

Wu, H.-C. & Warnemuende, K., 2000. Nonlinear acoustic nondestructive testing for concrete durability. In A. E. Aktan & S. R. Gosselin, eds. *Nondestructive Evaluation of Highways, Utilities, and Pipelines IV*. SPIE Press, pp. 501–507.

Zhang, Y. et al., 2016. Diffuse ultrasound monitoring of stress and damage development on a 15-ton concrete beam. *Journal of acoustical society of america*, 139(April), pp.1691–1701.

Zhang, Y. et al., 2011. Following stress level modification of real size concrete structures with CODA wave interferometry (CWI). *AIP Conference Proceedings*, 1335(2011), pp.1291–1298.

Zhang, Y. et al., 2017. Nonlinear Coda Wave Interferometry for the global evaluation of damage levels in complex solids. *Ultrasonics*, 73, pp.245–252.

Zhang, Y. et al., 2013. Nonlinear mixing of ultrasonic coda waves with lower frequency-swept pump waves for a global detection of defects in multiple scattering media. *Journal of Applied Physics*, 113(6), p.64905.

Zhang, Y. et al., 2012. Study of stress-induced velocity variation in concrete under direct tensile force and monitoring of the damage level by using thermally-compensated Coda Wave Interferometry. *Ultrasonics*, 52(8), pp.1038–1045.

Zhang, Y. et al., 2013. Validation of a thermal bias control technique for Coda Wave Interferometry (CWI). *Ultrasonics*, 53(3), pp.658–64.

Zhou, C. et al., 2013. Evaluation of fatigue cracks using nonlinearities of acousto-ultrasonic waves acquired by an active sensor network. *Smart Materials and Structures*, 22(1), p.15018.

Part II - Appended publications

Paper I

Efficiency of some voice coil transducers in low frequency reciprocal operations

Patrik Fröjd and Peter Ulriksen
Department of Engineering Geology, Faculty of Engineering, Lund University, John Ericssons väg 1, SE-22100 Lund, Sweden
patrik.frojd@tg.lth.se, peter.ulriksen@tg.lth.se

Abstract: The feasibility of using different voice coil transducers in applications with reciprocal transducers of mechanical waves is investigated. It was speculated that voice coil transducers could be a more efficient alternative to piezoelectric transducers in low frequency ranges. Five different voice coil transducers, originally constructed for either transmission or reception, were characterized in both modes of operation. A piezoelectric ceramic disk was used for comparison between the transducer types. The results show that voice coils indeed can function as reciprocal transducers and that the most sensitive of the evaluated transducers is more efficient than the piezoelectric disk for low frequencies.

Date Received: December 9, 2014 **Date Accepted:** May 22, 2015

1. Introduction

The purpose of this study is to investigate the feasibility of using different voice coil transducers in applications with transducers in reciprocal operation (i.e., both as transmitters and receivers of mechanical waves). The reciprocity of voice coils is established and utilized in reciprocal transducer calibration (e.g., Ackerman, 1957; Gabrielson, 1997; Levy and Bouche, 1956). Reciprocal operation is of interest in applications with networks of transducers in which transmitter-receiver pairs are alternated. One example of such applications are structural health monitoring (SHM) systems with transducers in a network taking turn to generate and receive propagating and standing waves in a structure. The possible number of transmitter-receiver pairs in such a network increases greatly if each transducer can be used to both send and receive.

Such SHM systems most commonly use lead zirconate titanate (PZT) transducers, which are either embedded in the structure or surface mounted (e.g., Liao *et al.*, 2011; Sabet and Yang, 2014; Song *et al.*, 2007; Yan *et al.*, 2013). The reciprocity of PZT transducers is well known, and the use of such transducers is widely spread (Chopra, 1996; Giurgiutiu and Zagrai, 2000; Lanza di Scalea *et al.*, 2007). PZT transducers are often used in high frequency modes, which work well when probing structures such as metal plates. For large structures with high damping characteristics, such as concrete structures, it can be of interest to utilize waves of lower frequency as these are known to propagate longer distances. In this letter the possibility of reciprocal transmission of mechanical waves of five different voice coil transducers is investigated, and compared to a PZT disk in the frequency range 10 Hz to 5 kHz. One common voice coil transducer is the geophone used in seismic measurements. It is normally only used as a receiver and then only below a couple of hundred Hertz.

2. Background

Voice coil transducers are based on the principle of a spring-mounted coil that moves within a magnetic field. Due to its own inertia, the coil remains stationary while the case moves with ambient vibrations or vice versa. The coils' relative motion through the magnetic field generates a voltage proportional to the velocity. If, instead, an

electric signal is applied over the poles, the moving coil will move within the magnetic field with a velocity proportional to the current. Conservation of energy implies that the responsivity of the coil-magnet system as a force transducer and its sensitivity as a velocity transducer are identical properties (Gabrielson, 1997; Wielandt, 2012). Thus, voice coil transducers can be used reciprocally as both receivers and transmitters of mechanical waves.

Inertial force actuators are often characterized by the frequency range in which they effectively output force. We want to extend the knowledge of how these transducers operate outside their anticipated range of working frequencies and how they work as receivers.

3. Experimental setup

The five types of voice coil transducers evaluated in this study are presented in Table 1. A PZT disk (Pz27, Meggit Sensing Systems, Denmark), 10 mm thick and 38 mm in diameter, is used as a piezoelectric reference.

Each transducer was evaluated in three steps: force responsivity, receiving sensitivity, and efficiency in transmission directly between a pair of identical transducers through a concrete block.

3.1 Force responsivity

The actuating abilities of the transducers were evaluated by measuring the force exerted by the transducers as a function of frequency. A Dynamic Signal Analyzer (35665A, Hewlet-Packard, Palo Alto, CA) (DSA) was used to step through source frequencies in the range of 10 to 5000 Hz and to calculate a frequency response spectrum of the signal from the force transducer measured for each source frequency. A power amplifier (type 2734, Brüel & Kjaer, Denmark) was used to amplify the driver signal from the DSA source before it was fed to the test transducer. The power amplifier signal was fed into the DSA (Ch. 1) for reference. The force exerted by the transducer was measured by a force transducer (type 8200, Brüel & Kjaer, Denmark), the output of which was amplified by a charge amplifier (type 2635, Brüel & Kjaer, Denmark) and then fed to the DSA (Ch. 2). A 150 kg concrete cube, with a 0.4 m side, acted as a firm fundament.

3.2 Receiving sensitivity

The DSA was used to step through a range of source frequencies and to calculate a frequency response spectrum of the receive signal from the test transducer, measured at each source frequency. The DSA Source, amplified by the 2734 power amplifier, was connected to a vibration exciter (type 4808, Brüel & Kjaer, Denmark), equipped with a an inline impedance head (type 8001, Brüel & Kjaer, Denmark). The test transducer was mounted on top of the impedance head. The accelerometer output of the impedance head was integrated by the 2635 charge amplifier and fed, as a velocity

Table 1. List of the voice coil transducers used in the study.

Transducer	Type	Manufacturer	Weight	Nominal impedance
SM-6 375Ω	Geophone	ION[a]	81 g	375 Ω
SM-6 3500Ω	Geophone	ION	81 g	3500 Ω
IFX30-100	Inertial force actuator	Motran Industries[b]	940 g	1.7 Ω
EX60S	Electro dynamical exciter	Visaton[c]	120 g	8 Ω
EX45S	Electro dynamical exciter	Visaton	60 g	8 Ω

[a]Ion, Houston, TX, http://www.iongeo.com/.
[b]Motran Industries, Valencia, CA, http://www.motran.com/.
[c]Visaton, Germany, http://www.visaton.com/en/.

measurement, to the DSA (Ch. 1) for reference. The force output of the impedance head was not used. The output from the voice coil transducer was fed to the DSA (Ch. 2).

3.3 Reciprocal concrete transmission efficiency

To verify that it is indeed possible to transmit mechanical waves through concrete using these voice coil transducers, measurements were made on the previously mentioned cubic concrete block. Two identical transducers were used for this experiment: one for transmission and one for reception. The reciprocity in the transmissions was investigated by repeating each measurement with reversed transducer configuration, so that the transducer that previously transmitted acted as receiver and vice versa.

Small metal plates were adhered to the center of two opposing sides of the block. These plates had threaded holes, which enabled the geophones to be exchanged and firmly fixed in place. The other voice coil transducers were fastened to the concrete using adhesive tape. The transducers were thus located horizontally on opposite sides of the concrete block.

The DSA source was used, via the power amplifier, to apply a sinusoidal signal with stepped frequency to the transducer that acted as a transmitter. The output of the power amplifier was fed into Ch. 1 of the DSA for reference. The output from the receiving transducer was fed into the DSA (Ch. 2). By dividing Ch. 2 with Ch. 1 the voltage transfer function was established. By then dividing by the transducer complex impedance the transmission efficiency was determined.

Because of eddy currents in the metal voice coil cases, generated by the magnetic field, it proved necessary to connect the case of the transducers to system signal ground in order to avoid galvanic coupling, through the concrete, between actuator and receiver.

4. Results

4.1 Force responsivity

The fast Fourier transform spectra of the output signals from the force transducer were recorded from the DSA. The force amplitude was divided by the current applied to the transducer in order to get a unit that facilitated comparison of the different transducer responsivities.

Figure 1(a) shows the transducer force responsivity for all transducers as a function of driver signal frequency. The plots are shown in decibel scale, normalized relative to the highest value in the diagram. The voice coil transducers all display a clear peak, which corresponds to the frequency at which the transducer exhibits resonance. This peak is naturally located at different frequencies for the different transducers, based on their weight and structure. This resonance frequency should not be confused with the natural frequency of the spring-coil system in the voice coils, which is, e.g., 14 Hz for the geophones. Spurious frequencies for the geophones can be seen in the interval 220–300 Hz. Between these and the resonance peak at ~3.1 kHz, the frequency response is rather flat which indicates a useful range of operation. At frequencies above the resonance peak the output from the voice coils declines rapidly. The other voice coil transducers show some spurious behavior at different frequencies, which corresponds to the irregularities in the spectra. By also analyzing the wide spectra of the response signals it was possible to monitor the presence of any harmonics. It was found that the geophones and the PZT disk displayed very weak harmonics (−80 dB). The other voice coils gave rise to slightly larger harmonics.

4.2 Receiving sensitivity

Figure 1(b) displays the sensitivity of all the investigated transducers, plotted as a function of vibration frequency. The plots are shown in decibel scale, normalized relative to the highest value in the diagram. The resonance peaks of the voice coil transducers are also clearly visible in this diagram. At 220–300 Hz, the spurious frequencies for the two geophones can be seen. Geophones are normally only used below these spurious

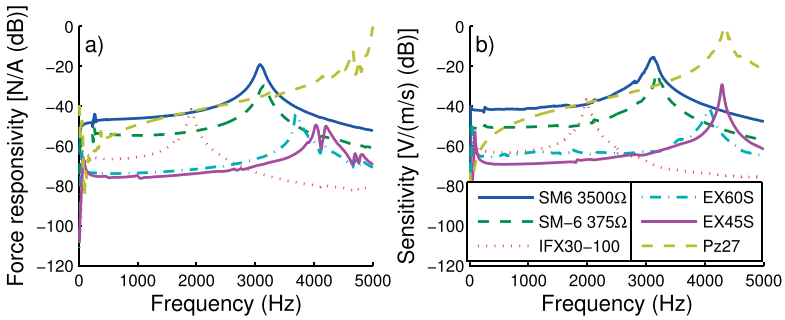

Fig. 1. (Color online) (a) The responsivity, in N/A, of the force output, at the same frequency as the driving sinusoidal signal, as a function of frequency, for the evaluated transducers. The amplitudes are in decibel scale, normalized relative to the highest value in the diagram. (b) The receiving sensitivity, in V/(m/s), at the same frequency as the vibrator input signal, of the evaluated transducers, as a function of vibration frequency. The amplitudes are in decibel scale, normalized relative to the highest value in the diagram.

frequencies. The similarity between the results for the voice coil transducers in Figs. 1(a) and 1(b) suggests reciprocity between transmission and receiving, as suggested by Wielandt (2012).

4.3 Reciprocal concrete transmission efficiency

Figure 2(a) shows the reciprocal transmission efficiency measurements for all the transducers tested and Fig. 2(b) shows the results with the interchanged transducers. The data is displayed in decibel scale normalized relative to the highest value in the diagram. The fact that the plots corresponding to the geophones in the diagrams are so similar supports the claim that these are useful as reciprocal transducers. The other transducers are not as similar, which might be explained by the difficulty in mounting them in a repeatable fashion, due to their surface area or weight. Numerical modeling suggests that the peaks between 4 and 5 kHz are natural frequencies of the concrete block. As expected from the results in Secs. 4.1 and 4.2, the SM-6 3500Ω geophone is the most efficient reciprocal transducer of the voice coil transducers. The PZT transducer seems to be as efficient as the geophone even for lower frequencies. However,

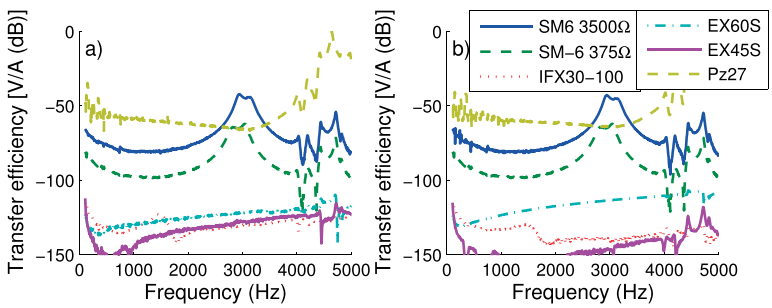

Fig. 2. (Color online) Transmission efficiency, in V/A, between a pair of identical transducers for all the transducers investigated in the study. All plots are in decibel scale, normalized relative to the highest value in the diagram. The measured signal in the PZT transducer for frequencies below ~3.2 kHz is electrical coupling between transmitter and receiver. In (a) one of the transducers, for each pair, acts as transmitter and the other as receiver. In (b) the transmission is reversed.

experiments where the PZT transducers were placed slightly apart from the concrete block, but otherwise in the same locations, were performed in order to investigate the possibility of capacitive coupling. It became apparent that the signal measured up to approximately 3.2 kHz was identical to the signal measured when the transducers were in contact with the concrete. Thus, the PZT data measured up to 3.2 kHz is from the electrical coupling between the two transducers, and is not a measure of mechanical vibrations. The effect was not removed by connecting the ground potential of the PZT transmitter and receiver. The receiving PZT also picked up ambient electrical disturbances in the room, for example, at the line frequency. Similar experiments were performed for the voice coil transducers but once the cases were grounded the electrical coupling was negligible. The electro dynamical exciters also picked up disturbances at the line frequency.

5. Conclusion

The data presented in this letter indicates that voice coil transducers can indeed be used as reciprocal transducers for mechanical waves in the frequency range ~100–5000 Hz. This, combined with their robustness, makes them suitable for applications in SHM, where they can be surface mounted. The mass and structure of the transducers give rise to a resonance peak for the transducers themselves. Depending on the type of measurement, this peak must be accounted for, so that it is not mistaken for a natural frequency of the monitored structure. On the other hand, it is obviously a frequency where the detection distance can be large.

Five different types of voice coil transducers were evaluated. The inertial force actuator and electro dynamical exciters are the most potent exciters, as they can exert the strongest force on the structure. They are, however, relatively insensitive as receivers. These transducers also generate relatively strong harmonics, which are not desired, as power is wasted on unintentional frequencies and potentially interesting nonlinear effects are caused by the transducers instead of the material.

The geophones proved to be the voice coil transducers best suited for reciprocal operation, due to their high sensitivity. This is confirmed by the results from the experiment where a signal was transmitted through a concrete block: the geophones displayed the highest output per input power. Of the two geophones, the higher impedance version, SM-6 3500Ω, proved to be the most efficient. These geophones are small, lightweight, robust, and relatively inexpensive when used, e.g., in reciprocal networks outdoors, on large concrete structures.

For frequencies higher than 5 kHz the PZT transducer excels while the response from all voice coils drops towards zero. However, the SM-6 3500Ω geophone was more effective than the PZT disk used in this study up to ~3.5 kHz. Additionally, in the reciprocal operation, the capacitive coupling between transmitter and receiver PZT, as well as the ambient electrical disturbances picked up by the receiver, obscured the signal from the mechanical vibrations for frequencies up to ~3.2 kHz.

Electrical coupling must be considered when using reciprocal transducer pairs. It was shown by Gabrielson (1997) that the radiated electromagnetic field from a geophone decayed as distance to the fourth power. Similar observations were made during the presented work; when placed within a few centimeters from each other, the electromagnetic coupling between two geophones was significant. When separated by the width of the concrete block this coupling was insignificant compared to the mechanical signal.

In the experimental setup in the study presented, the electrical coupling between voice coil transducers proved negligible—once the aluminum housings were connected to the ground potential pin to avoid galvanic coupling through the concrete. This, in addition to the apparent higher resilience to ambient electrical disturbances, speaks for voice coils as a viable alternative for PZT transducers in networks of reciprocal transducers where the frequencies of interest are below ~3–4 kHz.

References and links

Ackerman, E. (**1957**). "Reciprocity calibrations," Am. J. Phys. **25**(7), 454–460.

Chopra, I. (**1996**). "Review of current status of smart structures and integrated systems," in *1996 Symposium on Smart Structures and Materials*, edited by I. Chopra (Int. Soc. Opt. Photo), pp. 20–62.

Gabrielson, T. B. (**1997**). "Free-mass reciprocity calibration," J. Acoust. Soc. Am. **102**(5), 2800–2808.

Giurgiutiu, V., and Zagrai, A. N. (**2000**). "Characterization of piezoelectric wafer active sensors," J. Intel. Mat. Syst. Str. **11**(12), 959–976.

Lanza di Scalea, F., Matt, H., and Bartoli, I. (**2007**). "The response of rectangular piezoelectric sensors to Rayleigh and Lamb ultrasonic waves," J. Acoust. Soc. Am. **121**(1), 175–187.

Levy, S., and Bouche, R. R. (**1956**). "Calibration of vibration pickups by the reciprocity method," J. Res. Natl. Bur. Stand. **57**(4), 227–243.

Liao, W.-I., Wang, J. X., Song, G., Gu, H., Olmi, C., Mo, Y. L., and Loh, C. H. (**2011**). "Structural health monitoring of concrete columns subjected to seismic excitations using piezoceramic-based sensors," Smart Mater. Struct. **20**(12), 125015.

Sabet Divsholi, B., and Yang, Y. (**2014**). "Combined embedded and surface-bonded piezoelectric transducers for monitoring of concrete structures," NDT&E Int. **65**, 28–34.

Song, G., Gu, H., Mo, Y. L., Hsu, T. T. C., and Dhonde, H. (**2007**). "Concrete structural health monitoring using embedded piezoceramic transducers," Smart Mater. Struct. **16**(4), 959–968.

Wielandt, E. (**2012**). "Seismic sensors and their calibration," in *New Manual of Seismological Observatory Practice*, Part 2, edited by P. Bormann (IASPEI, GFZ German Research Centre for Geosciences), Chap. 5, pp. 1–49.

Yan, S., Wu, J., Sun, W., Ma, H., and Yan, H. (**2013**). "Development and application of structural health monitoring system based on piezoelectric sensors," Int. J. Distrib. Sens. N. **2013**, 1–12.

Paper II

Ultrasonics 80 (2017) 1–8

Contents lists available at ScienceDirect

Ultrasonics

journal homepage: www.elsevier.com/locate/ultras

Frequency selection for coda wave interferometry in concrete structures

Patrik Fröjd *, Peter Ulriksen

Department of Engineering Geology, Lund University, John Ericssons Väg 1, SE-221 00, Sweden

ARTICLE INFO

Article history:
Received 21 February 2017
Received in revised form 29 March 2017
Accepted 21 April 2017
Available online 23 April 2017

Keywords:
Coda wave
CWI
Structural health monitoring
Ultrasound
Diffuse field

ABSTRACT

This study contributes to the establishment of frequency recommendations for use in coda wave interferometry structural health monitoring (SHM) systems for concrete structures. To this end, codas with widely different central frequencies were used to detect boreholes with different diameters in a large concrete floor slab, and to track increasing damage in a small concrete beam subjected to bending loads. SHM results were obtained for damage that can be simulated by drilled holes on the scale of a few mm or microcracks due to bending. These results suggest that signals in the range of 50–150 kHz are suitable in large concrete structures where it is necessary to account for the high attenuation of high-frequency signals.

1. Introduction

Nondestructive testing (NDT) or structural health monitoring (SHM) methods based on ultrasonic measurements can be problematic in concrete due to the severe scattering of the waves in aggregates. This scattering redistributes energy from a coherent wave to a more diffuse propagation.

However, in coda wave interferometry (CWI), the trailing part of the transient signal (coda) is analyzed. These signals correspond to the diffuse field created by the scattering and reflections from the boundaries. Since the coda correspond to waves that have traversed the material for a relatively long time, it is more affected by damage in the material than signal parts that correspond to the direct propagation path. Analysis of coda waves is an attractive prospect for SHM applications, since not only the direct path between two transducers but also a larger volume can be probed.

The literature describes numerous studies where CWI has been implemented in both NDT and SHM applications and investigated for its ability to detect early onsets of cracking in concrete [1–4]. Recent publications report on methods to compensate for temperature effects on CWI measurements [5,6] and to measure nonlinear effects in the monitored material [7–9], thus furthering the usefulness of diffuse field measurements in SHM applications.

Different methods exist for analyzing coda waves, including the doublet method [10–12] and the stretching method [13–15]. The latter has been shown to be more precise and more stable toward noise [16]. The stretching method assumes that the variation in the material can be modeled as a homogeneous change in velocity, which results in a dilation of a measured waveform in time. The measured waveform is stretched with a range of stretching factors, and the factor that maximizes the correlation to the original waveform is a good estimate of the relative velocity variation in the material. However, for local damage, such as a lone crack or hole, the change cannot be estimated as a global, homogeneous velocity change. In such a case, it could be useful to simply calculate the decorrelation between the baseline and current waveform, possibly using different time windows in the coda [17,18].

The interaction between mechanical waves in concrete and the heterogeneities in the mix depends on the wavelength and the typical size of the heterogeneities. Following the naming convention used in the review by Planés and Larose [2], four frequency domains can be identified for scattering in concrete. The transitions between these regimes are smooth and depend greatly on the typical size of the aggregates used in the concrete mix.

The stationary wave regime, for frequencies below 10–20 kHz, is mostly associated with modal analysis. In this regime, the wavelength is on the same order of length as the structure as a whole, and thus it is much larger than the size of the aggregates in the concrete. The interaction between the waves and the aggregates is mostly negligible. There are, however, reflections from the structure boundaries, which lead to a diffuse wave field and a coda in a measured signal.

Larose et al. [19] used signals in the 1 kHz range to track variations in a concrete building due to temperature variations, and Ståhler et al. [20] used signals in similar frequency ranges to monitor stress changes in concrete during the launching of a bridge deck.

* Corresponding author.
E-mail address: patrik.frojd@tg.lth.se (P. Fröjd).

http://dx.doi.org/10.1016/j.ultras.2017.04.012
0041-624X/

The simple scattering regime, for frequencies between the stationary wave regime and up to approximately 100–150 kHz, is the range commonly used in the traditional ultrasonic investigation of concrete. The regime is defined by the wavelengths being shorter than the size of the structure, but longer than the size of the aggregates and reinforcement bars in the concrete. The waves interact weakly with the heterogeneities, and the codas in this regime thus often consist of a mix of scatterings and reflections from boundaries.

Several published accounts of coda wave analyses in concrete in this regime report on the successful detection of different changes to the structure. Niederleithinger et al. [21], Stähler et al. [20], and Fröjd and Ulriksen [22] provide examples where diffuse ultrasound, in the range of 50–70 kHz, is used to detect and track stress changes and/or cracking in concrete samples.

The multiple scattering regime, for frequencies between the simple-scattering regime and up to approximately 1 MHz, is the range where the ultrasound wavelengths are shorter than the size of the aggregates. In this regime, the waves are strongly affected by the heterogeneity and the direct/coherent wave is strongly attenuated. The measured signals then mostly consist of a coda created by multiple scatterings. Most of the publicized work on CWI in concrete operates in this regime, and it is here that the wave propagation can accurately be described by the solution of the diffusion equation.

Examples of work in concrete CWI in the multiple scattering regime include publications by Larose and Hall [15], Schurr et al. [3], and Zhang et al. [23]. Larose and Hall detected variations of relative velocity in the concrete sample due to stress changes with a resolution of $2 \cdot 10^{-5}$, and other publications report similarly high sensitivity.

The attenuation regime, for frequencies above 1 MHz, is the range where the ultrasound is so strongly attenuated, from both scattering and intrinsic absorption, that applications involving anything other than very small test objects in laboratories are infeasible. Applications with signals in this frequency regime thus have little use in practice, and are mostly neglected.

Methods for using diffuse waves to locate damage have been proposed that are based on modeling travel time variations and the decorrelation of coda waves [17,24,25]. A notable example is the LOCADIFF algorithm. In these methods, the multiply scattered, propagating wave fields are approximated as diffusion or radiative transfer, and an inversion process is used to fit these analytical models to experimentally measured data. This yields images of the location of a local change, and the resolution depends on the scattering properties of the waves and the material. The scattering properties can be described using the *scattering mean free path*, l, which is defined as the average distance between two scattering events, and the *transport mean free path*, l^*, which is the average travel distance after which each wave packet no longer contains information as to its original direction. If isotropic scattering is assumed, then $l = l^*$. If the scatterings are anisotropic, then $l < l^*$, since more than one scattering event is required to completely randomize the direction.

Alternatively, one can instead use the *scattering mean free time*, t, and *transport mean free time*, t^*, which correspond to the time between two scattering events and time after the wave direction is randomized, respectively.

Clearly, there are numerous examples of useful applications of CWI in concrete across widely different frequency ranges. In practical SHM applications with permanently installed transducers, it is of interest to monitor very large volumes, as civil structures can be many orders of magnitude larger than the test objects most often used in laboratory experiments. Depending on the circumstances, it might not be practical to operate in the multiple-scattering regime due to the severe attenuation of high-frequency ultrasound in concrete. For traditional ultrasonic imaging (using only the coherent wave), it is easier to select the frequency and transducer spacing, as the resolution and sensitivity are often directly related to the wavelength and the range is given by the attenuation of the coherent wave. To the authors' knowledge, there exist no similar recommendations when using CWI. We therefore aim to experimentally investigate the usefulness of CWI in a wide range of frequencies, encompassing the three first scattering regimes. The usefulness is measured by the difference in sensitivity to changes and by the difference in the transmission range.

This paper presents the results from two different experiments. In the first, CWI is used to detect drilled holes in a large concrete floor slab, which act as new scatterers. Drilled holes do not represent realistic damage to typical concrete structures, but they are useful approximations of cracks since they are well defined by their diameter and depth. Holes are drilled at different distances from the transducers in order to investigate the size of the probed area. In order to relate the size of the estimated probed area to the theoretical models mentioned above, the transport mean free path for the waves in the floor slab are also estimated using a diffusion model.

In the second experiment, a small concrete beam is damaged by applying bending loads, and CWI is used to track the deterioration. In both experiments, a wide range of central frequencies of the ultrasonic pulses is used.

This work takes a step toward the development of recommendations for implementing CWI in NDT or SHM applications in large concrete structures.

2. Materials and equipment

The test object used in the first experiment was an $800 \times 211 \times 8$ cm concrete floor slab. The mix had a water-cement ratio of 0.442, and the slab was reinforced with a steel mesh with a nominal diameter of 6 mm and 150 mm squares.

The test object used in the second experiment was an $80 \times 10 \times 15$ cm concrete beam. The concrete mix had a water-cement ratio of 0.6, and the beam was reinforced with a single steel bar with a nominal diameter of 8 mm.

Table 1 provides details on the concrete mix for both specimens.

As signals with vastly different central frequencies were used, different transducer pairs were necessary. The stationary-wave-regime signal was transmitted between a pair of SM-6 3500 Ω geophones from ION. The use of geophones as reciprocal transmitters and receivers of low-frequency mechanical waves in concrete has been investigated previously by the authors [26]. The geophones have a major resonant frequency at 3.1 kHz. The simple- and multiple-scattering regime signals were all transmitted by Ferroperm Pz26 piezoceramic disks with diameter 37.7 mm, and received by Ferroperm Pz37 piezoceramic disks with diameter 27 mm. Both types of piezoceramic discs have a resonant frequency of about 500 kHz. All transducers yield vertical excitation.

The signals were generated by an Agilent 33500B waveform generator and amplified to 200 Vpp. All signals were sampled by an Agilent InfiniiVision DSO-X 3014A oscilloscope. Custom-made

Table 1
Concrete composition for the floor slab and the small beam.

Components	Floor slab (kg/m^3)	Beam (kg/m^3)
Sand	1006	783
Aggregate (8–11 mm)	704	479
Aggregate (12–16 mm)	–	479
Cement	406	350
Water	101	210

switches enabled automatic switching between the various transducer pairs.

3. Experimental program

The excitation signals were all five-cycle, Hanning-windowed, sinusoidal pulses with different central frequencies. Five different frequencies were used: 500, 250, 150, 50, and 3.1 kHz. In concrete, these cover the first three useful scattering regimes; the wavelengths (based on shear velocity) of the 500 and 250 kHz waves are shorter than the size of the aggregates, and thus belong to the multiple scattering regime. The wavelengths of the 150 and 50 kHz waves are longer than the aggregates and thus belong to the simple scattering regime. The 3.1 kHz signals give rise to Lamb waves, with wavelengths on the same order of size as the test specimens, and thus belong to the stationary wave regime.

Each measurement was averaged five times, and processed with digital band-pass filters, centered on the central frequency of the excitation signal. Fig. 1 shows typical measured waveforms, after averaging and filtering, and their corresponding frequency spectra.

3.1. Holes in floor slab

The first experiment investigated how the choice of frequency influences the sensitivity of the CWI measurement to an extra scatterer that is on the same order of magnitude as the aggregates in the concrete. The transducers were placed at distances of approximately 20 wavelengths (based on the shear velocity). These correspond to 10, 20, 33, and 100 cm for the 500, 250, 150, and 50 kHz signals, respectively. The corresponding distance for the 3.1 kHz Lamb waves would be longer than the length of the slab. The geophone transducers were instead placed 4 m apart. For a structure this size, regardless of the placement of the low-frequency transducers, the measured signals will consist of waves that have been reflected from the boundaries many times. The distance between the geophones is therefore not crucial.

At the specified transducer distances for the different frequency transmissions, all signals had similar signal-to-noise ratios, ~50 dB, at the largest peak. This highlights the difference in order of magnitude of the attenuation and thus the useful maximum range between actuator and receiver, at the different signal frequencies.

The five pairs of transducers were placed with these individual distances, all centered at roughly the center of the concrete slab. Fig. 2 shows a sketch of the transducer placement.

The extra scatterers were introduced at different distances from the centerline by drilling holes in the concrete. The holes were located 0, 5, 10, 20 and 40 cm from the centerline, as shown in Fig. 2. Each hole was first drilled with a 4 mm diameter, then it was expanded to 8, 10, and 12 mm in steps. The holes were all ~1 cm deep. Eight measurements were taken at each hole for each diameter.

3.2. Bending cracks in beam

The second experiment was used to demonstrate the different sensitivities of CWI at different frequencies when detecting bending cracks in the small concrete beam. One pair of the PZT transducers was used for the 500, 250, 150, and 50 kHz signals, and one pair of the geophones was used for the 3.1 kHz signals. Both transducer pairs were placed 20 cm apart, centered on the lower side of the beam. An illustration of the experimental setup is shown in Fig. 3.

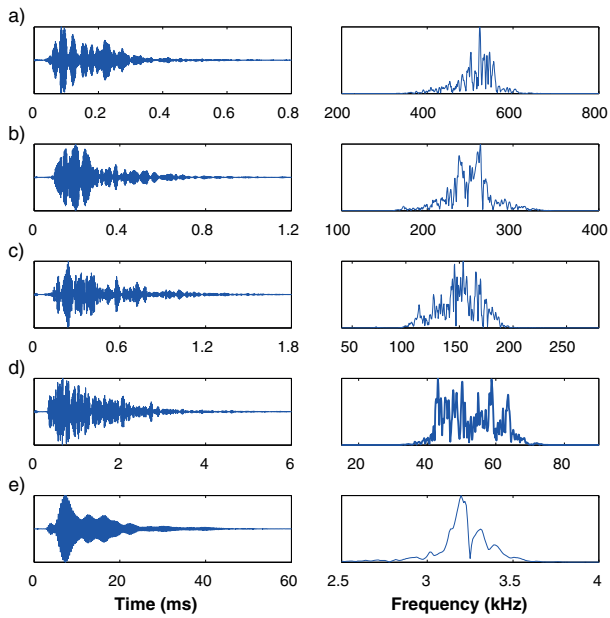

Fig. 1. Examples of measured waveforms in time domain (left) and frequency domain (right), for the different excitation signals: (a) 500 kHz, (b) 250 kHz, (c) 150 kHz, (d) 50 kHz, (e) 3.1 kHz.

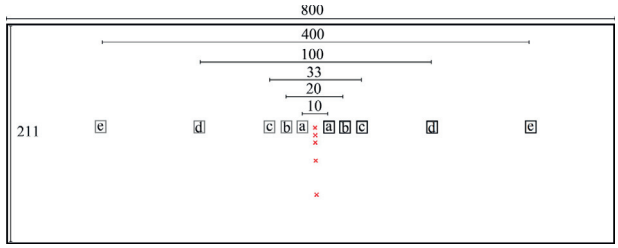

Fig. 2. Layout of the concrete floor slab, transducers, and boreholes. Dimensions are given in cm. The transducer pairs denoted by a-e in the Fig. were used for signals with frequencies 500, 250, 150, 50, and 3.1 kHz, respectively. The transducers to the right of the center were used as transmitters and those to the left as receivers. The red crosses indicate the location of the boreholes. The boreholes are located 0, 5, 10, 20 and 40 cm from the centerline, between the transducers. The sketch is not to scale and the transducers were placed slightly off-center on the slab due to other instrumentation on the concrete.

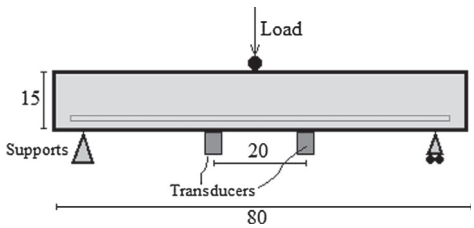

Fig. 3. Illustration of the experimental setup for the beam bending experiment. Dimensions are given in cm.

A downward load was applied at the center of the beam. The load was applied in steps with each step increasing the force ~0.5 kN. Between each load step, the load was released before the CWI measurements were performed. The measurements were thus made on the unloaded slab, and any effect on the coda should therefore be attributed to damage to the concrete, rather than stress. The measurement procedure was repeated until cracks were visible in the load phase. This occurred at a load of ~12 kN.

4. Data processing

4.1. Estimation of scattering properties

In order to estimate the scattering properties of the concrete in the floor slab at the different frequency ranges, the diffusion equation was fitted to the measured signals. A solution of the diffusion equation, in a finite 3D cuboid structure with sides a, b, and c, assuming isotropic scattering and no ultrasonic flux out from the boundaries from the concrete, is given by [27]:

$$\begin{aligned}\langle E(x,y,z,t)\rangle = E_0 e^{-\sigma t}\{1 + [g(x,x_0,a)g(y,y_0,b)g(z,z_0,c)] + [g(x,x_0,a) \\ + g(y,y_0,b) + g(z,z_0,c)] + [g(x,x_0,a)g(y,y_0,b) \\ + g(x,x_0,a)g(z,z_0,c) + g(y,y_0,b)g(z,z_0,c)]\}\end{aligned}$$

where

$$g(x,x_0,a) = 2\sum_{m=1}^{\infty}\cos\left(\frac{m\pi x}{a}\right)\cos\left(\frac{m\pi x_0}{a}\right)e^{-D\left(\frac{m\pi}{a}\right)^2 t}$$

Here, $\langle E(x,y,z,t)\rangle$ is the ensemble average energy density that can be thought of as the time evolution of the slowly varying envelope of the coda energy. The model assumes an impulse excitation with amplitude E_0 at point (x_0, y_0, z_0), which is the source location. The receiver position is given by (x, y, z), and a, b, and c are the dimensions of the structure. D is the diffusivity, which describes the rate at which the diffusion covers an area. If the waves are strongly scattered in the material, the diffusion process is slower, corresponding to a low value of D, and vice versa. The dissipation rate, σ, describes the exponential decay of the coda.

By fitting the diffusion equation to the envelope of the measured signals, the scattering parameters D and σ can be estimated. A least squares method was used for fitting.

It should be noted that for the lower-frequency signals, in the stationary-wave regime in particular, the "diffusivity" of the coda is created by boundary reflections rather than scattering, and the diffusion equation does not accurately describe the wave propagation. However, a rough approximation is still of interest, although the values for the lowest frequency are rather specific to the geometry of the structure. The estimation of the dissipation should be valid, however, since all energy decays due to intrinsic attenuation.

Using the estimated value of the diffusivity, it is possible to estimate the transport mean free path by [28]:

$$l^* = \frac{dD}{v_e}$$

where "d" is the dimensionality of the structure, which in this case is assumed to be 3 for the 500, 250, and 150 kHz signals and 2 for the 50 and 3.1 kHz signals. This is an approximation based on the relationship between the wavelengths and the thickness of the slab; for the lower frequencies, the slab can be approximated as a 2D structure. The average velocity of the transport of energy, v_e, could be thought of as the velocity of the envelope. A velocity of ~2500 m/s was measured in this setup, which agrees with the shear wave velocity in concrete.

4.2. Coda wave analysis

Since the drilled holes in the floor slab does not result in global, homogeneous velocity changes, the stretching method was not used for the drilled hole experiment. The influence of the holes was evaluated by calculating the decorrelation of the coda in a time window $[t_1, t_2]$:

$$DC = 1 - \frac{\int_{t_1}^{t_2}\varphi^0(t)\cdot\varphi(t)dt}{\sqrt{\int_{t_1}^{t_2}\varphi^0(t)^2dt\cdot\int_{t_1}^{t_2}\varphi(t)^2dt}}$$

where φ^0 is the reference measurement waveform, before the specimens are affected, and φ is each subsequent measurement waveform.

For the bending cracks in the beam, it is reasonable to assume that the overall effect on the propagating waves include a general

decrease in velocity, since microcracks can be formed over the entire cross section of the beam. Therefore the stretching method was employed, according to:

$$DC(\alpha_i) = 1 - \frac{\int_{t_1}^{t_2} \varphi^0(t(1+\alpha_i))\varphi(t)dt}{\sqrt{\int_{t_1}^{t_2} \varphi^0(t(1+\alpha_i))^2 dt \int_{t_1}^{t_2} \varphi(t)^2 dt}}$$

where α_i are different stretching factors. The α_i that minimizes the decorrelation coefficient is a good estimation of the relative modification of the propagation velocity. Both the relative velocity variation and remaining decorrelation, after optimal stretching, are used as damage indicators. Values of α_i in the interval $[-4 \cdot 10^{-3}, 4 \cdot 10^{-3}]$ with steps of $2 \cdot 10^{-5}$ were used in the stretching algorithm.

In both cases, the time windows were chosen to correspond to 100 periods of the waveform and were centered over the time when the waveform was attenuated to a SNR of ~25 dB. This corresponds to a significantly later time for the lower-frequency signals, since the attenuation is strongly dependent on frequency. For all signals this correspond to a time in the waveform after the waves have been scattered or reflected multiple times (i.e. several scattering mean free times), even for the simple scattering regime and stationary wave regime signals.

5. Results and discussion

5.1. Holes in floor slab

Table 2 shows the diffusivity and dissipation parameters that provide the best fit of the diffusion equation to the measured waveforms. The yielded values are in general agreement with the results from the literature [29]. The difference in dissipation again highlights the significantly increased attenuation for the higher-frequency signals. Also shown is the transport mean free path as estimated from the diffusivity. Fig. 4 shows an example waveform, from the 50 kHz transmissions, as well as the fitted diffusion model used to estimate the scattering properties.

Fig. 5 shows the results from the coda decorrelation measurements for the different central frequencies and for the different boreholes. Each subplot shows measurements with one central frequency, and each curve shows a specific distance between the borehole and the centerline, according to Fig. 2. The y-axis shows the coda decorrelation and the x-axis shows the measurement number. Eight measurements were performed at each borehole configuration, starting with eight measurements with no hole. The first of these measurements, with no hole, was used as the reference signal in the equation for decorrelation. The temperature was stable to within ±0.1 °C.

From Fig. 5, it can be seen that the absolute level of decorrelation increases with frequency. This is intuitive, as a hole of a certain diameter will affect a signal with a short wavelength more than one with a longer wavelength. However, the times when the borehole diameter was increased can clearly be seen, even in the plots corresponding to the simple-scattering regime (50 kHz)

Table 2
Results from fitting the diffusion equation to the measured waveforms in the concrete floor slab.

Frequency (kHz)	Diffusivity (m^2/s)	Dissipation (s^{-1})	Transport mean free path (cm)
500	8	13,000	1.0
250	18	10,000	2.1
150	39	7000	4.7
50	440	1200	35
3.1	~700	220	56

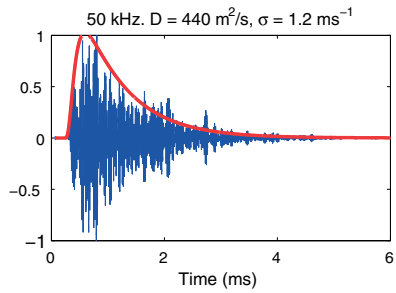

Fig. 4. An example of a normalized 50 kHz waveform measured in the concrete floor slab. The diffusion approximation is shown in red.

measurements. Even the smallest-diameter hole (4 mm) can be detected at this frequency, even though it corresponds to less than a tenth of a shear wavelength. This is smaller than the concrete aggregates and reinforcement bars.

The ability to resolve an event depends on the stability of the baseline measurements (measurements 2–8, in this case), which, in turn, depends on the signal-to-noise ratio and whether the variations are compensated for changes in environmental conditions.

The stationary-wave-regime signal measurements (3.1 kHz) cannot be used to detect the times for the drilling of holes in any useful capacity. This is not surprising, considering that the wavelength of the Lamb waves at these frequencies are on the order of one meter.

The influence of the distance of the hole to the direct line between the transducers and the decorrelation of the signals can clearly be seen in the figures. The sensitivity of the coda wave analysis decreases as the distance between the hole and the direct line increases. This is caused by two factors:

(1) The intrinsic absorption prevents far-traveling waves from influencing the measured signal. Evaluating the later parts of the codas results in a wider probed area, since more of the waves have time to travel further. However, the later parts of the signals will be more attenuated, resulting in lower signal-to-noise ratios.
(2) The probability that a measured wave packet has passed a certain point decreases with distance to the transducers and the direct connecting line between them. The second phenomenon can be visualized as a sensitivity kernel, as described by, e.g., Planés et al. [18], who showed that the width of the zone of high sensitivity between two transducers is on the order of one transport mean free path. Clearly, the higher-frequency signals (with shorter l^*) display a more rapid decline in sensitivity as a function of distance. There does not seem to be a significant difference in the effect of the holes within this high-sensitivity zone, which is in agreement with the resolution of sensitivity kernel–based imaging methods being on the order of l^*. The 150 kHz signal measurements seem to include the 10 cm holes in this high-sensitivity zone, which is more than the estimated l^*, but it should be noted that the estimate is a rough approximation. In general, our measurements are in agreement with this theory.

5.2. Bending cracks in beam

Fig. 6 shows the relative velocity change (lower) and remaining decorrelation, after stretching, (upper) of the different frequency

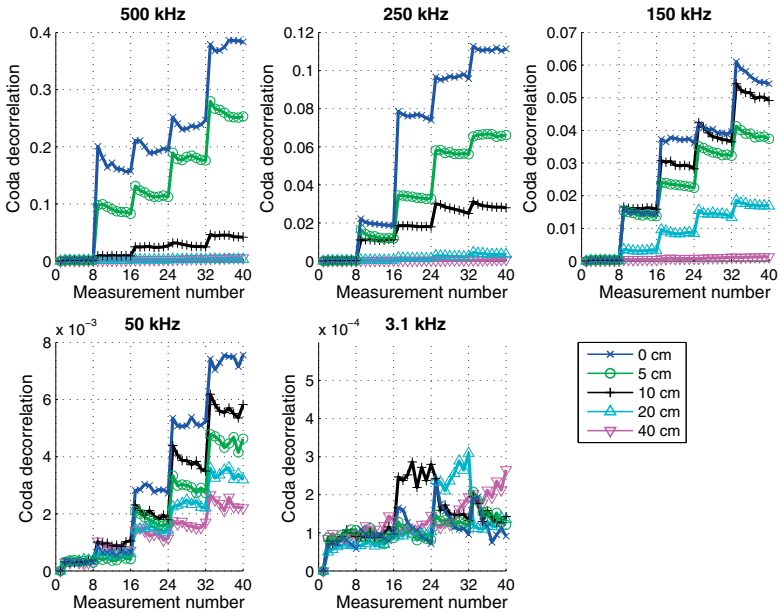

Fig. 5. Decorrelation of the coda at different central frequencies. Boreholes are drilled at every eighth measurement, with diameters 4, 8, 10, and 12 mm. Each curve shows measurements with different distances between the holes and the centerline between the transducer pair.

signals in the concrete beam subjected to a central load. The horizontal axis shows the bending load of the load step before each measurement. All measurements were performed after the load was released, to avoid measuring stress in the material. The temperature during the experiment was stable to within 0.1 °C.

In contrast to the case with drilled holes in the floor slab, it was not possible to know the exact damage state of the concrete at the various load steps. It was simply assumed that the level of damage in the concrete increased with the maximum bending load experienced by the beam. For low loads, it was assumed that only microscopic cracks formed. As the load increased, larger internal cracks were created, and at a load of ∼12 kN, the first visible crack appeared while the load was applied. The goal of this experiment was to demonstrate the relative difference in sensitivity to damage of the different frequency signals.

From Fig. 6, it is evident that the ultrasonic (50–500 kHz) CWI measurements registered an effect in the material at loads less than one-fourth of the load that produced visible cracks. This can be seen both from the relative velocity change and remaining decorrelation.

As the damage progresses, the relative velocity change decreases and the remaining decorrelation increase. After the beam has been loaded up to 8.5 kN, both the 500 and 250 kHz signals are so perturbed, and the decorrelation so high, that the estimated velocity change is not accurate. This data is shown with dotted lines in the relative velocity change plot, for improved visibility.

The 3.1 kHz signals display large fluctuations in the relative velocity change, with no clear relation to the progressing damage. At some points an increase in velocity is registered, which is

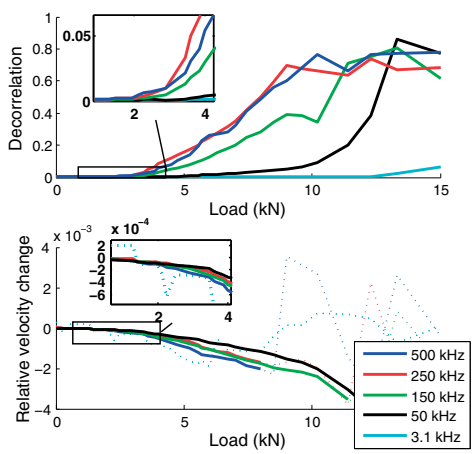

Fig. 6. Decorrelation (upper) and relative velocity change (lower) of the different frequency coda signals as a function of maximum bending load experienced by the beam. The relative velocity change measure is not relevant after the signal has been very distorted, since the degree of optimal stretching is somewhat random. These data are shown with dotted lines, in order to increase visibility in the graphs. The relative velocity change for the 3.1 kHz signals are also shown with a dotted line since the stretching method did not seem useful for this frequency.

counterintuitive. It is speculated that this is due to the fact that the coda, for these stationary wave regime signals, is created from the beam reverberating. In fact, there are several structural modes within the frequency spectra of the signal, which are excited. The time stretching procedure cannot be said to necessarily estimate the relative velocity change at these circumstances. Therefore, the line which corresponds to the 3.1 kHz signal in the lower subfigure in Fig. 6 is shown dotted, in order to increase visibility of the other lines. The decorrelation is a more straight-forward parameter, which should be applicable even if the measured coda is caused by modal reverberations. From the results it is clear that the stationary wave regime signals do not display significant decorrelation until after such loadings that visible cracks appear in the concrete.

The results from both decorrelation and relative velocity change measurements indicate that the 500 kHz measurements does not give much higher sensitivity than the 250 and 150 kHz measurements; all three configurations show some indication of change after ∼2 kN load. The 50 kHz measurements yield measurements with only slightly lower sensitivity in the decorrelation, and register a change after ∼3 kN load, though the absolute measurement values are lower than the high frequency counterparts. In the relative velocity change measurements, the 50 kHz signals display very similar sensitivity as the higher frequency signals.

5.3. General discussion

The combined results, from both experiments, indicate that CWI with signals in the simple-scattering regime (∼50–150 kHz in concrete) are quite suitable for SHM applications. These signals can be used to detect minor damage to concrete, by which we mean either a local hole or crack that is smaller than the aggregates in the concrete, or early signs of stress-induced cracking, such as a region of microcracks. The increase in sensitivity when using higher-frequency signals might not outweigh the downside of significantly higher attenuation, which necessitates a much denser transducer network in an SHM system. The simple-scattering-regime signals also exhibit a larger probed area between two transducers, which is also an attractive prospect in SHM applications.

In both the presented experiments, the time windows for the codas were placed at the times when the measured signals had an SNR of ∼25 dB. Selecting later coda windows yields measurements with greater sensitivity, but at the cost of lower SNR, which introduces more uncertainty and fluctuations. In SHM applications, in particular, care should be taken to choose a time window where a high-enough SNR is obtained, as noise and disturbances are likely to be more prevalent than in laboratory environments.

It should be noted that it is common to use chirp signals over a wide range of frequencies. Such a signal was not included in this study, as we focused on distinguishing the influences of different frequency signals. The benefits of including a wide range of frequencies in the signals are clear, but it should be noted that, for larger distances, the high-frequency components are significantly more attenuated than the lower-frequency components.

6. Conclusions

This study investigated the use of CWI in widely different scattering regimes to detect boreholes smaller than the largest aggregates in the concrete mix as well as cracks developing due to bending loads. As expected, it was found that the absolute decorrelation, and thus the sensitivity, was higher for the higher frequencies. However, it was shown that even 50 kHz signals in the simple-scattering regime can be used to detect holes in the range of 1/10 λ (∼4 mm) in the concrete, with the transmitting and receiving transducers separated by significantly larger distances than the higher-frequency signals. Furthermore, it was confirmed that the lower-frequency signals could detect holes that were located further from the centerline between the transducers. This is in agreement with the results presented by Planés et al. [18], which suggests that the width of the sensitive area of diffuse waves, between two transducers, is on the order of the transport mean free path.

Similar conclusions were drawn from the tracking of developing cracks due to bending loads; although the higher frequency signals detect earlier signs of damage, the simple-scattering-regime signals, in the range of 50–150 kHz, are not much less sensitive. This could in part be explained by the fact that significantly later parts of the codas can be analyzed for the lower-frequency signals at the same signal-to-noise-ratio. These later parts of the codas correspond to waves that are more scattered.

The results contribute to the determination of recommended choice of frequency and transducer placement in the design of CWI SHM systems for concrete structures, based on the size and type of expected damage and the general size of the structure to be monitored. For realistic concrete structures, which often are very large, the advantage in transmission range of simple-scattering-regime signals is great. Clearly, 50–150 kHz signals can readily be used to detect mm-scale damage, and higher-frequency signals might not be necessary. For more detailed information on optimal placement of the transducers and on the choice of frequency, in a specific application, simulations are recommended.

It has been shown that signals in the range of a few kHz in the stationary wave regime are not able to detect cm-scale holes in concrete, nor microcracks due to bending loads before cracks are visible. However, previous studies have demonstrated the use of such signals for monitoring stress changes, and in such applications, the very weak attenuation enables very long distances between transducers.

Acknowledgments

This work was supported by Swedish Research Council Formas [grant number 244-2012-1001].

References

[1] Y. Lu, J.E. Michaels, A methodology for structural health monitoring with diffuse ultrasonic waves in the presence of temperature variations, Ultrasonics 43 (2005) 717–731, http://dx.doi.org/10.1016/j.ultras.2005.05.001.
[2] T. Planès, E. Larose, A review of ultrasonic Coda Wave Interferometry in concrete, Cem. Concr. Res. 53 (2013) 248–255, http://dx.doi.org/10.1016/j.cemconres.2013.07.009.
[3] D.P. Schurr, J.-Y. Kim, K.G. Sabra, L.J. Jacobs, Damage detection in concrete using coda wave interferometry, NDT E Int. 44 (2011) 728–735, http://dx.doi.org/10.1016/j.ndteint.2011.07.009.
[4] O. Abraham, Y. Zhang, X. Chapeleau, O. Durand, V. Tournat, Monitoring of a large cracked concrete sample with non-linear mixing of ultrasonic coda waves, in: 7th Eur. Work. Struct. Heal. Monit., Nantes, 2014, pp. 1412–1418.
[5] Y. Zhang, O. Abraham, X. Chapeleau, L.-M. Cottineau, V. Tournat, A. Le Duff, B. Lascoup, O. Durand, Study of concrete's behavior under 4-point bending load using Coda Wave Interferometry (CWI) analysis, in: 39th Annu. Rev. Prog. Quantative Nondestruct. Eval., 2013, pp. 398–404. doi:http://dx.doi.org/10.1063/1.4789075.
[6] Y. Zhang, O. Abraham, V. Tournat, A. Le Duff, B. Lascoup, A. Loukili, F. Grondin, O. Durand, Validation of a thermal bias control technique for Coda Wave Interferometry (CWI), Ultrasonics 53 (2013) 658–664, http://dx.doi.org/10.1016/j.ultras.2012.08.003.
[7] B. Hilloulin, Y. Zhang, O. Abraham, A. Loukili, F. Grondin, O. Durand, V. Tournat, Small crack detection in cementitious materials using nonlinear coda wave modulation, NDT E Int. 68 (2014) 98–104, http://dx.doi.org/10.1016/j.ndteint.2014.08.010.
[8] Y. Zhang, V. Tournat, O. Abraham, O. Durand, S. Letourneur, A. Le Duff, B. Lascoup, Nonlinear mixing of ultrasonic coda waves with lower frequency-swept pump waves for a global detection of defects in multiple scattering media, J. Appl. Phys. 113 (2013) 64905, http://dx.doi.org/10.1063/1.4791585.

[9] Y. Zhang, V. Tournat, O. Abraham, I. Français, A. Le Duff, Nonlinear Coda Wave Interferometry for the global evaluation of damage levels in complex solids, Ultrasonics 73 (2017) 245–252, http://dx.doi.org/10.1016/j.ultras.2016.09.015.
[10] R. Snieder, A. Grêt, H. Douma, J. Scales, Coda wave interferometry for estimating nonlinear behavior in seismic velocity, Science 295 (2002) 2253–2255, http://dx.doi.org/10.1126/science.1070015.
[11] G. Poupinet, W.L. Ellsworth, J. Frechet, Monitoring velocity variations in the crust using earthquake doublets: an application to the Calaveras Fault, California, J. Geophys. Res. 89 (1984) 5719, http://dx.doi.org/10.1029/JB089iB07p05719.
[12] P.M. Roberts, Development of the active doublet method for measuring small velocity and attenuation changes in solids, J. Acoust. Soc. Am. 91 (1992) 3291, http://dx.doi.org/10.1121/1.402864.
[13] C. Sens-Schönfelder, U. Wegler, Passive image interferometry and seasonal variations of seismic velocities at Merapi Volcano, Indonesia, Geophys. Res. Lett. 33 (2006) L21302, http://dx.doi.org/10.1029/2006GL027797.
[14] O. Lobkis, R. Weaver, Coda-wave interferometry in finite solids: recovery of P-to-S conversion rates in an elastodynamic billiard, Phys. Rev. Lett. 90 (2003) 254302, http://dx.doi.org/10.1103/PhysRevLett. 90.254302.
[15] E. Larose, S. Hall, Monitoring stress related velocity variation in concrete with a 2.10^-5 relative resolution using diffuse ultrasound, J. Acoust. Soc. Am. 125 (2009) 1853–1856.
[16] C. Hadziioannou, E. Larose, O. Coutant, P. Roux, M. Campillo, Stability of monitoring weak changes in multiply scattering media with ambient noise correlation: laboratory experiments, J. Acoust. Soc. Am. 125 (2009) 3688–3695, http://dx.doi.org/10.1121/1.3125345.
[17] T. Planès, E. Larose, V. Rossetto, L. Margerin, LOCADIFF: Locating a weak change with diffuse ultrasound, AIP Conf. Proc. 1511 (2013) 405–411, http://dx.doi.org/10.1063/1.4789076.
[18] T. Planès, E. Larose, L. Margerin, C. Sens-schönfelder, Decorrelation and phase-shift of coda waves induced by local changes: multiple scattering approach and numerical validation, Waves Random Complex Media 24 (2014) 99–125, http://dx.doi.org/10.1080/17455030.2014.880821.
[19] E. Larose, J. de Rosny, L. Margerin, D. Anache, P. Gouedard, M. Campillo, B. van Tiggelen, Observation of multiple scattering of kHz vibrations in a concrete structure and application to monitoring weak changes, Phys. Rev. E. Stat. Nonlin. Soft Matter Phys. 73 (2006) 16609, http://dx.doi.org/10.1103/PhysRevE.73.016609.
[20] S.C. Stähler, C. Sens-Schönfelder, E. Niederleithinger, Monitoring stress changes in a concrete bridge with coda wave interferometry, J. Acoust. Soc. Am. 129 (2011) 1945–1952, http://dx.doi.org/10.1121/1.3553226.
[21] E. Niederleithinger, Coda wave interferometry used to localize compressional load effects in a concrete specimen, in: EWSHM-7th Eur. Work. Struct. Heal. Monit., 2014, pp. 1427–1433. <http://hal.inria.fr/hal-01021036/>.
[22] P. Fröjd, P. Ulriksen, Amplitude and phase measurements of continuous diffuse fields for structural health monitoring of concrete structures, NDT E Int. 77 (2015) 35–41, http://dx.doi.org/10.1016/j.ndteint.2015.10.003.
[23] Y. Zhang, O. Abraham, E. Larose, T. Planes, A. Le Duff, B. Lascoup, V. Tournat, R. El Guerjouma, L.M. Cottineau, O. Durand, Following stress level modification of real size concrete structures with CODA wave interferometry (CWI), AIP Conf. Proc. 1335 (2011) 1291–1298, http://dx.doi.org/10.1063/1.3592082.
[24] C. Pacheco, R. Snieder, Time-lapse travel time change of multiply scattered acoustic waves, J. Acoust. Soc. Am. 118 (2005) 1300–1310, http://dx.doi.org/10.1121/1.2000827.
[25] E. Larose, T. Planes, V. Rossetto, L. Margerin, Locating a small change in a multiple scattering environment, Appl. Phys. Lett. 96 (2010) 2013–2016, http://dx.doi.org/10.1063/1.3431269.
[26] P. Fröjd, P. Ulriksen, Efficiency of some voice coil transducers in low frequency reciprocal operations, J. Acoust. Soc. Am. 137 (2015) EL490-5, http://dx.doi.org/10.1121/1.4922011.
[27] F. Deroo, J.-Y. Kim, J. Qu, K. Sabra, L.J. Jacobs, Detection of damage in concrete using diffuse ultrasound, J. Acoust. Soc. Am. 127 (2010) 3315–3318, http://dx.doi.org/10.1121/1.3409480.
[28] P. Sheng, Introduction to Wave Scattering, Localization and Mesoscopic Phenomena, Academic Press Inc., San Diego, 1995.
[29] P. Anugonda, J.S. Wiehn, J.A. Turner, Diffusion of ultrasound in concrete, Ultrasonics 39 (2001) 429–435, http://dx.doi.org/10.1016/S0041-624X(01)00077-4.

Paper III

NDT&E International 77 (2016) 35–41

Contents lists available at ScienceDirect

NDT&E International

journal homepage: www.elsevier.com/locate/ndteint

Amplitude and phase measurements of continuous diffuse fields for structural health monitoring of concrete structures

P. Fröjd *, P. Ulriksen

Department of Engineering Geology, Lund University, John Ericssons väg 1, 221 00, Lund, Sweden

ARTICLE INFO

Article history:
Received 10 July 2015
Received in revised form
1 October 2015
Accepted 4 October 2015
Available online 14 October 2015

Keywords:
Structural health monitoring
Ultrasonic NDT
Continuous wave
Lock-in amplifier
Coda wave

ABSTRACT

Measuring amplitude and phase of continuous ultrasonic waves with a lock-in amplifier is shown to give similarly sensitive indicators of concrete damage as pulsed coda wave analysis, but maintains its sensitivity at considerably much lower signal levels. Continuous and pulsed measurements were performed on a concrete slab subjected to cyclically increased damage level. In the unloaded phase each measurement type was performed at varying transmit signal levels. The result indicates the possibility of using a larger distance between transducers in high frequency health monitoring systems of concrete structures, where attenuation of propagating waves is strong.

1. Introduction

There is an increasing demand on the reliability and safety of civil structures as these are growing in numbers and getting older. In general, early warnings of degradation or damage is desired, without invasive test procedures. For this reason, much effort has been put into developing the fields of non-destructive testing (NDT) and structural health monitoring (SHM).

Ultrasonic waves, with a variety of methods, have been successfully used in NDT of concrete structures [1,2]. Measuring velocity, attenuation and nonlinearity of propagating ultrasonic pulses have been shown to give indicators of cracking, with increasing sensitivity in the order mentioned [3–5]. Methods based on guided-waves commonly involve only analysis of the direct propagating wave, and thus only investigate the direct path between two sensors. This is not optimal in SHM of large civil structures where it is necessary to monitor as large a volume as possible, with the fixed sensor locations. One method which addresses this issue is to transmit a signal and measure the diffuse field created by boundary reflections and waves scattered by the heterogeneities in the concrete. By analyzing these trailing parts of the measured signal (coda waves), a larger volume is probed. Although it is, by definition, not possible to attribute features in the diffuse signal to any one specific bulk or guided wave mode, it has been shown that they are very sensitive to material changes [6–9]. This sensitivity can be attributed to the fact that the trailing parts of the measured signal correspond to waves which have traversed a relatively large volume and has thus been more affected by change in the material than the parts corresponding to the direct propagation path.

A major challenge in using the diffuse field is its sensitivity to changes in transducer location and coupling conditions between measurements. This issue is largely circumvented in SHM since the transducers are permanently fixed to the structure. Piezoceramic transducers (PZT) are commonly used, either embedded into the concrete or mounted on the surface. These are used both as transmitters and receivers of the mechanical waves and thus provide an efficient solution for SHM applications. In contrast, hammer impact hits, although generating strong pulses which can travel relatively far, are not suitable for SHM applications since they are not perfectly reproducible and cannot be used for reciprocal transmission and reception.

The implementation of coda wave analysis in both NDT and SHM applications and the ability of the method to detect early onsets of cracking in concrete have been extensively investigated [10–14]. There exist different methods for analyzing coda waves, including the doublet method [7–9] and the stretching method [6,15,16] among which the latter of these has been shown to be more precise and more stable towards noise [17].

Coda wave analysis has been used to follow other changes to concrete than cracking; thermal damage to the material is shown in [13] and velocity variations in the medium due to stress (acoustoelastic effect) can be followed clearly in e.g. [18,19]. In these works it is also shown that coda wave analysis is very

* Corresponding author: Tel.: +46 46 222 89 83.
E-mail address: patrik.frojd@tg.lth.se (P. Fröjd).

http://dx.doi.org/10.1016/j.ndteint.2015.10.003

sensitive to temperature variations, and some bias control technique is necessary to increase resolution and avoid false indications of damage. Further temperature bias control techniques are presented in [20]. Measuring the acoustoelastic effect yields information on nonlinear characteristics of the probed structure, which is known to be sensitive to microscopic damage. Recent research [21,22] shows alternative methods for detecting such nonlinearities with coda waves. In these studies low frequency "pump" acoustic signals are input to the structure while high frequency coda wave analysis is performed. Due to microcracking in the concrete, providing nonlinearity, the high frequency coda wave signals are modulated with the low frequency pump signals. By using different amplitudes of the pump signal and investigating the effect on the high frequency signal a measure of the nonlinear behavior of the material is yielded. Such measurements are shown to be more sensitive to microcracks, than linear parameter measurements, and less sensitive to temperature variations.

One issue with coda wave analysis, and guided waves in general, in civil structures is the fact that the attenuation of mechanical waves is substantial in concrete. This makes covering large areas difficult as the transducers have to be placed at close distance. For this reason, the prospect of being able to detect weaker signals, and thus increase transmission range, is appealing.

One method of achieving this is to use single frequency tones as excitation, as opposed to transient bursts. If a single frequency is transmitted continuously a steady-state diffuse field will stabilize after a short period of time, consisting of direct propagation, reflections in boundaries and scattered waves. The signal measured at any receiver location will then be a superposition of all different propagation paths between actuator and receiver. This removes any temporal information in the measured signal, which impedes spatial resolution. However, an advantage is the increase in energy of the scattered and reflected waves, which otherwise rapidly attenuate below the noise floor. Furthermore, continuous signals can be detected at low amplitudes, even well below the noise floor. This gives potential to increase the distance between transducers and thus enabling monitoring of larger structures.

In published work by Yan et al. [23], Liao et al. [24] and Song et al. [25] continuous waves were used in SHM of concrete beams subjected to damage. The frequency of the continuous transmission was swept over an interval and the energy at different frequency bands was calculated using wavelet package decomposition. Damage to the concrete was correlated with a decrease in energy.

Weaver et al. have presented interesting work, where devices are described and demonstrated which output high energy ultrasonic signals with extremely narrow band-widths. These can be regarded as ultrasonic analogues to optical lasers. Different systems are described, e.g. one where a piezoelectric transducer is part of a nonlinear electronic circuit which will oscillate with a certain frequency [26]. It was shown that an externally applied acoustic wave field can stimulate coherent acoustic emissions from the oscillator, with the same frequency as the external waves, as long as this frequency is close to that of the self-oscillations of the circuit. Several such oscillators can lock in to each other leading to a net increase in energy in a coherent, narrow-band signal. In other work, the authors describe systems where the input of a transmitter is connected to the output of a receiving transducer, in a feed-back loop [27,28]. The result is a narrow-band signal, whose frequency depend on the properties of the propagation medium. Such a system can be used for monitoring changes to a structure, with high sensitivity. These techniques are not implemented in this study, but are of interest in applications where single-frequency measurements are performed, as they have potential to increase transmission efficiency.

Although studies exist where continuous transmission have been used for SHM purposes, to the authors' knowledge, there is no comprehensive comparison of pulsed and continuous transmission for SHM applications. The presented study therefore investigates the use of straightforward amplitude and phase measurements from single-frequency continuous acoustic transmissions as indicators of damage and compares the sensitivity to pulsed coda wave analysis. The measurements of the continuous signals were performed with a lock-in amplifier, which is known to be able to detect very low signal levels. In order to simulate increased transducer distance, the amplitudes of the transmitted signals were gradually reduced.

2. Materials and equipment

2.1. Concrete sample

The tests were conducted on a concrete slab with dimensions $1.2 \times 0.8 \times 0.15$ m^3 and a water-cement-ratio of 0.45. The material composition of the concrete is given in Table 1. The slab was reinforced with a steel mesh (nominal diameter=6 mm) in the tension face, with 6 reinforcement bars in the direction of the strain and 7 perpendicular. Fig. 1 shows the layout of the reinforcement. The slab was cured in room temperature for 31 days, sealed with plastic sheets, before the testing.

2.2. Ultrasonic transducers

Piezo ceramic discs (Ferroperm Pz 27) with diameter 38 mm and thickness 10 mm were used as ultrasonic transducers. The discs were glued to 25-mm-high aluminum cylinders. BNC connectors were installed into threaded holes in the cylinders and connected to either pole of the ceramic discs. The transducers, PZT disc and aluminum cylinder combined, have a major resonant frequency at 47 kHz.

2.3. Pulsed transmission

For the transient measurements, an Agilent 33500B Waveform Generator was used to output a 5-cycle, Hanning-windowed, sinusoidal pulse with a center frequency of 47 kHz as excitation of the transmitter. Fig. 2 shows the excitation pulse in time and frequency domain. The signals measured by the receiver were put through a Krohn-Hite 3905B Multichannel Filter set to high-pass, with a 5 kHz cut-off frequency, and a gain of 20 dB. The filtered and amplified signal was sampled with an Agilent InfiniiVision DSO-X 3014A oscilloscope.

2.4. Continuous transmission

For the continuous measurements, the transmitter was excited by a continuous sinusoidal wave of frequency 47 kHz, generated by the 33500B waveform generator. The signal was left on for 300 ms

Table 1
Composition of concrete.

Components	Values (kg/m^3)
Cement	400
Fine aggregate (0–8 mm)	890
Coarse aggregate (8–11 mm)	445
Coarse aggregate (11–16 mm)	445
Water	180
Superplasticizer (polycarboxylate, Sikament EVO 26)	0.83

before any measurements were made, providing sufficient time for the development of a steady state.

The signals from the receiving transducer were put through the Krohn-Hite filter, with the same settings as for the pulse transmissions, and sampled with a Signal Recovery 7210 Multi-channel Lock-In Amplifier. The lock-in amplifier outputs the amplitude of the measured signal and its phase, relative to the driver signal (provided by the signal generator).

3. Acoustical measurements

3.1. Measurement procedure

The concrete slab was instrumented with the two PZT transducers on the tension face, 700 mm apart and centered on the slab. The transducer to the right of the center acted as actuator and the one to the left as receiver. The transducer locations are displayed in Fig. 1.

The slab was placed with supports 100 mm from the edges. Using a hydraulic testing machine, the load was applied as a line along the width of the slab so as to create cracks centered between transmitter and receiver. The loading protocol used was to apply an increasing load in steps, release the load between steps and then perform the acoustic measurements. Thus, the measurements were performed on an unloaded slab and developed cracks were, at least partially, closed. Each load level was chosen to be 2 kN greater than the previous one. A load cell in the testing machine measured the applied load and a displacement transducer measured the deflection of the slab.

Directly after the release of each load step, both transient and continuous transmission acoustic measurements were performed at different voltage levels of the driving signal, ranging from 10 V to 1 mV. This was made in order to simulate an increased distance between the transducers, by decreasing signal-to-noise ratio, and investigate the lower limit for where the two methods can detect damage. At each voltage level, 20 pulsed transmission measurements were performed in order to enable averaging.

The choice of 47 kHz signals gives a shear wave wavelength of ~4 cm, which is slightly larger than the largest aggregates in the concrete. This means that the transmissions were in the simple scattering regime [12]. The coda thus consists of some scattered waves, but mostly of reflections in the boundaries. The number of reflections, and their amplitude at the receiver position, depend on the geometry of the concrete slab. With the specimen dimensions and transducer placement used in the presented study, many reflections in the boundaries were measured with the same order of magnitude as the direct propagation wave.

Coda wave analysis is often performed with higher frequency signals, which are more sensitive to changes but are more quickly attenuated in the material. Like in all ultrasonic measurements, there is a trade-off between range and resolution or sensitivity, and since the aim of the study is to investigate the use of diffuse field measurements in large structures a relatively low frequency was chosen.

The signal frequency was chosen since it was the resonance frequency of the transducers. The frequency is much higher than the major resonant frequencies of the concrete specimen, and the characteristics of the transducers are assumed to influence the transmissions more than the modes of the slab.

3.2. Data processing

For both modes of transmission, damage was estimated by analyzing attenuation and velocity change as the concrete slab is damaged. For the pulsed transmission, this was done with the

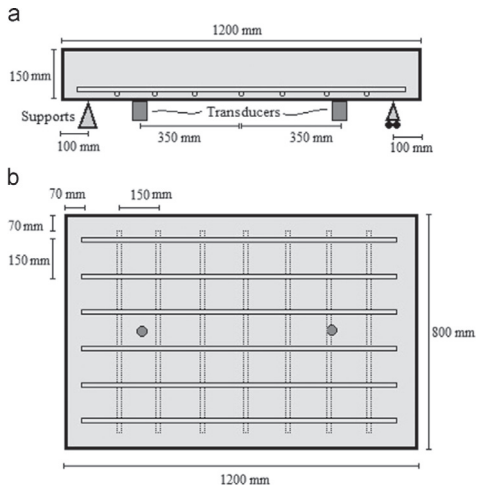

Fig. 1. Concrete dimensions, reinforcement layout and transducer locations. Concrete slab seen from the side (a) and from above (b).

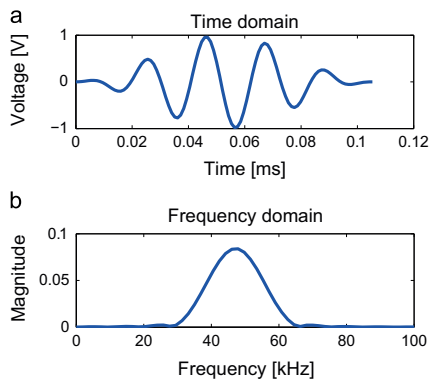

Fig. 2. Excitation signal for pulse measurements in time (upper) and frequency (lower) domain.

energy dissipation method [29] and the stretching method [6,15,16]. Before evaluation of damage the measured pulses were averaged over the 20 samples and passed through a digital 5-pole Butterworth band-pass filter with cut-off frequencies at 30 and 70 kHz in order to suppress noise. In the frequency range of interest, the noise was approximately white.

For the energy dissipation evaluations, the energy content of each measured waveform was calculated with

$$E = \sum_{k=1}^{N} \left[\frac{1}{2}(A_k + A_{k+1})\right]^2 \cdot \Delta t$$

where A_k is the amplitude of the signal at sample k, Δt is the time step and N is the number of samples. The energy measured for pulses transmitted through the undamaged sample was used as baseline. The dissipated energy for each state of damage was

defined as the ratio between the current pulse energy and the baseline energy.

The stretching method was used to estimate the variation of velocity between two diffuse ultrasonic pulse signals. The baseline coda signal was interpolated at times $t(1+\alpha)$ in a time window $[t_1\ t_2]$. This corresponds to a stretching or compression of the reference signal which was then compared to the measurement signal from the possibly damaged structure by computing the correlation coefficient:

$$CC(\alpha_i) = \frac{\int_{t_1}^{t_2} u_r(t(1+\alpha_i))u_d(t)dt}{\sqrt{\int_{t_1}^{t_2} u_r^2(t(1+\alpha_i))dt \int_{t_1}^{t_2} u_d^2(t)dt}}$$

where u_r and u_d are the reference signal and the signal from the damaged structure respectively and α_i are different stretching factors. The α that maximizes the correlation coefficient is equal to the relative modification of the propagation velocity.

For each continuous measurement, only two scalar values were acquired; amplitude and phase, relative to the exciting signal. According to the manufacturer, the dynamic reserve of the lock-in amplifier is better than 80 dB i.e. 10^{-4} and the phase accuracy is 2°.

Attenuation was evaluated as the ratio between each measured amplitude and that of the baseline signal. Changes in phase give an indication of change in velocity in the medium. Since the measured phase is that of the scattered wave field the velocity change is an average of all propagation paths between the transducers.

Measurements were performed at different levels of transmission signal amplitude. The signal-to-noise ratio (SNR) was evaluated at each transmission level according to

$$SNR = 10 \cdot \log_{10}\left(\frac{A_{sig}}{A_{noise}}\right)^2$$

where A_{sig} is the amplitude of the highest peak in the pulse, measured on the undamaged concrete slab and A_{noise} is the root-mean-square of the white noise in the measured signal, after band-pass filtering.

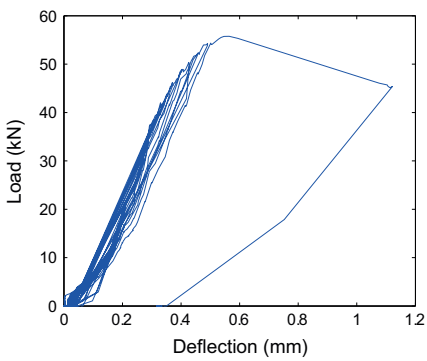

Fig. 3. Response of the concrete to the loading procedure. The reinforcement bars yielded at ~57 kN load. Acoustical measurements were performed while the slab was not loaded.

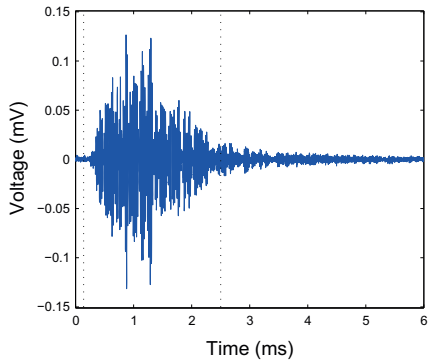

Fig. 4. Averaged and filtered pulse measurement. Vertical, dotted lines show time window used in the coda wave analysis.

4. Results and discussion

In order to induce damage in the material, the concrete slab was loaded and unloaded according to the cyclic loading procedure. The applied load was increased until the reinforcement bars yielded. After this, an applied load could not be maintained at a constant level.

Fig. 3 shows the response of the beam during the loading procedure. The reinforcement bars yielded at ~57 kN load. Cracks were only visible on the surface of the concrete just before yielding of the reinforcement bars. After unloading of each load step, both continuous and pulse measurements were performed. Fig. 4 shows the average of 20 measured pulses, filtered with a digital band-pass filter. It can be seen that multiple reflections are recorded and mixed, which support the claim that the waveform is diffuse. A 3D estimation, using the equivalent spherical volume, yields an average of ~11 reflections, assuming a velocity of 2600 m/s for a window of 2.5 ms. A similar method of estimating the number of reflections is used in e.g. [30].

It is known that the late part of the coda is more sensitive since this part corresponds to waves reflected more times than the earlier parts. However, it was observed that this part was obscured at low SNR, and since a consistent reference was desired for all SNR levels, the parts of the signal with high amplitude was used. The time window used is visualized in Fig. 4.

4.1. Energy/amplitude measurements

After each unloading of the concrete slab, new acoustical measurements were performed, and the amplitude of the continuous signals and the energy content of the pulses were measured. These are shown in Fig. 5 as a function of the concrete deflection during the preceding load step. The values are normalized with regard to the first measured energy/amplitude. Each sub-figure shows the amplitude and energy ratio for decreasing transmission signal levels. The uppermost left sub-figure shows data from measurements with a high signal-to-noise ratio. It can clearly be seen that the transmitted signal is increasingly attenuated as the concrete is loaded. The continuous and pulse transmissions show very similar sensitivity to the damage.

However, as the transmission signal level is decreased the pulse measurements become less coherent, and show little or no relation to the level of damage in the concrete. It is clear that the pulse

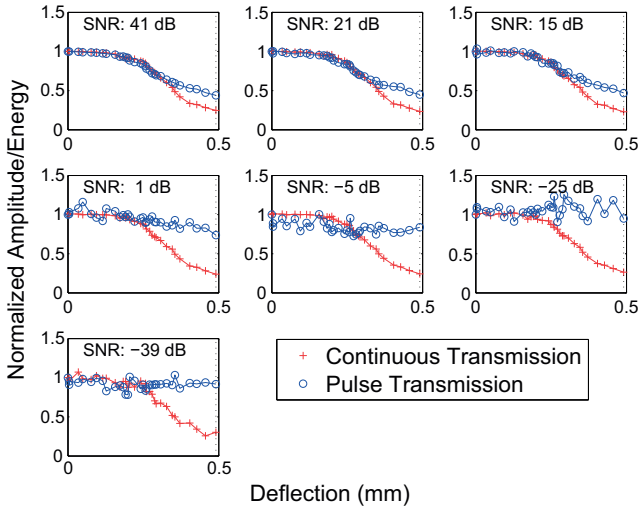

Fig. 5. Amplitude measurements from continuous measurements and energy measurements from pulse measurements as a function of deflection of the concrete slab. The amplitude and energy are normalized relative the baseline measurement. The horizontal axis of each subplot corresponds to the deflection of the concrete slab during the preceding load step. Each consecutive subplot shows measurements for decreasing signal-to-noise (SNR) ratio. The dotted, vertical line correspond to the deflection of the last load step before yielding.

is simply not measurable below the noise, even after averaging and filtering. The continuous signal data, however, measured by the lock-in amplifier, maintains its sensitivity to changes in the concrete even for extremely low signal levels; only for the lowest SNR is there some variance in the data at each load level. The results indicate that the continuous transmission display the same sensitivity as pulsed transmission, but is functional at lower signal levels.

4.2. Relative velocity/phase measurements

The relative velocity change of the pulses were computed using the stretching method in order to provide an indication of damage. The pulses measured after each load step were stretched with relative velocity change factors such as to maximize the correlation with the baseline signal. Fig. 6a shows the relative velocity change as a function of deflection of the concrete slab at the preceding load step. The figure shows data from the highest signal-to-noise ratio, ~41 dB. Fig. 6b shows the corresponding correlation after stretching. It can clearly be seen that the velocity decreases as the concrete is damaged. It can also be seen that the correlation decreases with increasing damage, since the shape of the pulse is increasingly warped. For very low values of correlation the corresponding value of relative velocity change is meaningless. This is the case after reinforcement bars have yielded, after ~0.5 mm deflection; the calculated velocity change is large, but the correlation is very low.

In order to compare the sensitivity of the time-stretch measurements for pulse transmission and the phase measurements for the continuous transmission, both data sets were normalized to the minimum value in the set of measurements before yielding of the reinforcement bars. These normalized relative values are shown in Fig. 7, as a function of previous deflection of the slab. Each sub-figure displays similar measurements with decreasing signal-to-noise ratio.

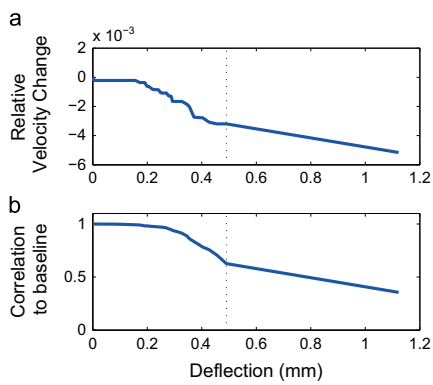

Fig. 6. (a) Relative velocity change as a function of deflection of the concrete slab, as calculated with the time-stretch method. Each value stretches the measured pulse in such a way as to maximize the correlation with the baseline. (b) Correlation with the baseline for each measured pulse after stretching with the optimal relative velocity change. The dotted black line corresponds to the deflection at breaking point for the slab.

As can be seen in Fig. 7, for the transmissions with high signal-to-noise ratio, the velocity and phase measurements display very similar sensitivity to damage, with a clear relation to the previously experienced deflection of the concrete slab. It should be noted that, after yielding of the reinforcements bars, the pulse measurements do not correlate to the baseline signal and the absolute values of these data are meaningless. These values are therefore not shown in the figure.

Similarly as for the attenuation measurements, in Fig. 5, it is clear from Fig. 7 that for very low SNR the pulse measurements cannot distinguish between the pristine and damaged concrete

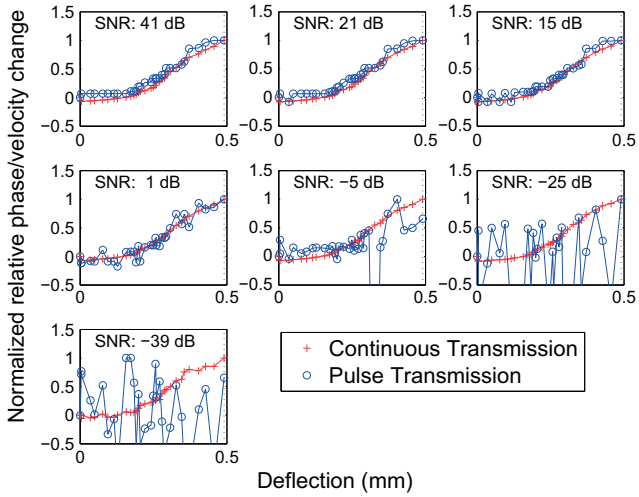

Fig. 7. Phase measurements from continuous measurements and relative velocity change measurements from pulse measurements as a function of deflection of the concrete slab. The phase and velocity change are normalized relative the minimum value of the set of measurements before the yielding of the reinforcement bars. The horizontal axis of each subplot corresponds to the deflection of the concrete slab during the preceding load step. Each consecutive subplot shows measurements for decreasing signal-to-noise (SNR) ratio. The dotted, vertical line correspond to the deflection of the last load step before yielding.

due to the signal being buried under the noise. The phase measurement maintains it sensitivity even at extremely low signal levels.

The results show that both amplitude and phase measurement of continuous waves give indications of damage equal to similar measurements with pulse transmission, with the added benefit of being able to detect much weaker signals. The pulse transmissions lose their sensitivity to damage when the measured signal is of the same order of magnitude as the noise, while the continuous measurements maintain their sensitivity even at a SNR of ~ -40 dB, and possibly lower. The presented pulse measurements are averaged with 20 samples. Theoretically, SNR increases with the square-root of the number of samples, provided that the noise is truly white and the channel is stable. Under such conditions, this means that the pulse measurements would need to be averaged 10,000 times in order to maintain sensitivity at -40 dB SNR.

The phase measurements give slightly earlier warning than the amplitude measurements, but both values are obtained simultaneously from the lock-in amplifier which means it is very little effort to design an SHM application which makes use of both parameters. The time-stretching method is computationally intensive as each measurement is correlated to many stretched baseline signals. In contrast, the phase measurements are read from the lock-in amplifier in almost real-time.

The results from the study indicate the usefulness of the measurement method for the specific concrete slab, with given dimensions and damage. However, an advantage with using multiple scattered waveforms is that increasing complexity in the geometry of the test object does not impede the measurements; more boundaries simply increase the diffusivity of the waveform. It should be noted that decreasing the transmission signal amplitude should be considered a rough approximation of increasing the distance between the transducers; in this experiment the geometry, and thus possible propagation paths, remain the same for the different simulated transducer distances. This is generally not the case for real life structures.

If continuous measurements are used, it is of great importance to establish that no parasitic electrical coupling exist between the transducers as this might hide the mechanical signal. This is less of an issue in pulse transmission, as transmission and reception is separated in time. In the presented study, this was done by observing that no signal was measured with the same experimental set-up, but with the transducers without contact with the concrete. Also, the fact that the measured signal clearly shows almost identical correlation to damage level in the concrete, as the pulsed measurements, greatly indicates that the coupling is mechanical.

The methodology demonstrated in this paper could make higher frequency signals practical in continuous monitoring of even large concrete structures. In this study signals with frequencies of ~ 50 kHz were used, which yields wavelengths of several centimeters. In order to detect smaller damage higher frequencies are typically used. For SHM purposes, however, this has not been practical due to the high attenuation in concrete.

The measurement procedure can easily be expanded to use signals with swept frequency. By sweeping across a suitable frequency range pulse measurements can be recreated with an inverse Fourier transformation. Sweeps which include lower frequency regions can utilize structural modes to possibly extend operational range further.

5. Conclusions

Amplitude and phase measurements of continuous, single-frequency ultrasonic signals as indicators of damage in a reinforced concrete slab have been evaluated. The measurements have been benchmarked to energy and velocity measurements of ultrasonic pulse measurements, with a central frequency the same as the continuous signal.

It has been shown that the continuous-signal measurements and pulse measurements display remarkably similar sensitivity to

damage, both with regard to attenuation and velocity changes, for the given excitation signals and specimen geometries.

Further studies are necessary to compare continuous transmission signals and pulsed coda wave analysis at other frequencies. It should be noted that other excitation signals for the coda wave analysis, such as chirps, can yield higher sensitivities, and that the sensitivity can be further increased by measuring nonlinear parameters, e.g. with low frequency wave modulation. The prospect of using similar nonlinearity measurements for continuous wave transmissions is of future interest.

The choice of time window in coda wave analysis is not trivial in applications with low SNR; particularly for nonlinearity measurements it has been shown that it is crucial to use very late parts of the signals [22]. However, the later parts of the coda are most obscured by noise and increased attenuation. There is thus a trade-off in sensitivity and robustness.

It has been demonstrated that continuous measurements, with a lock-in amplifier, can easily be performed at much lower signal levels than for pulse measurements, while maintaining the sensitivity to damage in the concrete. This suggests that it is possible to increase the transducer distance, or increase frequency, in SHM applications. This would be very beneficial in the monitoring of civil structures, as these can be very large and because the attenuation of mechanical waves is high in concrete. These measurements are also insensitive to variations in the noise environment of the monitored structure.

Acknowledgments

This work was supported by Swedish Research Council Formas [Grant number 244-2012-1001].

References

[1] McCann D, Forde M. Review of NDT methods in the assessment of concrete and masonry structures. NDT E Int 2001;34:71–84. http://dx.doi.org/10.1016/S0963-8695(00)00032-3.

[2] Garnier V, Piwakowski B, Abraham O, Villain G, Payan C, Chaix JF. Acoustic techniques for concrete evaluation: improvements, comparisons and consistency. Constr Build Mater 2013;43:598–613. http://dx.doi.org/10.1016/j.conbuildmat.2013.01.035.

[3] Daponte P, Maceri F, Olivito RS. Ultrasonic signal-processing techniques for the measurement of damage growth in structural materials. IEEE Trans Instrum Meas 1995;44:1003–8. http://dx.doi.org/10.1109/19.475146.

[4] Van Hauwaert A, Thimus J-F, Delannay F. Use of ultrasonics to follow crack growth. Ultrasonics 1998;36:209–17. http://dx.doi.org/10.1016/S0041-624X(97)00129-7.

[5] Warnemuende K, Wu H-C. Actively modulated acoustic nondestructive evaluation of concrete. Cem Concr Res 2004;34:563–70. http://dx.doi.org/10.1016/j.cemconres.2003.09.008.

[6] Larose E, Hall S. Monitoring stress related velocity variation in concrete with a 2.10-5 relative resolution using diffuse ultrasound. J Acoust Soc Am 2009;125:1853–6.

[7] Poupinet G, Ellsworth WL, Frechet J. Monitoring velocity variations in the crust using earthquake doublets: an application to the Calaveras Fault, California. J Geophys Res 1984;89:5719. http://dx.doi.org/10.1029/JB089iB07p05719.

[8] Roberts PM. Development of the active doublet method for measuring small velocity and attenuation changes in solids. J Acoust Soc Am 1992;91:3291. http://dx.doi.org/10.1121/1.402864.

[9] Snieder R, Grêt A, Douma H, Scales J. Coda wave interferometry for estimating nonlinear behavior in seismic velocity. Science 2002;295:2253–5. http://dx.doi.org/10.1126/science.1070015.

[10] Deroo F, Kim J-Y, Qu J, Sabra K, Jacobs LJ. Detection of damage in concrete using diffuse ultrasound. J Acoust Soc Am 2010;127:3315–8. http://dx.doi.org/10.1121/1.3409480.

[11] Lu Y, Michaels JE. A methodology for structural health monitoring with diffuse ultrasonic waves in the presence of temperature variations. Ultrasonics 2005;43:717–31. http://dx.doi.org/10.1016/j.ultras.2005.05.001.

[12] Planès T, Larose E. A review of ultrasonic Coda Wave Interferometry in concrete. Cem Concr Res 2013;53:248–55. http://dx.doi.org/10.1016/j.cemconres.2013.07.009.

[13] Schurr DP, Kim J-Y, Sabra KG, Jacobs LJ. Damage detection in concrete using coda wave interferometry. NDT E Int 2011;44:728–35. http://dx.doi.org/10.1016/j.ndteint.2011.07.009.

[14] Abraham O, Zhang Y, Chapeleau X, Durand O, Tournat V. Monitoring of a large cracked concrete sample with non-linear mixing of ultrasonic coda waves. In: Proceedings of the 7th European Workshop on Structural Health Monitoring, Nantes; 2014. p. 1412–18.

[15] Sens-Schönfelder C, Wegler U. Passive image interferometry and seasonal variations of seismic velocities at Merapi Volcano, Indonesia. Geophys Res Lett 2006;33:L21302. http://dx.doi.org/10.1029/2006GL027797.

[16] Lobkis O, Weaver R. Coda-Wave Interferometry in finite solids: recovery of P-to-S Conversion rates in an elastodynamic billiard. Phys Rev Lett 2003;90:254302. http://dx.doi.org/10.1103/PhysRevLett.90.254302.

[17] Hadziioannou C, Larose E, Coutant O, Roux P, Campillo M. Stability of monitoring weak changes in multiply scattering media with ambient noise correlation: laboratory experiments. J Acoust Soc Am 2009;125:3688–95.

[18] Zhang Y, Abraham O, Grondin F, Loukili A, Tournat V, Le Duff A, et al. Study of stress-induced velocity variation in concrete under direct tensile force and monitoring of the damage level by using thermally-compensated Coda Wave Interferometry. Ultrasonics 2012;52:1038–45. http://dx.doi.org/10.1016/j.ultras.2012.08.011.

[19] Zhang Y, Abraham O, Chapeleau X, Cottineau L-M, Tournat V, Le Duff A, et al. Study of concrete's behavior under 4-point bending load using Coda Wave Interferometry (CWI) analysis; 2013. p. 398–4 doi: 10.1063/1.4789075.

[20] Zhang Y, Abraham O, Tournat V, Le Duff A, Lascoup B, Loukili A, et al. Validation of a thermal bias control technique for Coda Wave Interferometry (CWI). Ultrasonics 2013;53:658–64. http://dx.doi.org/10.1016/j.ultras.2012.08.003.

[21] Zhang Y, Tournat V, Abraham O, Durand O, Letourneur S, Le Duff A, et al. Nonlinear mixing of ultrasonic coda waves with lower frequency-swept pump waves for a global detection of defects in multiple scattering media. J Appl Phys 2013;113:064905. http://dx.doi.org/10.1063/1.4791585.

[22] Hilloulin B, Zhang Y, Abraham O, Loukili A, Grondin F, Durand O, et al. Small crack detection in cementitious materials using nonlinear coda wave modulation. NDT E Int 2014;68:98–104. http://dx.doi.org/10.1016/j.ndteint.2014.08.010.

[23] Yan S, Sun W, Song G, Gu H, Huo L-S, Liu B, et al. Health monitoring of reinforced concrete shear walls using smart aggregates. Smart Mater Struct 2009;18:047001. http://dx.doi.org/10.1088/0964-1726/18/4/047001.

[24] Liao W-I, Wang JX, Song G, Gu H, Olmi C, Mo YL, et al. Structural health monitoring of concrete columns subjected to seismic excitations using piezoceramic-based sensors. Smart Mater Struct 2011;20:125015. http://dx.doi.org/10.1088/0964-1726/20/12/125015.

[25] Song G, Gu H, Mo YL, Hsu TTC, Dhonde H. Concrete structural health monitoring using embedded piezoceramic transducers. Smart Mater Struct 2007;16:959–68. http://dx.doi.org/10.1088/0964-1726/16/4/003.

[26] Weaver RL, Lobkis OI, Yamilov A. Entrainment and stimulated emission of ultrasonic piezoelectric auto-oscillators. J Acoust Soc Am 2007;122:3409–18. http://dx.doi.org/10.1121/1.2800315.

[27] Weaver RL, Lobkis OI. On the linewidth of the ultrasonic Larsen effect in a reverberant body. J Acoust Soc Am 2006;120:102. http://dx.doi.org/10.1121/1.2205128.

[28] Lobkis OI, Weaver RL. On the Larsen effect to monitor small fast changes in materials. J Acoust Soc Am 2009;125:1894–905. http://dx.doi.org/10.1121/1.3081530.

[29] Moradi-Marani F, Rivard P, Lamarche C-P, Kodjo SA. Evaluating the damage in reinforced concrete slabs under bending test with the energy of ultrasonic waves. Constr Build Mater 2014;73:663–73. http://dx.doi.org/10.1016/j.conbuildmat.2014.09.050.

[30] Duroux A, Sabra KG, Ayers J, Ruzzene M. Extracting guided waves from cross-correlations of elastic diffuse fields: applications to remote structural health monitoring. J Acoust Soc Am 2010;127:204–15. http://dx.doi.org/10.1121/1.3257602.

Paper IV

Original Article

SHM Structural Health Monitoring

Structural Health Monitoring
2016, Vol. 15(4) 403–412

DOI: 10.1177/1475921716642139
shm.sagepub.com
SAGE

Continuous wave measurements in a network of transducers for structural health monitoring of a large concrete floor slab

Patrik Fröjd and Peter Ulriksen

Abstract

Local, superficial damage was detected and localized on an 8 × 2-m concrete floor slab using a structural health monitoring system. A total of 30 piezoelectric transducers, placed in a grid, transmitted and received continuous ultrasonic waves that were measured using a lock-in amplifier. Tomography was used to create images from the measured amplitude and phase of the continuous waves between all possible transducer pairs. The location of damage induced by impact hits was visible in the resulting images. The signals could easily be detected even between the most distant transducer pairs, indicating the possibility of monitoring even very large concrete structures.

Keywords

Structural health monitoring, ultrasound, diffuse field, continuous wave, lock-in amplifier

Introduction

Minor damage and small cracks in concrete can quickly lead to more severe damage, for example, by exposing the reinforcement bars to the environment. Thus, early signs of damage and degradation need to be detected. To this end, much effort has been devoted to the fields of non-destructive testing (NDT) and structural health monitoring (SHM).

Ultrasonic waves have been successfully used in NDT of concrete structures.[1,2] Measurements of the velocity, attenuation, and nonlinearity of propagating ultrasonic pulses have been shown to be indicators of cracking, with increasing sensitivity in the order mentioned.[3–5] Methods based on guided waves commonly only involve an analysis of the direct propagating wave, and thus they only investigate the direct path between two sensors. This is not optimal for SHM of large civil structures, as it is necessary to monitor as large a volume as possible using fixed sensor locations.

In coda wave interferometry (CWI), the trailing part of the transient signal is included in the analysis. These signals correspond to the diffuse field created by reflections from the boundaries and scattering from heterogeneities in the material. It is not possible to attribute features in the diffuse signal to any one specific bulk or guided-wave mode, nor is it possible to determine the propagation path traveled by a wave corresponding to a particular part of the signal. However, it has been shown that CWI is very sensitive to changes in the material.[6–9] This sensitivity can be attributed to the fact that the trailing parts of the measured signal correspond to waves that have traversed a relatively large volume and they may have traversed the damaged region repeatedly. These waves, thus, have been more affected by damage in the material than the parts corresponding to the direct propagation path.

The literature describes numerous studies where CWI has been implemented in both NDT and SHM applications and investigated for its ability to detect early onsets of cracking in concrete.[10–14] Recent publications report on methods to compensate for temperature effects on CWI measurements[15–17] and to measure nonlinear effects in the monitored material,[18,19] thus furthering the usefulness of diffuse field measurements in SHM applications.

Department of Engineering Geology, Lund University, Lund, Sweden

Corresponding author:
Patrik Fröjd, Department of Engineering Geology, Lund University, John Ericssons Väg 1, SE-221 00 Lund, Sweden.
Email: patrik.frojd@tg.lth.se

However, one issue with coda wave analysis (and guided waves in general) in civil structures is the fact that mechanical waves experience substantial attenuation in concrete. This makes it difficult to cover large areas as the transducers have to be placed close together. For this reason, the prospect of detecting weaker signals, thereby increasing the transmission range, is appealing.

One method of improving the detection capability is to use single-frequency tones as the excitation instead of transient bursts. If a single frequency is transmitted continuously, then after a short period of time, a steady state will stabilize that consists of direct propagation, reflections from the boundaries, and scattered waves. The signal measured at any receiver location will be a superposition of all the different propagation paths between the actuator and receiver. This removes any temporal information in the measured signal, which impedes spatial resolution. However, an advantage is the increase in energy of the scattered and reflected waves, which would otherwise rapidly attenuate below the noise floor. Furthermore, if a lock-in amplifier is used as a coherent detector, then continuous signals can be detected at low amplitudes, even well below the noise floor. This has the potential to increase the distance between transducers and thus enable the monitoring of larger structures given a fixed number of sensors. It also has the potential to measure higher signal frequencies, which are known to be more sensitive to damage but are quickly attenuated by the concrete at significant distances.

Yan et al.,[20] Liao et al.,[21] and Song et al.[22] used continuous waves in SHM of concrete beams subjected to damage. The frequency of the continuous transmission was swept over an interval, and the energy at different frequency bands was calculated using wavelet package decomposition. The damage to the concrete was correlated with a decrease in energy. Lobkis and Weaver[23] also proposed the use of continuous wave transmissions to monitor changes in materials. In their work, the monitored structure acts as the propagation medium in an ultrasonic feedback system, and changes in the material were shown to affect the frequency of the resulting continuous tone.

In previously published work by the authors,[24] we showed that, in a reinforced concrete slab subjected to bending loads, the amplitude and phase measurements of continuous wave excitations can indicate damage with a sensitivity comparable to that of pulsed coda wave analysis. We also showed that measurements of the continuous waves maintain their sensitivity to damage in the specimen at signal-to-noise ratios far below the functional limit of pulsed wave measurements, even after the filtering and averaging of the latter.

Locating damage in concrete, when using multiple scattered and reflected wave measurements, is not straightforward due to the diffuse nature of the acquired signals. However, methods for locating damage have been proposed based on modeling travel time variations of coda waves[25] and decorrelation.[26,27] In these methods, the multiply scattered propagating wave fields are modeled as diffusion, where analytical solutions of the propagation of the average intensity in space and time are used. These tomographic methods require full waveform measurements of the diffuse wave fields, which is why they are not applicable when transmitting continuous waves and measuring with a lock-in amplifier, since this yields only scalar values of amplitude and phase. Yan et al.[20] located damage to some degree, when using continuous waves, through dividing a shear wall into horizontal and vertical subdomains and assigning each domain the value of the damage index measured by one transducer pair per domain. A similar approach is used in this work; the structure under test is divided into a set of subdomains and each domain is evaluated by averaging amplitude and phase measurements from a large number of transducer pairs.

The purpose of this study is to investigate the possibility of detecting and locating any superficial damage on a large concrete floor slab using continuous wave measurements. Reciprocal piezoelectric transducers were surface mounted in a grid on the floor, and a monitoring system was implemented that enabled reciprocal measurements between all sensors in the network.

Materials and equipment

Floor module

The floor module was a composite of an $8000 \times 2110 \times 80$-mm concrete slab on top of glued, laminated timber (glulam) beams. The glulam beams were attached to the concrete slab with screws that protruded diagonally from the beams and were cast into the concrete. Figure 1 provides details on the dimensions of the floor module, and Table 1 lists the material composition of the concrete. The water–cement ratio for the concrete was 0.442. The slab was cured for more than 28 days at 20°C at the production facility of the manufacturer, after which it was transported to the testing facility. The concrete slab was reinforced with a steel mesh with a nominal diameter of 6 and 150 mm^2.

Ultrasonic transducers

Piezoceramic disks (Ferroperm Pz 27) with a diameter of 38 mm and a thickness of 10 mm were used as the ultrasonic transducers. The disks were glued to 25-mm-high aluminum cylinders. Bayonet Neill–Concelman (BNC) connectors were installed into threaded holes in

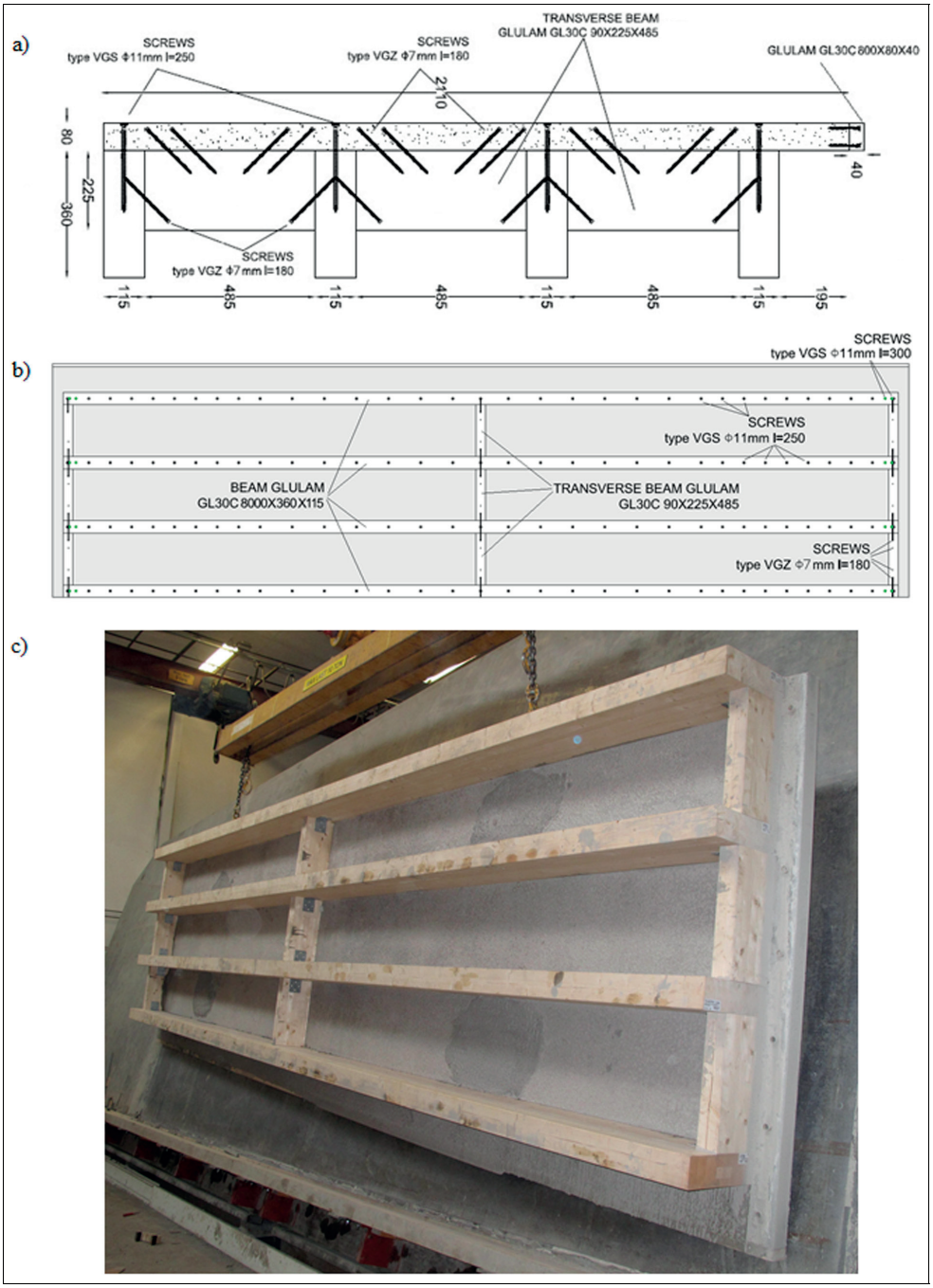

Figure 1. (a) Sketch of the floor module as seen from the short side, (b) sketch of the floor module as seen from below, and (c) photograph of the floor module as seen at an angle from below. All dimensions are in mm.

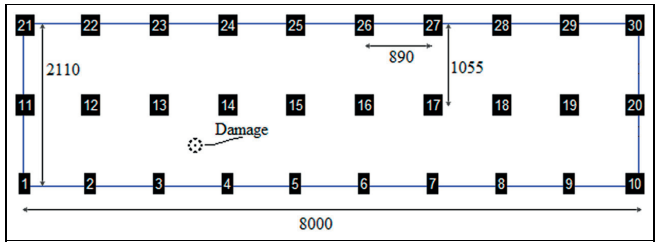

Figure 2. Layout and numbering of transducers. Dimensions are given in mm.

Table 1. Composition of concrete.

Components	Values (kg/m^3)
Sand	1006
Aggregate (8–11 mm)	704
Cement	406
Water	101
Superplasticizer (Sika HD 100)	3.8
Air-entraining agent (SikaAer S)	0.4

the cylinders and connected to each pole of the ceramic disks. Combined, the transducers, lead zirconate titanate (PZT) disk, and aluminum cylinder have major resonant frequencies around 50 kHz.

A total of 30 steel disks with a diameter of 40 mm and a thickness of 5 mm were glued onto the upper side of the concrete floor slab with an even distribution in a 3 × 10 grid. Each disk had a threaded hole by which the transducers could be attached. The layout and numbering of the transducers are shown in Figure 2.

Measurement equipment

The excitation signal was generated by an Agilent 33500B waveform generator and amplified by an A.A. Lab Systems LTD A-303 amplifier. Measurements were performed with a Signal Recovery 7210 multichannel digital signal processing (DSP) lock-in amplifier that can measure up to 32 channels simultaneously. The lock-in amplifier outputs the amplitude of the measured signal and its phase relative to the driver signal (provided by the waveform generator).

A custom-made multiplexer from SubVision was used to switch the transmission and reception channels arbitrarily between the signal generator and the lock-in amplifier.

Experimental program

For each measurement, one transmitting transducer was excited by a continuous 50 kHz sinusoidal wave. After the amplifier stage, the amplitude was 60 Vpp. The signal was left on for 100 ms before any measurements were made, providing sufficient time to reach a steady state. The lock-in amplifier measured the amplitude and phase at all 29 transducers that were not transmitting. The multiplexer then switched so that the next transducer in line operated as the transmitter and the rest as receivers. Thus, in each measurement cycle, every transducer acted once as transmitter, while all others acted as receivers. This resulted in 30 × 29 data pairs. There was no external filtering or pre-amplification of the input signals to the lock-in amplifier.

Damage was gradually induced by use of a HILTI DX2 bolt gun with 6.8/11 M10 DX cartridges, power level "green" ("light"). The bolt gun was not loaded with any bolts, but the piston was used to inflict impact damage in a repeatable manner. The location of the shots on the floor slab is indicated in Figure 2.

The first shot was fired at the center of the area between transducers 3, 4, 13, and 14. Subsequent shots were fired in a 15-cm-diameter circle around the location of the first shot. Figure 3 shows the order of the shots and the damage to the concrete. The visible damage to the concrete was superficial, with the deepest hole about 5 mm. The width of the holes varied from less than 1 to 4.5 cm. Some superficial cracking can be seen around the holes, for example, around hole number 1.

A total of 10 measurement cycles were performed with the undamaged concrete floor slab. The data from the first five measurements are used as the baseline. After the measurements on the undamaged slab, shots were fired every five measurement cycles. Table 2 shows after which shot (as numbered in Figure 3) the different measurement cycles were done. Shots 6–9 were all fired together before the last five measurement cycles.

Data processing

The lock-in amplifier measured the amplitude and phase of the steady-state wave field at each receiver location, yielding two-dimensional measurements.

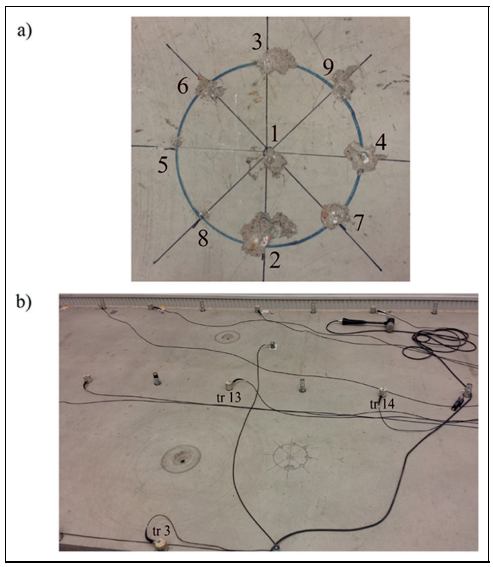

Figure 3. Photographs of the damage to the concrete from the bolt gun shots: (a) close-up of the damaged area. The numbers signify the order the shots were fired in; (b) damaged area in relation to surrounding transducers. Closest in-picture transducers are numbered. Other types of transducers, not referenced in this article, and two of the threaded holes used for lifting the floor slab are also seen.

Table 2. Definition of the damage levels.

Damage level	Shots fired	Measurement cycle numbers
Baseline	–	1–5
0	–	6–10
1	1	11–15
2	1, 2	16–20
3	1, 2, 3	21–25
4	1, 2, 3, 4	26–30
5	1, 2, 3, 4, 5	31–35
6	1, 2, 3, 4, 5, 6, 7, 8, 9	36–40

Each measurement was evaluated with Mahalanobis distance,[28] in amplitude–phase space, from the baseline data set. Equation (1) shows the Mahalanobis distance with transducer i as the transmitter and transducer j as the receiver

$$D_{i,j} = \sqrt{\left(x_{i,j}^{d} - \overline{X_{i,j}^{b}}\right)^{T} S^{-1} \left(x_{i,j}^{d} - \overline{X_{i,j}^{b}}\right)} \qquad (1)$$

where $x_{i,j}^{d}$ is an amplitude and phase measurement from the potentially damaged structure, $\overline{X_{i,j}^{b}}$ is the mean vector of the baseline data set, and S is the baseline covariance matrix. Superscript T indicates a transpose.

Mahalanobis distance equals the distance from the mean of the baseline data set, expressed as the number of standard deviations of the baseline data in the specific direction in amplitude–phase space.

This damage indication system takes into account fluctuations in the baseline data set. If the baseline measurements have large variations in a certain direction in amplitude–phase space, then a larger absolute deviation from the mean of the baseline is needed in this direction to identify a measurement value as an outlier.

Since the continuous transmission will create a diffuse field through wave scatterings and boundary reflections, all pairs are affected by changes in the concrete, not just those pairs whose direct propagation path exactly crosses the area of damage. The benefit of this is that the waves reaching the receiver will have traversed the damaged area multiple times, and this yields high sensitivity. The drawback is that it impedes spatial localization.

However, there is some correlation to the transducer pair configuration relative to the damaged region. The attenuation in the concrete is such that waves that have traveled further will have less energy than those that traveled a more direct path. This means that the part of the wave corresponding to the direct propagation path, or close to this, contains the most energy. It is reasonable to assume that those transducer pairs with the damaged region between them are affected more by the damage than the other pairs.

In order to investigate this, the floor slab was divided into a grid having the same layout as the grid formed by the transducers. Each box in the grid was assigned a value corresponding to the mean of Mahalanobis distance for all transducer pairs whose direct propagation path intersects the box. Figure 4 shows, as an example, lines between the transducers in the pairs which are included in the evaluation of the grid coordinate between transducers 3, 4, 13, and 14. The grid coordinate is highlighted in red. Since all transducers are used reciprocally as transmitters and receivers, each one transducer pair provides two measurements, with reversed transmission. For example, the grid coordinate corresponding to the location of damage includes both measurements from transmissions between transducers 3 and 4 and between transducers 4 and 3.

Results and discussions

The lock-in amplifier enabled transmission between even the furthest transducers. The measured signal

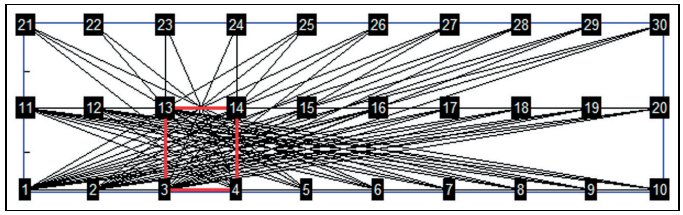

Figure 4. Lines connecting the transducer pairs from which measurements were used to evaluate the grid coordinate corresponding to the location of the damage (between transducers 3, 4, 13, and 14, as outlined in red).

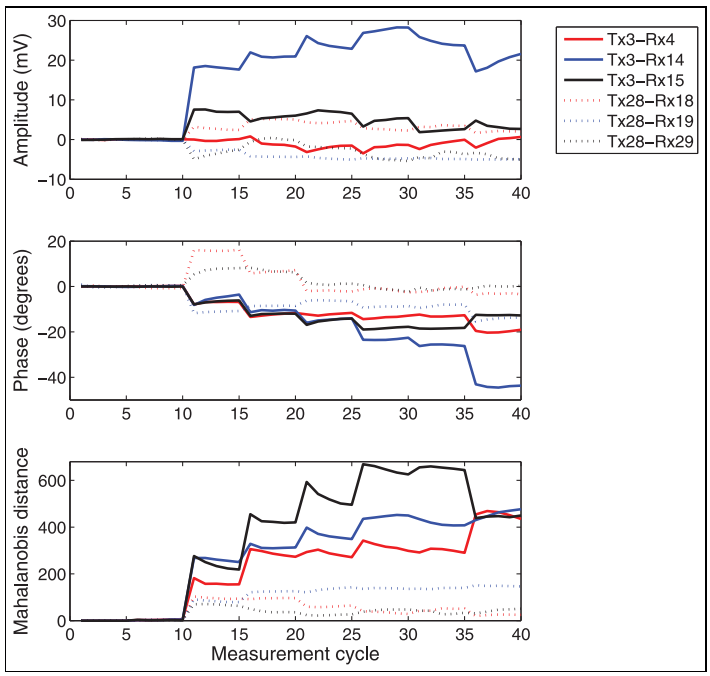

Figure 5. Data measured from transducers 4, 14, and 15 when transducer 3 acted as transmitter (solid lines) and from transducers 18, 19, and 29 when transducer 28 acted as transmitter (dotted lines). The *x*-axis shows the measurement cycle number. The first five measurements are the baseline when no damage has yet occurred. After the 10th measurement, the damage level is increased with shots made with the bolt gun after every five measurement cycles. The mean offset of the baseline data is removed from the amplitude and phase data sets. Top: amplitude measurements, center: phase measurements, and bottom: Mahalanobis distance.

level between transducers 21 and 10 (distance of ~8.2 m) was on the order of 50 μV_{rms}. Signals of this level are far below the noise floor, but the impressive capabilities of the lock-in amplifier enabled their detection.

Figure 5 shows the data measured at receivers 4, 14, and 15 while transducer number 3 is acting as transmitter, and the data measured at receivers 18, 19, and 29 when transducer 28 acted as transmitter. The measurements with transducer 3 as transmitter are close to the location of damage and those with transducer 28 as transmitter are further away from the damage. The plots in Figure 5 show the amplitude, phase, and Mahalanobis distance as a function of the measurement cycle number. The mean offsets of the baseline values have been subtracted from the amplitude and

phase data. Similar data sets were developed for every transmitter–receiver pair.

All diagrams show deviations from the baseline after the 10th measurement cycle when the first shot was fired. Further changes can be seen every five measurements, as more shots are fired at the concrete. As seen from Figure 5, the data measured with the damage between the transducers react, on average, more to the damage than the data from the transducers further from it. Some exceptions occur, as with the amplitude measurements between transducers 3 and 4.

Interestingly, the amplitudes measured by several receivers increase as the concrete is damaged. If there had been no reflections of the ultrasonic waves at the boundaries or scattering from heterogeneities, one would measure a wave traveling only along the direct propagation path. If cracks were to appear in this path, the measured amplitude would decrease due to increased attenuation and scattering. However, since we measure the sum of all possible propagation paths in a continuous wave field, it is not trivial to predict the effects on amplitude and phase. This is less of an issue in SHM than in traditional NDT, since the main goal of SHM is to detect deviations from the baseline. Even more confusing are the data sets in which the amplitude first decreases with damage and then begins to increase with further damage. This could be explained in part by the initial formation of small cracks that mostly attenuate the signals. However, as the level of damage increases, the size of the cracks act more like reflectors and the emerging wave field happens to yield higher energies at the receiving transducer location than it does with the undamaged structure. Further research is needed to better understand such behavior.

Mahalanobis distance takes into account both the amplitude and phase values for each measurement and yields data with better correlation to the damage level than if the components are analyzed separately.

The previously described algorithm was used to investigate the possibility of localizing the damage. The floor slab was divided into a grid, and the mean Mahalanobis distance of all transducer pairs that had a direct connecting line intersecting each individual grid box was calculated in a tomographic style. Figure 6 shows such data from one measurement at each of the different damage levels.

The imaging method successfully identifies the grid coordinate of the damage as the box with the highest mean Mahalanobis distance from the baseline data. Additionally, it is evident that the deviation from the baseline increases as the damage level increases. This increase is seen over the entire floor slab, and there is a misleading, particularly, high, indication in the grid box 8–9–18–19, but at all damage levels the correct grid box is assigned the highest value.

It should be noted that even the first damage level yields a mean Mahalanobis distance of 72 in the grid box corresponding to the damaged area. This is a substantial deviation, corresponding to 72 standard deviations from the mean of the baseline data set, and the possibility of detecting even slighter damage seems likely.

It is of interest to see if similar localization is possible with a sparser network of transducers. An example is shown in Figure 7(a), where only transducers 4, 8, 11, 20, 22, 26, and 30 are used. It is evident from the figure that it is possible to localize the damage with sparser networks. Further removal of transducers resulted in a gradual loss of ability to locate the damage.

Figure 7(b) shows a lower resolution localization using only the data from the four transducers in the corners of the slab. This is encouraging for the scalability of the system; a system similar to that in this study but with several meters between the closest transducers would have great utility. Scaling the experiment is not straightforward, however, as the distance to the reflective boundaries affects the emerging diffuse wave field.

It should be stressed that the shading of the boxes in the grid is based on the means of all values from the transducer pairs with direct propagation paths crossing the box. Looking only at one or a very few pairs can yield false negative indications of damage in the vicinity of the pair or false positive indications at other locations. Further research is needed to fully understand this instability, but averaging over a number of transducer pairs mitigates the effects of such outliers.

Conclusion

It has been shown that amplitude and phase measurements of single-frequency steady-state wave fields can successfully be used to detect small superficial damage in a concrete slab. Mahalanobis distance from baseline measurements was used as an indicator of damage. This distance increased as further damage was introduced to the floor slab.

Using a lock-in amplifier, useful signals were detectable even between transducer pairs placed 8.2 m apart. This was achieved with an excitation signal amplitude of 60 Vpp, which is relatively low compared to many other presented guided-wave SHM applications. An even greater range is expected if the excitation signal is increased further, although care must be taken when using continuous transmissions to avoid accidentally measuring the electrical coupling in the measurement system. The proposed measurement technique, thus, has the potential for monitoring even larger structures.

Using a 50-kHz transmission frequency, it was possible to locate the damaged region within an area slightly

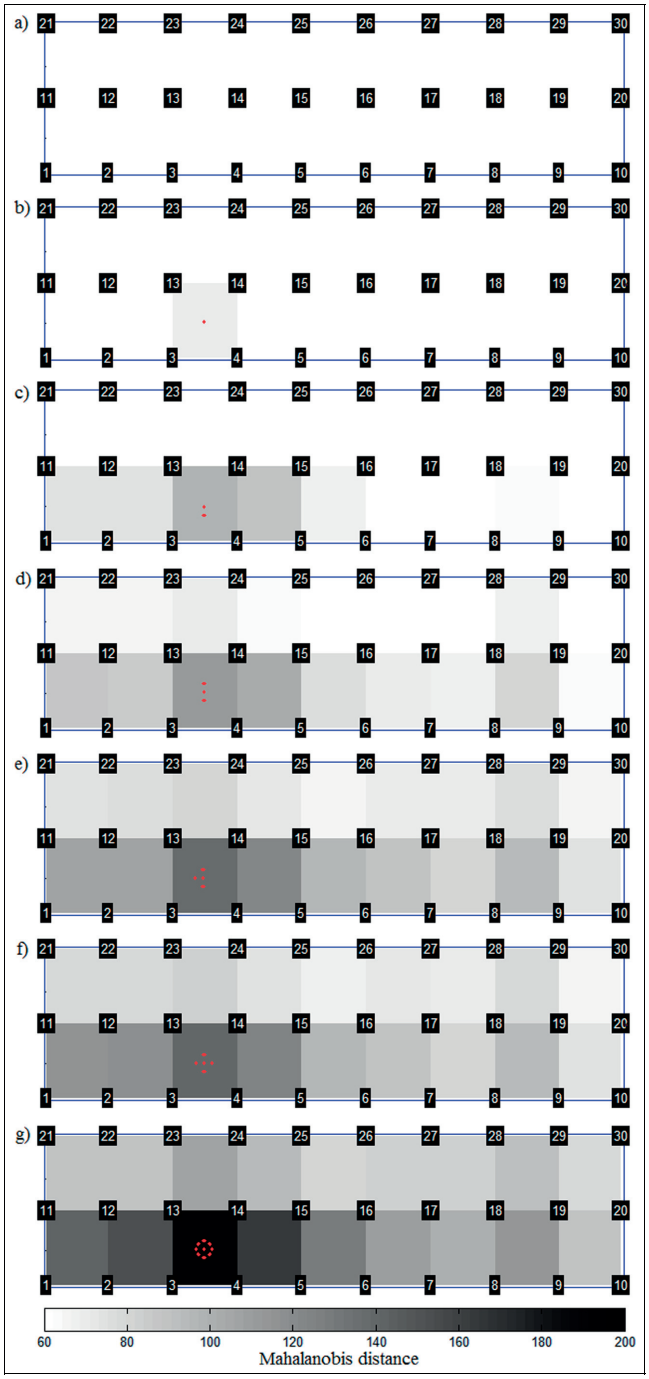

Figure 6. Mahalanobis distance from the baseline data for measurements at different damage levels: (a)–(g) damage levels 0–6. The red dots indicate locations of bolt gun shots.

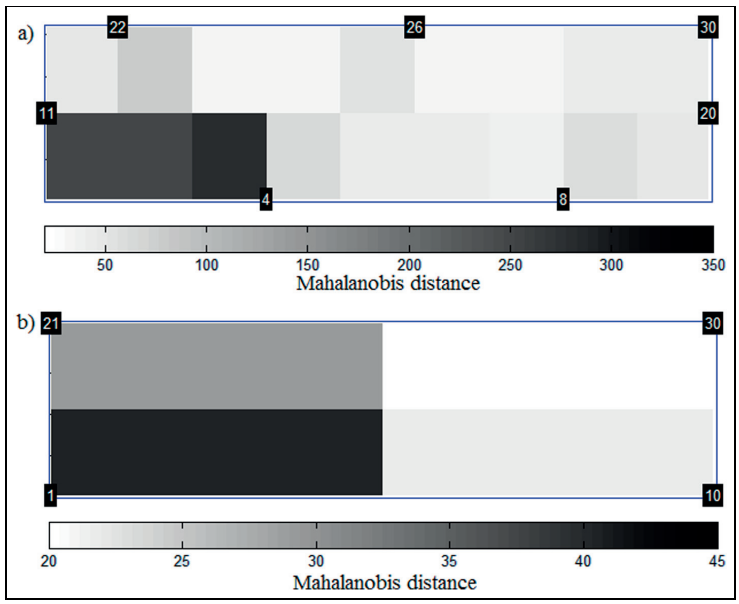

Figure 7. Mahalanobis distance from the baseline data for sparse networks of transducers at damage level 6: (a) transducers 4, 8, 11, 20, 22, 26, and 30 were used and (b) transducers 1, 10, 21, and 30 were used.

less than 1 m^2 through averaging of all transducer pair combinations.

Fluctuations are a source of error in the measurements. It is speculated that these fluctuations are caused by temperature variations leading to slight shifts in the transfer functions between each transducer pair, resulting in fluctuations in the efficiency of the chosen transmission frequency. A possible method to avoid this sensitivity is to step through a number of frequencies.

Further research is needed to be able to predict the effect of different changes in the material on the amplitude and phase of the transmitted signal between two transducers. However, by averaging the result over a number of transducer pairs and calculating Mahalanobis distance from the baseline, it is possible to detect and locate damage and to differentiate between damage levels of varying severity.

Acknowledgements

The authors would like to give special thanks to the manufacturers of the concrete floor module. The concrete slab was constructed by Hedareds Sand & Betong AB, and the glulam beams were created by Moelven Töreboda AB.

Declaration of Conflicting Interests

The author(s) declared no potential conflicts of interest with respect to the research, authorship, and/or publication of this article.

Funding

The author(s) disclosed receipt of the following financial support for the research, authorship, and/or publication of this article: This work was supported by the Swedish Research Council Formas (grant no. 244-2012-1001).

References

1. McCann D and Forde M. Review of NDT methods in the assessment of concrete and masonry structures. *NDT&E Int* 2001; 34: 71–84.
2. Garnier V, Piwakowski B, Abraham O, et al. Acoustic techniques for concrete evaluation: improvements, comparisons and consistency. *Constr Build Mater* 2013; 43: 598–613.
3. Daponte P, Maceri F and Olivito RS. Ultrasonic signal-processing techniques for the measurement of damage growth in structural materials. *IEEE T Instrum Meas* 1995; 44: 1003–1008.
4. Van Hauwaert A, Thimus J-F and Delannay F. Use of ultrasonics to follow crack growth. *Ultrasonics* 1998; 36: 209–217.
5. Warnemuende K and Wu H-C. Actively modulated acoustic nondestructive evaluation of concrete. *Cement Concrete Res* 2004; 34: 563–570.
6. Larose E and Hall S. Monitoring stress related velocity variation in concrete with a 2.10^{-5} relative resolution using diffuse ultrasound. *J Acoust Soc Am* 2009; 125: 1853–1856.

7. Poupinet G, Ellsworth WL and Frechet J. Monitoring velocity variations in the crust using earthquake doublets: an application to the Calaveras Fault, California. *J Geophys Res* 1984; 89: 5719.
8. Roberts PM. Development of the active doublet method for measuring small velocity and attenuation changes in solids. *J Acoust Soc Am* 1992; 91: 3291.
9. Snieder R, Grêt A, Douma H, et al. Coda wave interferometry for estimating nonlinear behavior in seismic velocity. *Science* 2002; 295: 2253–2255.
10. Deroo F, Kim J-Y, Qu J, et al. Detection of damage in concrete using diffuse ultrasound. *J Acoust Soc Am* 2010; 127: 3315–3318.
11. Lu Y and Michaels JE. A methodology for structural health monitoring with diffuse ultrasonic waves in the presence of temperature variations. *Ultrasonics* 2005; 43: 717–731.
12. Planès T and Larose E. A review of ultrasonic Coda Wave Interferometry in concrete. *Cement Concrete Res* 2013; 53: 248–255.
13. Schurr DP, Kim J-Y, Sabra KG, et al. Damage detection in concrete using coda wave interferometry. *NDT&E Int* 2011; 44: 728–735.
14. Abraham O, Zhang Y, Chapeleau X, et al. Monitoring of a large cracked concrete sample with non-linear mixing of ultrasonic coda waves. In: *7th European workshop on structural health monitoring*, Nantes, July 8–11, 2014, pp. 1412–1418. Inria.
15. Zhang Y, Abraham O, Grondin F, et al. Study of stress-induced velocity variation in concrete under direct tensile force and monitoring of the damage level by using thermally-compensated Coda Wave Interferometry. *Ultrasonics* 2012; 52: 1038–1045.
16. Zhang Y, Abraham O, Chapeleau X, et al. Study of concrete's behavior under 4-point bending load using Coda Wave Interferometry (CWI) analysis. In: *The 39th annual review of progress in quantitative nondestructive evaluation*, Denver, CO, 15–20 July, 2012 (Proceedings given out 2013), pp. 398–404. AIP Publishing.
17. Zhang Y, Abraham O, Tournat V, et al. Validation of a thermal bias control technique for Coda Wave Interferometry (CWI). *Ultrasonics* 2013; 53: 658–664.
18. Zhang Y, Tournat V, Abraham O, et al. Nonlinear mixing of ultrasonic coda waves with lower frequency-swept pump waves for a global detection of defects in multiple scattering media. *J Appl Phys* 2013; 113: 064905.
19. Hilloulin B, Zhang Y, Abraham O, et al. Small crack detection in cementitious materials using nonlinear coda wave modulation. *NDT&E Int* 2014; 68: 98–104.
20. Yan S, Sun W, Song G, et al. Health monitoring of reinforced concrete shear walls using smart aggregates. *Smart Mater Struct* 2009; 18: 047001.
21. Liao W-I, Wang JX, Song G, et al. Structural health monitoring of concrete columns subjected to seismic excitations using piezoceramic-based sensors. *Smart Mater Struct* 2011; 20: 125015.
22. Song G, Gu H, Mo YL, et al. Concrete structural health monitoring using embedded piezoceramic transducers. *Smart Mater Struct* 2007; 16: 959–968.
23. Lobkis OI and Weaver RL. On the Larsen effect to monitor small fast changes in materials. *J Acoust Soc Am* 2009; 125: 1894–1905.
24. Fröjd P and Ulriksen P. Amplitude and phase measurements of continuous diffuse fields for structural health monitoring of concrete structures. *NDT&E Int* 2016; 77: 35–41.
25. Pacheco C and Snieder R. Time-lapse travel time change of multiply scattered acoustic waves. *J Acoust Soc Am* 2005; 118: 1300–1310.
26. Larose E, Planes T, Rossetto V, et al. Locating a small change in a multiple scattering environment. *Appl Phys Lett* 2010; 96: 2013–2016.
27. Planès T, Larose E, Rossetto V, et al. LOCADIFF: locating a weak change with diffuse ultrasound. In: *AIP conference proceedings*, Denver, CO, 15–20 July 2012, pp. 405–411. New York: AIP Publishing.
28. Mahalanobis PC. On the generalised distance in statistics. *Proc Natl Inst Sci India* 1936; 2: 49–55.

Paper V

Original Article

SHM
Structural Health Monitoring

Structural Health Monitoring
1–10

DOI: 10.1177/1475921717699878
journals.sagepub.com/home/shm
SAGE

Detecting damage events in concrete using diffuse ultrasound structural health monitoring during strong environmental variations

Patrik Fröjd and Peter Ulriksen

Abstract

Diffuse ultrasonic wave measurements used in structural health monitoring applications can detect damage in concrete. However, the accuracy is very susceptible to environmental variations. In this study, a large concrete floor slab was monitored using diffuse wave fields that were generated by continuous-wave transmissions between ultrasonic transducers. The slab was monitored for several weeks while being subjected to changes in environmental conditions. Subsequently, it was damaged using impact hits, resulting in centimeter-scale cracking. The variations caused by the environment masked the effects of the damage in the measurements. To address this issue, the Mahalanobis distance was used to distinguish between the influence of the damage and the influence of the environmental variations. The Mahalanobis model uses amplitude and phase measurements of continuous waves at a set of different frequencies as inputs. A moving window approach was applied to the baseline data set to account for slow trends. This study shows that this technique greatly suppresses most of the variations caused by environmental conditions. All damage events in our data set have been detected.

Keywords

Structural health monitoring, ultrasound, diffuse field, continuous wave, lock-in amplifier, Mahalanobis distance, environmental variations

Introduction

Structural health monitoring (SHM) systems that can continuously monitor the condition of concrete structures would help to address the ever increasing demand for safety and efficiency of civil structures, especially in light of the aging infrastructure in many countries. Unfortunately, it is far from trivial to implement SHM systems in concrete structures, due to their large sizes and the complexity of the material. Modal analysis is a useful tool for detecting damage from changes in global vibrational properties of the structure. However, these low-frequency methods are generally not able to detect small localized damages. Early detection of small cracks in concrete is important, as these cracks can quickly lead to more serious damages, for example, by exposing reinforcement bars to the environment. To localize these kinds of damages, higher frequency vibrations are necessary and ultrasonic methods can be employed. The use of ultrasonic methods in concrete is complicated since the aggregates and reinforcement bars inside the material are of a similar size as the wavelength of the mechanical waves. This leads to severe multiple scattering, which redistributes the energy from the directly propagating part of a transferred pulse to a diffuse wave field. When measuring a transient pulse traveling through concrete, these diffuse waves appear as a tail behind the direct propagating part of the wave. This trailing part of the wave is called the coda. It has been shown that proper analysis of coda waves, for example, by coda wave interferometry[1,2] (CWI), yields measurements which are much more sensitive to changes in the propagation material than any analysis of only the direct propagating wave by, for example, measuring time of flight. This high sensitivity is due to the multiple scattering of the late arriving waves; since they have longer travel times, they

Department of Engineering Geology, Lund University, Lund, Sweden

Corresponding author:
Patrik Fröjd, Department of Engineering Geology, Lund University, John Ericssons Väg 1, SE-221 00 Lund, Sweden.
Email: patrik.frojd@tg.lth.se

are more affected by changes in effective velocity than the direct propagating part. CWI is recently used quite often for non-destructive testing (NDT) or SHM purposes in concrete. We refer to the review article by Planés and Larose[3] for an overview.

The diffuse nature of high-frequency waves in concrete makes it impractical to implement different wave mode analyses, such as those used in metal plate structures, as the different dispersion modes are quickly concealed by the multiple scattered waves. However, one advantage of diffuse wave measurements is that they can be used to probe more than just the material located in a direct line between the transmitting and receiving transducers. This is because the multiple scattered waves traverse a wider region of the material. Thus, CWI could fill the gap between global, but insensitive, modal analysis methods and local, detailed NDT point measurements. This is a very promising prospect for SHM applications. The region of influence of diffuse waves between two transducers can be estimated by modeling the propagation of energy either as diffusion or using radiative transfer models.[1,4,5] These models can be used to construct sensitivity kernels that provide a spatial map of the sensitivity of the diffuse waves to changes in the material. These kernels have been shown to be complex, particularly if anisotropic scattering is considered,[6] but, in general, a high sensitivity region exists close to, and between, the transmitting and receiving transducers. These sensitivity kernels can be used in inversion procedures, such as the LOCADIFF algorithm, for locating local changes to the material.[7–11]

In concrete, one issue with CWI and ultrasonic methods in general is the high attenuation of high-frequency waves, caused by both scattering and intrinsic absorption. This attenuation, combined with often noisy environments for civil structures, means that the transducers cannot be separated by large distance before the signal-to-noise ratio (SNR) decreases below useful levels. We have previously shown that for detecting bending damage in a concrete slab, the transmission of single-frequency, continuous waves and their sampling with a lock-in amplifier can produce data with similar sensitivity as transient CWI, but at much lower SNR levels.[12] This allows larger distances to be used between transducers in a network, even in the presence of high-frequency noise. When a single frequency is transmitted continuously, a steady state is shortly reached that contains direct propagation, reflections from the boundaries, and scattered waves.

Localization methods such as LOCADIFF require measurements of transient time series, which are not available when measuring with a lock-in amplifier. Instead, we have earlier proposed a tomographic procedure that provides a rough localization of a small defect in a large concrete floor slab.[13] A similar method is used in this work.

One of the greatest challenges in SHM is the sensitivity of measurements to environmental or operational variations (EOVs). Examples of such conditions are temperature, humidity, wind, and traffic. EOVs can lead to false indications of damage in the structure and often affect measurements even more than the real damage. Unfortunately, the high sensitivity of coda waves also means that such methods are very susceptible to EOVs.[14,15]

Some prior studies have used a reference specimen to compensate for measurement fluctuations in CWI measurements caused by temperature variations.[16,17] The reference specimen was subjected to the same temperature variations as the test specimen, but was not subjected to any loads. This thermal bias control technique worked well to remove undesired variations, particularly when it was combined with measurements of nonlinear parameters that are less sensitive to temperature variations.[18] Another method is the optimal baseline selection method (also known as the look-up table method), which stores a number of baseline data sets acquired at different environmental situations.[19–21] Each new measurement is then evaluated against the baseline with which it is most similar. This has been shown to work well with diffuse ultrasound measurements subjected to temperature variations.[22] Salvermoser et al.[23] showed a strong correlation between velocity change and temperature, measured on a concrete bridge. Linear regression parameters could then be found which could be used to scale the measured temperature to estimate the effect on the velocity. By subtracting this estimated temperature-induced variation from the measured relative velocity change, only changes caused by damage should remain.

Unfortunately, a reference specimen will not always be available in real structures, and furthermore, most structures will be exposed to many EOVs other than global temperature variations. For instance, sunshine will occasionally heat some parts of a structure, while other sections remain cool. Exposure to EOVs will give rise to complicated behaviors, and statistical methods are needed for data normalization, possibly combined with a machine learning method. One popular tool for data normalization in SHM applications is the Mahalanobis[24] distance. It has been used in a number of studies to successfully compensate for temperature variations and to detect outliers corresponding to damage.[25–27] Other data normalization methods exist, for example cointegration, and we refer to the book by Farrar and Worden[21] for more information on data normalization and machine learning approaches for handling EOVs in SHM.

For this work, a large concrete floor slab was monitored for several weeks while subjected to significant temperature variations and complex sunshine patterns. These changes occurred naturally due to the slab's location in a laboratory hall with large windows. The monitoring system consisted of a distributed network of piezoelectric transducers which were used to transmit or receive continuous waves on command. The monitoring system is the same as used in our previously published work,[13] where it was shown to successfully detect damage in short-term acquisitions, where the data were not significantly affected by EOVs. The same localization procedure was applied here. A number of frequencies were used in order to increase the level of information yielded by each measurement cycle. Baseline measurements were gathered for more than 2 weeks before damage was introduced to the concrete. The purpose of this work is to demonstrate the use of the Mahalanobis distance as a data normalization procedure that can compensate for the influence of EOVs on diffuse wave field SHM measurements and to show that this enables the detection of a sudden damaging event.

Materials and equipment

Floor slab

The floor slab was an 8000 × 2110 × 80 mm composite concrete slab on top of glued, laminated timber beams (glulam). The concrete slab was reinforced with a steel mesh with a nominal diameter of 6 mm, and 150 mm squares. We refer to our previously published work[13] for more details of the geometry of the floor slab and the material composition of the concrete.

Ultrasonic transducers

Piezo ceramic disks (Ferroperm Pz 27) with 38 mm diameter and 10 mm thickness were used as ultrasonic transducers. The disks were glued to 25-mm-high aluminum cylinders. Bayonet Neill–Concelman (BNC) connectors were installed into threaded holes in the cylinders and connected to each pole of the ceramic disks. The transducers (lead zirconate titanate (PZT) disk and aluminum cylinder combined) have major resonant frequencies around 40–50 kHz, as well as some weaker resonances around 10–15 kHz.

Steel disks with 40 mm diameter and 5 mm thickness were glued onto the upper side of the concrete floor slab in a regular grid distribution. Each disk had a threaded hole for attaching the transducers. Eight transducers were used in this study. The layout and numbering of the transducers are shown in Figure 1.

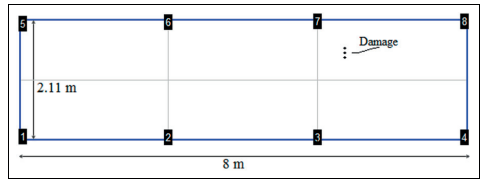

Figure 1. Layout and numbering of transducers and the location of the induced damage. The gray grid lines are those used in the tomographic procedure.

Measurement equipment

The excitation signal was generated by an Agilent 33500B waveform generator and amplified by an A.A. Lab Systems LTD A-303 amplifier. Measurements were performed with a Signal Recovery 7210 multichannel digital signal processing (DSP) lock-in amplifier that can measure up to 32 channels simultaneously. The lock-in amplifier outputs the amplitude of the measured signal and its phase relative to the driver signal (provided by the waveform generator).

A custom-made multiplexer from SubVision was used to switch the transmission and reception channels arbitrarily between the signal generator and the lock-in amplifier.

Experimental program

To obtain each measurement, one of the eight transducers was excited by a continuous sinusoidal wave with an amplitude of 60 Vpp. The signal started 100 ms before any measurements were made, providing sufficient time to reach a steady state. The lock-in amplifier measured the amplitude and phase at the seven transducers that were not transmitting. The multiplexer then switched to the next transducer in line to serve as the transmitter. The entire procedure was repeated at various frequencies: 13, 40, 42, 46, 48, and 50 kHz. These frequencies were chosen to correspond to the resonant frequencies of the transducers. The lowest frequency (13 kHz) was speculated to be less sensitive to damage than the higher frequency signals, but still sensitive to temperature variations. Low-frequency diffuse wave field measurements have been shown to be useful for measuring changes caused by variation in temperature.[14] Thus, they can be useful in the algorithm to differentiate between changes caused by damage and those caused by temperature.

In each measurement cycle, transmissions with all transducer combinations were repeated for each of the six frequencies, so that, in each cycle, 8 × 7 × 6 measurements were made. Each measurement cycle took

Figure 2. (Left) Photograph of the floor slab and the laboratory hall. Not all transducers seen in the photograph were used in this study. (Right) Close-up of the damage to the concrete. A ruler is included for reference.

approximately 1 min. This time can very likely be reduced by optimizing the control system. There was no external filtering or pre-amplification of the input signals to the lock-in amplifier.

The concrete floor slab was stored in a laboratory hall with windows covering one wall. This enabled the sun to shine into the laboratory, which heated the room considerably and resulted in day-night temperature cycles in the room with heterogeneous heating as the sunlight moved over the floor. Measurements were taken while the slab was left undamaged for 19 days. After that time, the concrete was locally damaged using a HILTI DX2 bolt gun with 6.8/11 M10 DX cartridges, power level "green" ("light"). The bolt gun was not loaded with bolts, but the piston was used to damage the concrete. The location of the damage is shown in Figure 1. Two shots were performed on the 20th day, and an additional shot was made a day later. After this, the floor was left undisturbed for several more days before the experiment was terminated, resulting in a total of 25 days of measurements. Figure 2 shows a photograph of the floor slab in the laboratory setting and a close view of the damage from the bolt gun impacts. The resulting damage consisted of small holes with surrounding cracked regions. The holes were 4–5 mm deep in the center, and the cracked regions ranged from 1 to 3 cm.

Amplitude and phase measurements, as described above, were performed during the entire experiment at ~35-min intervals. Two Velleman DVM171THD data loggers, placed on the floor slab, were used to log the temperature in the laboratory during the experiment, and the recorded temperature varied between 20°C and 27°C.

Data normalization

The lock-in amplifier measured the amplitude and phase of the steady-state wave field for each of the six frequencies at each receiver location. These can be viewed as 12-dimensional measurement points that have very complex behavior when subjected to changes in environmental conditions, such as temperature, or operational variations in the measurement system.

It can be very difficult to see trends in multivariate data or see deviations from previous system behaviors. One popular tool to evaluate such data is the Mahalanobis distance. A set of multivariate data points, the baseline, is used as a reference. Each new data point is evaluated as the distance between it and the center of the baseline data set. This distance is expressed as the number of standard deviations of the baseline in the direction, in multidimensional space, in which the new point is separated from the center. In this article, it is understood that "Mahalanobis distance" implies the Mahalanobis distance of the current sample to the baseline.

In this case, the amplitudes and phases of the six different frequency measurements are used as features in the Mahalanobis distance, and these define the dimensions in a 12-dimensional space. The general idea is that damage to the concrete will shift the measured data, in this space, in a direction that is orthogonal to the variations caused by, for example, temperature variations. Since this shift is in a direction where the baseline does not have a high variation, it will result in a relatively large Mahalanobis distance.

The following equation shows the calculation of Mahalanobis distance with transducer i as the transmitter and transducer j as the receiver

$$D_{i,j} = \sqrt{\left(x_{i,j}^{d} - \overline{X_{i,j}^{b}}\right)^{T} S^{-1} \left(x_{i,j}^{d} - \overline{X_{i,j}^{b}}\right)}$$

$x_{i,j}^{d}$ is a 12-dimensional six-frequency amplitude and phase measurement from the potentially damaged

structure, $\overline{X_{i,j}^{b}}$ is the mean vector of the baseline data set, and S is the baseline covariance matrix. Superscript T indicates a transpose.

The baseline consisted of 300 data points corresponding to measurements over approximately 1 week. If the baseline period is too short, even small variations in environmental conditions from day to day will result in large Mahalanobis distances. A week was deemed appropriate for the current experiment. However, apart from the daily variations in temperature, the floor and the transducers were also subjected to slow variations; for example, larger scale weather conditions changed approximately weekly. This led to the baseline becoming quickly outdated, which in turn led to an increasing Mahalanobis distance over time even though no damage was inflicted. To account for these slow variations, a moving window approach was implemented in which the baseline was continuously updated with new data points and old points were discarded. An example of a moving window algorithm was presented by Jeng,[28] based on principal component analysis rather than the Mahalanobis distance.

Different results will be yielded depending on the "lag" of the baseline, that is, the time between the end of the baseline and the evaluated data point. In this implementation, no lag was introduced, so each measured data point was evaluated using a baseline consisting of the 300 previous points. This was well suited for sudden, instantaneous damage, as there was a sharp line dividing the subset of data from the non-damaged structure and the subset from the damaged structure. One effect of not using any lag was that the next sample (the second sample after the damage was introduced) was evaluated with a baseline which contained information that was also from the damaged structure. Therefore, the model learned this behavior and the point was given a low Mahalanobis distance. The result was that sudden damaging events appeared as sharp spikes in the timelines, even though the damage, of course, remained in the structure. Increasing the baseline lag smoothed the peak in time.

Localization

Since a continuous transmission, as mentioned previously, creates a diffuse field through wave scatterings and boundary reflections, all transducer pairs are potentially affected by changes in the concrete, not just those pairs whose direct propagation path exactly crosses the area of damage. As mentioned, the benefit of this is that the waves reaching the receiver will have traversed material for longer periods of time, which yields high sensitivity. It also means that a damaged region does not have to be located directly between two transducers to be detectable. The drawback is that it impedes spatial localization.

The influence of changes in the propagation material on diffuse waves is extremely difficult to predict. By modeling the diffuse propagation with either diffusion or radiative transfer models, it is possible to construct sensitivity kernels between a transmitter and a receiver.[4–6] These models confirm that the influence of a change on diffusely propagating waves is greater if the change is located close to either the transmitter or receiver or if it is somewhat in between the two. In a previous article,[13] the authors showed that a simple tomographic procedure can be used to provide rough localization of damage if a network of transducers is employed. In this procedure, the structure is divided by a grid. A value corresponding to the mean of the resulting Mahalanobis distance for all transducer pairs whose direct propagation path intersects the box is assigned to each grid cell.

Results and discussion

During the entire 25-day experiment, the temperature in the laboratory varied between 20°C and 27°C and sunshine heated both the floor slab and the transducers in complicated patterns. Figure 3 shows the measured temperature from one of the data loggers. It should be stressed that this temperature measurement only represents the temperature at one specific location on the floor slab; significant differences were noticed over the surface of the slab during sunny days due to the sun movement patterns. However, the temperature data in Figure 3 provide a good indication of the general temperature in the room at any given time, and 24-h cycles are clearly visible. The upper x-axis in Figure 3 displays the time in hours, and, for reference, the lower x-axis displays the corresponding sample numbers for the SHM system. The vertical gray lines indicate the times of the bolt gun shots.

The effect of these variations can easily be seen in the raw data. Figure 4 shows example amplitude and phase data as a function of time (sample number) between transducers 7 and 3 for the 50 kHz signals. Similar data were acquired for every transducer pair combination and for each of the six chosen frequencies.

As detailed above, impact hits were used to damage the concrete on the 20th day, just before samples 727 and 735, and once again on the next day, just before sample 773. The location of the damage is shown in Figure 1. The times of the shots are not obvious from the curves in Figure 4, as the fluctuations in the data due to environmental conditions obscure the damage events. In previous work, we have shown that similar damage can easily be detected with such 50-kHz

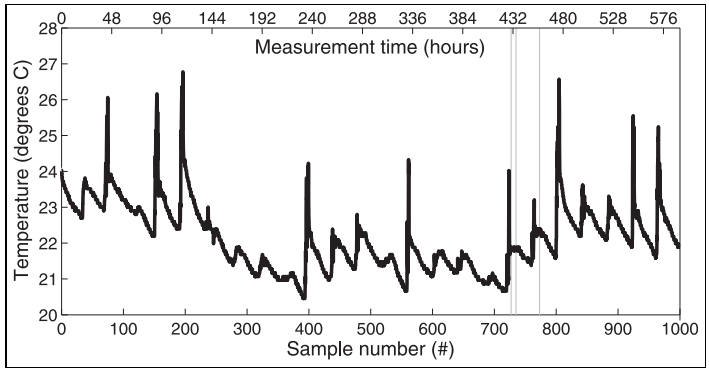

Figure 3. Temperature in the laboratory during the 25-day experiment. The gray vertical lines indicate the times of the damage events.

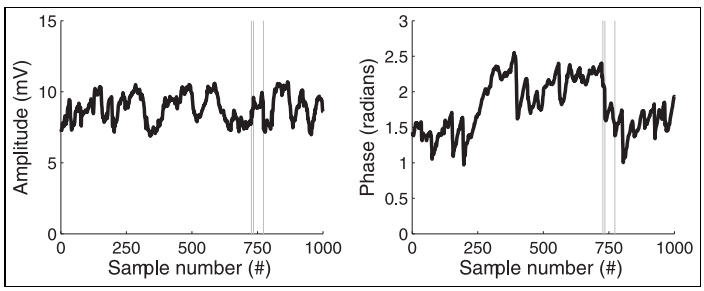

Figure 4. (left) Amplitude and (right) phase as a function of sample number for the frequency 50 kHz. Data are taken between transducers 7 and 3. The gray vertical lines indicate the times of the damage events.

continuous-wave measurements, viewing either amplitude or phase, in static environmental conditions.[13]

The variations caused by the EOV are also illustrated in Figure 5(a) to (g), which shows the resulting images from the tomography procedure for a few select times using only the 50 kHz phase measurements. The gray scale corresponds to the deviations from the mean of the baseline data set, expressed in the number of standard deviations of the baseline set (averaged over the grid boxes in the tomography). This corresponds to a one-dimensional version of the Mahalanobis distance. The sample numbers 400, 600, 700, 727, 735, 773, and 805 are shown. False-positive indications are given at random times, as seen in Figure 5(a) to (c), and there is no noticeable difference before and after the damage. This illustrates the inability of the system to separate the effects of damage and EOV, when using only one of the measured parameter at a time. Similar results are yielded for any of the 12 measured parameters.

It is likely that the effects visible here would be less pronounced if, for example, transducers embedded into the concrete had been used instead of surface-mounted transducers that are more exposed to the environment. However, for the purposes of this study, it does not matter if the variations are introduced due to the concrete or due to the transducers, as both kinds of effects need to be accounted for in a realistic application.

Figure 6 shows the Mahalanobis distance between transducers 7 and 3 as a function of time (sample number). The Mahalanobis distance of each sample is calculated from the amplitude and phase values of all frequencies, and it is relative to a baseline consisting of the 300 preceding samples (corresponding to 1 week's measurements) without any baseline lag. The first 300 measurements are used as the first baseline and are set to zero. For every new measurement, the baseline window is moved one sample ahead. Figure 6 shows some inherent deviation from the baseline at all times, with

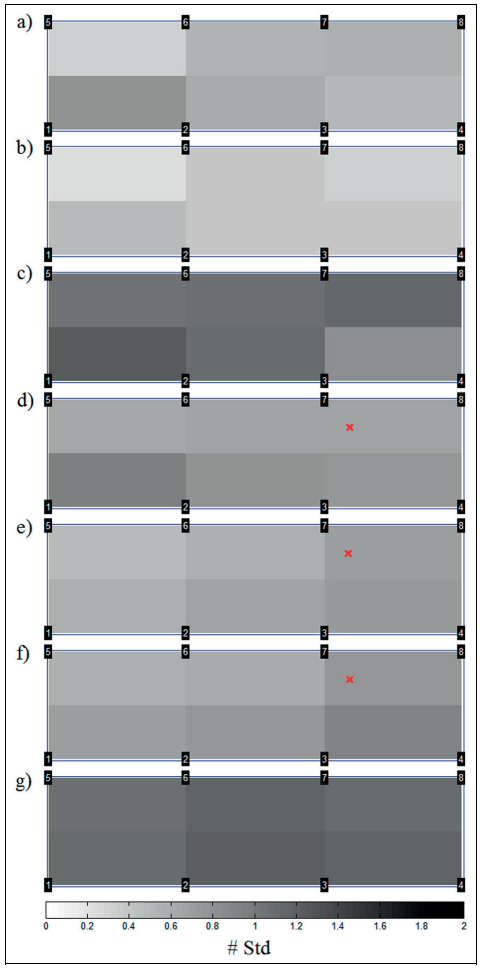

Figure 5. Results from the tomographic procedure at different times, using only phase data from the 50 kHz measurements. Sample numbers are (a) 400, (b) 600, (c) 700, (d) 727, (e) 735, (f) 773, and (g) 805. The red crosses denote the location of the damage. The gray scale signifies the deviation of the phase from the baseline data set, expressed in number of standard deviations of the baseline set. It is not possible to distinguish the healthy state from the damaged states using these images.

some variation. This is expected, since the EOV compensation is not perfect and there are some uncertainties in each measurement. However, some measurements clearly stand out in Figure 6, and these can be distinguished from the normal condition by the choice of a threshold value. These cases occur at sample numbers 727, 735, and 773, with a slightly wider peak at ~805. The first three correspond to three clearly resolved damage events. The peak around 805 is not caused directly by a damage event, but is a false positive that is not successfully suppressed by the algorithm. There are two possible explanations. First, as can be seen from Figure 3, this was a particularly warm day with strong sunlight. The weather had changed suddenly from the previous 7 days, and the baseline did not contain enough data. Second, the temperature peak occurs on the first day after the last damage event. It is reasonable to assume that the influence of the EOVs on the measurements can be altered by the damage, for example by tension reliefs and exposure of inner materials, and that the Mahalanobis model has not yet "learned" this new behavior. If this is the case, then the variation is partly and indirectly caused by the damage, and it should rightfully be detected by the SHM system.

Figure 7(a) to (g) shows the resulting images from the tomographic procedure at the same time stamps as in Figure 5, but in this case, the Mahalanobis distance is the damage indicator. Here, thresholds can easily be set to show no indications when there is no damage (Figure 7(a) to (c)). The time stamps corresponding to the damage events (Figure 7(d) to (f)) clearly indicate a deviation from normal behavior, and they also provide a rough indication as to between which transducers the damage occurred. Some indications are seen all over the slab, which is expected since the continuous diffuse wave fields consist of multiple scattered waves and boundary reflections. This phenomenon is expected to be somewhat less pronounced in larger structures where the transducers generally will be placed further from reflective boundaries.

The images corresponding to the false positive at 805 (Figure 7(g)) show a slightly more homogeneous deviation over the slab, which is expected for a deviation caused by global EOVs. However, the grid coordinate containing the damaged area shows a slightly higher deviation than the rest of the slab. This possibly supports the reasoning described above—that this peak, at least in part, is caused indirectly by real damage.

The presented result did not use a lag in the moving window for the baseline. This led to sharp spikes for sudden events. After that, the damaged condition is included in the baseline and the behavior is classified as normal. This is suitable only for the detection of sudden events, which is the scope of this article. For slower degradation processes, a lag is needed between the baseline and each analyzed measurement. In a realistic scenario for a large structure that is exposed to the environment, one option is to use a lag of an entire year. The baseline period would correspond to the same season from the previous year. Alternatively, the method could be combined with the optimal baseline

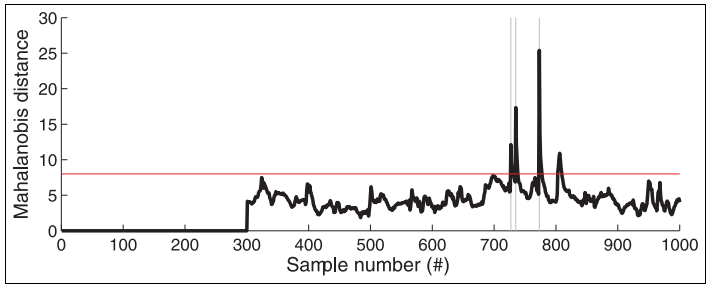

Figure 6. Mahalanobis distance for the measurements between transducers 7 and 3. A threshold line is set at a Mahalanobis distance of 8 (red horizontal line). The gray vertical lines indicate the times of the damage events.

selection method mentioned in the Introduction section. Then, any slowly evolving damages should be detected as slow trends in the data. The possibility to detect slow deterioration in the material of a structure, with this method, will need to be verified in future studies.

Further improvements to the presented monitoring system could be to increase the number of frequencies used in the continuous-wave measurements. This would increase the dimensionality of each measurement. Then, principal component analysis could be used to remove some of the variations caused by the environmental conditions before applying the Mahalanobis distance tool, as described by Cross et al.[29] Applying this technique to the data in this study did not improve the results. However, it could be of use if the dimensionality of the data is increased.

It should be stated that some parameters, such as selected frequencies, novelty threshold, and baseline lag, of the proposed SHM system have to be chosen from experience. Some will likely have to be tuned after the system has been in operation for a period of time, in order to find optimal settings.

The measurements in this study could likely be improved by the use of more sophisticated transducers, possibly embedded into the concrete, for example, those recently developed by Niederleithinger et al.[30] The optimal placement of the transducers is not trivial and depends on the chosen frequencies and the geometry of the structure which is to be monitored.

Conclusion

Narrowband amplitude and phase measurements of diffuse wave fields, created by continuous-wave transmissions at different frequencies, were used to detect minor damage to a large concrete floor slab. A similar system has previously been shown to successfully detect and localize damage in mostly static environmental conditions. In this study, the system monitored the floor slab

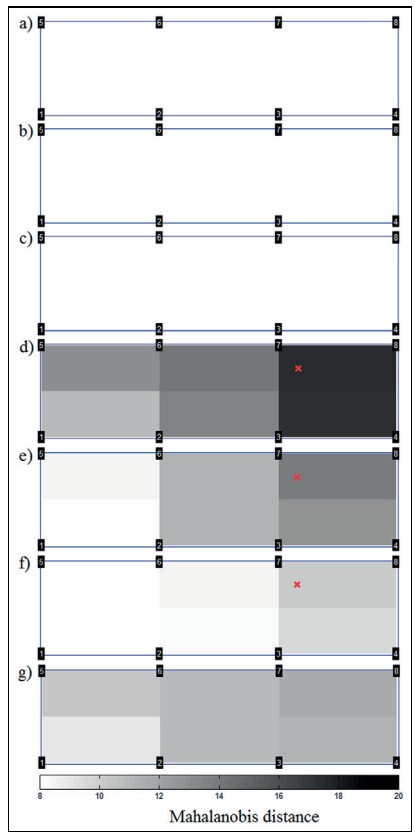

Figure 7. Results from the tomographic procedure after data normalization using the Mahalanobis distance. Sampling times (sample numbers) are (a) 400, (b) 600, (c) 700, (d) 727, (e) 735, (f) 773, and (g) 805. The red crosses denote the location of the damage. The damaged states can clearly be separated from the healthy state.

over 25 days, during which it was subjected to varying temperatures and sunlight exposure. These environmental conditions greatly influenced the measured data, and the resulting variations completely concealed the effect of the inflicted damage to the concrete. However, it was demonstrated that the variations caused by the environment could be largely suppressed using the Mahalanobis distance from a moving window baseline data set. Sudden damage events, which left centimeter-scale cracks in the concrete, could clearly be detected after this data normalization. Subsequently, a tomographic procedure, described in prior work by the authors, can be implemented to provide a rough localization of the damage.

Some of the environmentally caused variations remained after the data normalization. The most notable was a false-positive indication, on the same scale as the damage events, which was detected on a particularly warm and sunny day. This issue may be minimized in long-term measurements, where longer baselines can be used, which will include data from more environmental variations.

Nevertheless, the results from this study are encouraging for the use of diffuse ultrasonic wave fields in SHM applications for concrete structures, as the usability of such measurements are known to be very susceptible to environmental and operational variations.

Acknowledgements

The authors would like to specially thank the manufacturers of the concrete floor module. The concrete slab was constructed by Hedareds Sand & Betong AB, and the glulam beams were created by Moelven Töreboda AB.

Declaration of conflicting interests

The author(s) declared no potential conflicts of interest with respect to the research, authorship, and/or publication of this article.

Funding

The author(s) disclosed receipt of the following financial support for the research, authorship, and/or publication of this article: This work was supported by Swedish Research Council Formas (grant no. 244-2012-1001).

References

1. Pacheco C and Snieder R. Time-lapse travel time change of multiply scattered acoustic waves. *J Acoust Soc Am* 2005; 118: 1300–1310.
2. Snieder R. The theory of coda wave interferometry. *Pure Appl Geophys* 2006; 163: 455–473.
3. Planès T and Larose E. A review of ultrasonic Coda Wave Interferometry in concrete. *Cement Concrete Res* 2013; 53: 248–255.
4. Planès T, Larose E, Margerin L, et al. Decorrelation and phase-shift of coda waves induced by local changes: multiple scattering approach and numerical validation. *Wave Random Complex* 2014; 24: 99–125.
5. Mayor J, Margerin L and Calvet M. Sensitivity of coda waves to spatial variations of absorption and scattering: radiative transfer theory and 2-D examples. *Geophys J Int* 2014; 197: 1117–1137.
6. Margerin L, Planès T, Mayor J, et al. Sensitivity kernels for coda-wave interferometry and scattering tomography: theory and numerical evaluation in two-dimensional anisotropically scattering media. *Geophys J Int* 2016; 204: 650–666.
7. Kanu C and Snieder R. Time-lapse imaging of a localized weak change with multiply scattered waves using numerical-based sensitivity kernel. *J Geophys Res* 2015; 120: 5595–5605.
8. Planeäs T, Larose E, Rossetto V, et al. LOCADIFF: locating a weak change with diffuse ultrasound. *AIP Conf Proc* 2013; 1511(1): 405–411.
9. Rossetto V, Margerin L, Planeäs T, et al. Locating a weak change using diffuse waves: theoretical approach and inversion procedure. *J Appl Phys* 2011; 109: 34903.
10. Planès T, Larose E, Rossetto V, et al. Imaging multiple local changes in heterogeneous media with diffuse waves. *J Acoust Soc Am* 2015; 137: 660–667.
11. Zhang Y, Planes T, Obermann A, et al. Diffuse ultrasound monitoring of stress and damage development on a 15-ton concrete beam. *J Acoust Soc Am* 2016; 139: 1691–1701.
12. Fröjd P and Ulriksen P. Amplitude and phase measurements of continuous diffuse fields for structural health monitoring of concrete structures. *NDT&E Int* 2016; 77: 35–41.
13. Frojd P and Ulriksen P. Continuous wave measurements in a network of transducers for structural health monitoring of a large concrete floor slab. *Struct Health Monit* 2016; 15: 403–412.
14. Larose E, de Rosny J, Margerin L, et al. Observation of multiple scattering of kHz vibrations in a concrete structure and application to monitoring weak changes. *Phys Rev E* 2006; 73: 16609.
15. Niederleithinger E and Wunderlich C. Influence of small temperature variations on the ultrasonic velocity in concrete. *AIP Conf Proc* 2013; 1511: 390–397.
16. Zhang Y, Abraham O, Tournat V, et al. Validation of a thermal bias control technique for Coda Wave Interferometry (CWI). *Ultrasonics* 2012; 53: 658–664.
17. Zhang Y, Abraham O, Grondin F, et al. Study of stress-induced velocity variation in concrete under direct tensile force and monitoring of the damage level by using thermally-compensated Coda Wave Interferometry. *Ultrasonics* 2012; 52: 1038–1045.

18. Hilloulin B, Zhang Y, Abraham O, et al. Small crack detection in cementitious materials using nonlinear coda wave modulation. *NDT&E Int* 2014; 68: 98–104.
19. Konstantinidis G, Wilcox PD and Drinkwater BW. An investigation into the temperature stability of using permanently attached sensors. *IEEE Sens J* 2007; 7: 905–912.
20. Clarke T, Simonetti F and Cawley P. Guided wave health monitoring of complex structures by sparse array systems: influence of temperature changes on performance. *J Sound Vib* 2010; 329: 2306–2322.
21. Farrar CR and Worden K. *Structural health monitoring: a machine learning perspective*. Chichester: John Wiley & Sons, 2013.
22. Lu Y and Michaels JE. A methodology for structural health monitoring with diffuse ultrasonic waves in the presence of temperature variations. *Ultrasonics* 2005; 43: 717–731.
23. Salvermoser J, Hadziioannou C and Stähler SC. Structural monitoring of a highway bridge using passive noise recordings from street traffic. *J Acoust Soc Am* 2005; 138: 3864–3872.
24. Mahalanobis PC. On the generalised distance in statistics. *Proc Natl Inst Sci India* 1936; 2: 49–55.
25. Worden K, Manson G and Fieller NRJ. Damage detection using outlier analysis. *J Sound Vib* 2000; 229: 647–667.
26. Markou M and Singh S. Novelty detection: a review—part 1: statistical approaches. *Signal Process* 2003; 83: 2481–2497.
27. Yan A-M, Kerschen G, De Boe P, et al. Structural damage diagnosis under varying environmental conditions—part I: a linear analysis. *Mech Syst Signal Pr* 2005; 19: 847–864.
28. Jeng J-C. Adaptive process monitoring using efficient recursive PCA and moving window PCA algorithms. *J Taiwan Inst Chem E* 2010; 41: 475–481.
29. Cross EJ, Manson G, Worden K, et al. Features for damage detection with insensitivity to environmental and operational variations. *Proc R Soc Lon Ser: A* 2012; 468: 4098–4122.
30. Niederleithinger E, Wolf J, Mielentz F, et al. Embedded ultrasonic transducers for active and passive concrete monitoring. *Sensors* 2015; 15: 9756–9772.